Design, Development and Evaluation of Wearable Nanovibration Delivery Devices for Use in Osteoporosis Intervention

Richard Gibson

Department of Biomedical Engineering

Declaration

This thesis is the result of the author's original research. It has been composed by the author and has not been previously submitted for examination which has led to the award of a degree.

Signed: Date:

Abstract

Osteoporosis is a condition in which bone mineral density is lost making bones susceptible to fracture and reducing quality of life. In light of this, potential therapies to reduce the loss of bone mineral density or increase the creation of new bone cells are of interest.

This doctoral thesis summarises an investigation into the feasibility of using nanoscale mechanical vibration, also known as nanokicking/nanovibration, as an avenue to stimulate the growth of bone cells in vivo via the design and implementation of a wearable device applied to the surface of an osteoporotic region. Nanovibration is the application of low frequency vibration (1000 Hz) to a target area which has been shown to successfully stimulate the growth of bone cells in vitro using a displacement amplitude measured in the nanometre scale (2.5 - 100 nm).

The wearable nanovibration delivery device for the preliminary clinical evaluation was effective in that it was able to be worn for up to 2 hours and record the level of nanovibration transmission from the vibration source to the measurement device at the opposite side of the bone. This initial study demonstrated its viability in concept from an engineering perspective and noted potential improvements for future studies in this area.

The device was successfully scaled down for use on rats and used in a live animal trial to both apply and measure controlled nanovibration from the source to the opposite side of a target area of bone. The results from the animal trial showed no evidence that bone mineral density loss was affected at the target region.

Both studies indicated that nanovibration was being successfully transmitted to the other side of the bone. This was supported by FEA modelling as well as characterisation experiments in bone sample media granting confidence to these findings and quantifying the transmission of vibration through the bone region in terms of vibration amplitude as well as the reduction in vibration amplitude through the macroscopic bone regions applicable to the target region.

The wearable devices designed were used for their intended purpose to deliver and measure nanovibration but had no measurable positive effect on bone mineral density during the animal trials. The feedback from the studies provides information regarding future investigations into transferring the capacity to promote bone cell stimulation via nanovibration in-vitro to an in-vivo technique with potential applicability, and provide feedback on ergonomics, design features, and use limitations.

Publications Arising from This Work

The following article was written in parallel to this thesis featuring nanoscale transduction devices designed as part of this project as part of the animal studies covered in this thesis. Results relevant to the outcomes of this thesis were kindly shared by the authors. In addition, partial design and development progress reports were presented at BioMedEng19 featuring designs and concepts covered as part of the wearable device development method.

J A Williams, P Campsie, R Gibson, et. al., 2024, Developing and Investigating a Nanovibration Intervention for the Prevention/Reversal of Bone Loss Following Spinal Cord Injury, ACS Nano, 18 (27), 17630-17641

Table of Contents

List of Tables

List of Figures

Acknowledgements

I offer my thanks to Prof. Stuart Reid for their assistance and guidance throughout a (very) long and complex project and introducing me to many aspects of research and science beyond engineering and biomedical. I must also offer thanks to Dr. Jonathan Williams and Dr. Paul Campsie, both of whom were invaluable for their technical expertise and constant support.

John Riddel's knowledge and role in supporting the animal trials was indispensable, without which the animal studies would not have been possible. His group at the University of Glasgow were always a delight to work with. Thanks to the other members working on nanokicking projects, such as Peter Childs and Matthew Dalby and their teams as well.

The kind assistance from the Spinal Cord Injuries Unit at the Queen Elizabeth Hospital and Dr. Mariel Purcell was crucial, and having the opportunity to be involved in a preliminary clinical evaluation in such an environment formed a core experience I continue to draw on in new areas of medical device engineering.

Many thanks to Stephen Murray for his help with the many, many 3D prints I demanded as well as his help liaising with the John Scott Abattoir for bovine samples.

Thanks to my co-students in the lab, Svetoslava, Callum, Chalisa, Olivia, Gavin, Curtis and Sean for making my time at the University of Strathclyde more enjoyable.

Many thanks to my mother and father, Gillian and Neil, for their help during a very long writing period and through COVID-19, without whom I may not be sane. Thanks also to Diane Salman for her help providing a fresh perspective.

Abbreviations

aBMD ..... Areal Bone Mineral Density

ANOVA ..... Analysis of Variance

ASIA ..... American Spinal Injuries Association

BMD ..... Bone Mineral Density

CAD ..... Computer Assisted Design

CED ..... Cambridge Electronic Design

CT ..... Computed Tomography

DC ..... Direct Current

DEC ..... Departmental Ethics Committee

DEXA ..... Dual-Energy X-Ray Absorptiometry

DXA ..... Dual x-ray absorptiometry

DXRA ..... Dual x-ray absorptiometry

FDM ..... Fused Deposition Modelling

FEA ..... Finite Element Analysis

HDPE ..... High-Density Polyethylene

HU ..... Hounsfield Units

LED ..... Light Emitting Diode

LIPUS ..... Low-intensity Pulsed Ultrasound

NHS ..... National Health Service

OP-AMP ..... Operational Amplifier

PC ..... Personal Computer

PCB ..... Printed Circuit Board

PLA ..... Polylactic Acid

PP ..... Peak-Peak

pQCT ..... Peripheral Quantitative Computed Tomography

QCT ..... Quantitative Computer Tomography

SCI ..... Spinal Cord Injury

SCISCI ..... Scottish Centre for Innovation in Spinal Cord Injury

SD ..... Secure Digital

SLI ..... Scanning Laser Interferometer

USA ..... United States of America

vBMD ..... Volumetric Bone Mineral Density

VOI ..... Volume of Interest

WBV ..... Whole Body Vibration

WHO ..... World Health Organisation

1. Introduction

This thesis is the result of an investigation into the design, build and application of a wearable device to deliver mechanical vibrations on the nanometre scale, referred to as nanovibrations (1; 2; 3; 4), to a target area of bone in order to evaluate this application's usefulness in alleviating osteoporosis. This technique is also referred to as nanokicking. Osteoporosis describes the loss of bone mineral density resulting in bone fragility and damage which has a cost both in financial terms and in terms of the quality of life experienced (5; 6; 7).

1.1 Clinical Motivation

Osteoporosis is a condition that affects 200 million people worldwide (8). In the United Kingdom, the National Health Service (NHS) estimates that it affects over 3 million people, representing an estimated 4.4 billion pounds each year in costs to the public health sector (7). Osteoporosis is characterised by a reduction in bone mineral density (BMD) and bone mass, which accounts for an estimated 70% of bone strength, contributing to a loss of bone strength and an increase in fracture risk, with proximal femur fractures as a result of osteoporosis making up 20% of fractures (9).

Osteoporosis is defined by the NHS and World Health Organisation (WHO) as having a BMD of more than 2.5 standard deviations below the mean normal value of a young adult as assessed using a standard Dual-Energy X-ray Absorptiometry (DEXA) scan (5; 10). This leads to the bones being more fragile and susceptible to fracture following higher impact shocks such as falls as well as regular activity (9).

Though osteoporosis is prevalent in older, particularly female populations due to hormonal and metabolic changes resulting from the ageing process, it can affect all age groups and genders. It can also result from muscle loss with a reduction in mechanical stress on the bone, which is referred to as disuse, and trauma. In the case of highly traumatic injuries such as spinal cord injuries, the loss of bone strength due to bone mineral density decrease can be severe, and traditional physical therapies more strenuous (11; 12).

To help address osteoporosis, various treatments have been and are being explored by scientists worldwide, covered in detail in Chapter 2 of this thesis.

This thesis is the result of an investigation into the potential to use bespoke equipment designed to apply nanoscale vibration, referred to colloquially as 'nanokicking' or nanovibration, to bone in-vivo to positively affect bone mineral density. Nanokicking involves low-frequency vibration, ranging between 250 and 2000 Hz and of with an vibration amplitude of up to 100 nm, and following positive results in-vitro, is considered as a possible means to affect bone mineral density in-vivo. Terms such as nanovibration, nanokicking, and nanoscale vibration refer to the same concept in this thesis and may be considered synonymous, however the term nanovibration is used hereafter for consistency.

1.2 Aims and Objectives

Nanovibration has been used in-vitro to stimulate bone cell growth via osteoblastogenesis in mesenchymal stem cells (2), a process explored more closely in the following literature review below but that features key commonalities. Nanovibration, or 'nanokicking' features vibrations of the order of tens of

nanometres (ranging between 1 and 100 nm) at relatively low frequency (commonly ranging between 250 and 2000 Hz, though frequencies as low as 150 and 5000 Hz have been studied). Whilst the emerging technology is already proving a promising avenue to produce bone graft material in-vitro by using nanovibration to stimulate stacks of mesenchymal stem cells at audible frequencies (13), it also presents an opportunity to explore the use of nanoscale mechanotransduction vibration as a potential direct therapy intervention in-vivo due to the low fracture risk associated with nanovibrations. This is in contrast to the use of physical exercise, which carries with it fracture risks (14), and whole-body vibration (WBV), which can be strenuous for patients with spinal cord injuries and other conditions (15) and is time consuming, compromising the independence and mobility of the patient and presenting continuing costs to health services. This makes patient groups unable or less able to undergo traditional therapies, such as patients suffering from spinal cord injuries (SCI), especially vulnerable to osteoporosis, who already suffer from restrictions to mobility and activity as a result of their injury.

BMD loss has been shown to occur post-SCI (16) and conditioning therapies are difficult to perform on patients who have lost lower limb functionality, which can lead to slower patient improvement. The increase of fracture risk due to osteoporosis in SCI patients and the slow recovery time make it especially valuable to explore alternative therapies for treating osteoporosis in this group, which resulted in this being the focus group of patients for the human study portion of this thesis.

The benefit that any easily applicable device would have, such as a wearable device capable of reducing or reversing the loss of BMD in a disuse osteoporosis patient, would be valuable as it could contribute to an improved quality of life for the patient as well as open up another treatment route for health experts to apply to SCI patients unable to perform conventional physical exercises regularly. Low-amplitude mechanical interventions that can be applied passively, thereby reducing both risk of fracture and enabling greater access to potential treatment, is therefore especially valuable for SCI patients.

The Literature Review Chapter 2 provides the base information to establish how bones maintain density, how osteoporosis develops, and how changes to BMD are measured as well as outline existing osteoporosis therapies and how they work.

The Materials and Methods Chapter 3 describes the methods by which the nanovibration devices were designed and implemented in a series of studies, as well as the experiments done to investigate the use of the wearable device by patients with SCI, the effect on BMD that using the device has as part of an animal trial, and characterisation experiments using FEA and measurements on bovine samples. The results of the above experiments are presented in the Results Chapter 4.

Chapter 5 Discussion aims to comment on the results, elaborate on the limitations of each experiment, provide context necessary to interpret the results, and comment on possible avenues for future work. These are then summarised in Chapter 6 Conclusion.

The hypothesis that is therefore defined for this work is that nanovibration as used in similar nanovibrational work in-vitro is capable of producing a benefit in-vivo. In order to pursue this hypothesis, at this stage of research, what is assessed is the feasibility of delivering nanovibrations to at least one target region of interest in a repeatable and measurable manner. The aim of the original work in this thesis is to examine the potential for using nanovibration as an osteoporosis therapy via a bespoke prototype wearable nanovibration device designed for this project. This can be broken down into two measurable objectives, described in the following sections.

1.2.1 Design a Prototype Wearable Nanovibration Delivery Device for Use by SCI Patients

In order to investigate whether the use of mechanical vibration stimulation at the nanoscale is a valuable therapy to pursue, it is required to conceive of and design a device which is:

- Capable of delivering consistent, controlled and measurable vibration stimulation to a patient at the location of interest (in this instance an osteoporotic region such as the hip, knee or ankle (11)) during up to 4 hour sessions repeated regularly multiple times per week over the course of up to 4 months as supported by patient tolerance. The vibration must be delivered to the region of interest; confidence of which shall be ensured via vibration transmission supporting experiments.

- Wearable and can be used independently by either clinical staff or the patients themselves if they have upper limb functionality.
- Capable of delivering a level of stimulation at the same frequencies (150 – 2000 Hz) and comparable amplitudes (approx. between 5 – 40 nm) as early in-vitro studies (13, 2) to the target region in the bone; for the purposes of this work, 1000 Hz was selected as a target frequency. Vibration must be delivered directly to the bone, with confidence that comparable vibration exists within the bone region.

In addition to this, testing and characterisation of the vibration amplitude at the target region in the bone was carried out to provide confidence that vibration was present inside the trabecular region of bone as well as better understand the behaviour of low-frequency vibration at the nanoscale. This was done via finite element analysis (FEA) modelling and laboratory experiments on proxy media. The design and its use were validated based on the above factors considered, and ultimately the feasibility of using a device in real-life use cases was determined.

Given the difficulties in gathering sufficient participants to determine statistical significance of the effect of nanovibration on BMD, as well as difficulties inherent to recruiting participants suffering from variable injuries and different lifestyles, the studies using the prototype wearable nanovibration device were aimed solely to determine the viability and limitations of using a wearable device as a delivery mechanism. In order to assess whether the proposed stimulation may have an effect on BMD at the proposed session durations, however, it was deemed necessary to implement an animal trial into the study, detailed below.

1.2.2 Design a Prototype Nanovibration Delivery Device for Use in an Animal Study

In order to complement and support the studies done using human participants, the animal study portion of the project provides a body of data for analysis relating to the effect of nanovibrations on BMD by applying nanovibrations to the bone. Kind permission to present the results from this study was obtained from Dr. Jonathan Williams (17), who ran the animal study using the equipment designed as part of this project and who supplied results presented in section 4.2.3 of this thesis. The animal study provides a more controlled and repeatable set-up enabling for any potential positive effect to be observed repeatably, as well as manage a larger sample size inaccessible with human participants within practical limitations. In order to perform during the study the animal device needed to:

- Be miniaturised to fit on a rat hind limb.
- Provide consistent, controllable and measurable vibration of the same frequency as for the human focussed studies and at amplitudes between 40 nm and 100 nm for a period of study for up to 4 hours as part of daily nanovibration delivery sessions.
- Minimise manual intervention from the study controller over the time of the study.

The BMD was assessed at the target region using computer tomography scanning. The aim of the study was to determine whether nanovibration has an application in therapy, and to what degree. This will also help decide the future of the technology and give insight into any subsequent investigation; this work aims to

use the effect of nanovibration as seen during the animal trials to discuss and determine the feasibility of using nanovibration delivery as a means to affect positively BMD over realistically feasible session durations.

1.2.3 Scope and Limitations

This work establishes the overall feasibility of applying the proposed technology via the use of a preliminary clinical evaluation and investigations on human participants combined with animal studies. At this stage of development, it is not intended to demonstrate clinical efficacy on bone mineral density, only to establish via investigation on human participants the ergonomic and practical viability, establish evidence of positive effect via animal studies, and provide adequate confidence of vibration transmission via supporting experiments.

All supplemental experiments aim to provide context and information within the goal of demonstrating practical viability.

1.3 Original Contribution

This thesis contributes several novel contributions to the field of nanovibration delivered in-vivo as well as inform feasibility limitations discovered as part of the project.

- This thesis investigates the feasibility of using wearable, active devices with a vibration measurement component as a potential tool for patients suffering from spinal cord injuries.
- This thesis describes the design and use of nanovibration devices used in animal trials in order to characterize the effects of the stimulation in-vivo

following rapid bone loss due to spinal cord injury. It reports the first null result in animal trials at the dose attempted.

- This thesis combines FEA analysis proof-of-concept models and vibration characterisation experiments on bovine femurs using laser interferometry measurement tools to support understanding of nanovibration transmission through bone as a bulk media, in order to support future work and support the conclusions of this thesis.

1.4 Chapter Overview

This investigation follows existing work in vitro to improve bone density with the aim of evaluating the potential to improve bone density in vivo from applying nanovibration techniques via a wearable device. The investigation can be broken down as follows:

- Chapter 1: Introduction outlining the top-level objectives and motivation of the study, as well as limitations to the study at this stage of development.
- Chapter 2: Overview of key literature and background information sufficient to interpret the methods and results. A brief overview of bone mineral density therapies is included for context of existing treatments.
- Chapter 3: Description of all materials and methods used as part of the project. This section covers both design methods and experimental methods, both simulated and physical in nature.
- Chapter 4: Covers all results gathered during the project that can be discussed. This chapter covers results gathered as part of the animal trials, preliminary clinical evaluation, finite element analysis simulations, vibration transmission characterisation on analogue and biological tissue

samples, and feedback gathered from the design and usability of the wearable device.

- Chapter 5: Discusses the results and observations. This chapter aims to comment on and objectively weigh the factors contributing to the overall feasibility of the proposed technique as per the aims and objectives of the project.
- Chapter 6: Concludes on the project outcomes, and propose suggestions and speculations for future work.

2. Literature Review

The literature review establishes how bones maintain their density, how osteoporosis can develop and existing information and therapies aimed at improving BMD.

2.1 Bone Morphology

Bone is a complex biological structure; it serves to provide structural integrity and protection for various organs, supports the majority of the load during physical activity as well as transmitting forces to affect the surrounding environment (18).

Within the bone itself there are several types of region, among them being dense compact or cortical bone, and cancellous or trabecular bone, which has a sponge-like shape and can distribute forces across a larger area. The complex geometry of bone renders it anisotropic as a material, that is to say, it will exhibit different mechanical characteristics depending on the direction of application of force.

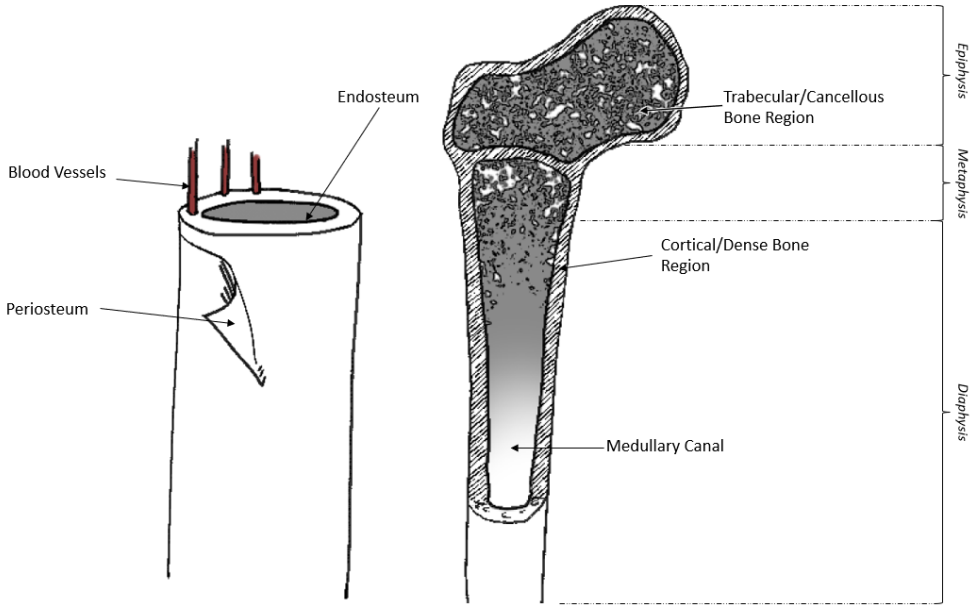

Figure 1: Bone diagram showing/illustrating the different layers/types of bone tissues in the femur bone and its regions

Figure 1 above shows the makeup of a long bone such as a femur. This is made of a diaphysis and an epiphysis. The diaphysis is the main shaft of the bone and is hollow, containing the medullary cavity which is used to store bone marrow. The structure of the diaphysis is dense and compact cortical bone. The epiphysis is situated at the proximal and distal ends of the bone. This region is wider and formed internally of mostly trabecular bone. Between the trabeculae, small structures that make up a spongy formation inside the trabecular region, is red bone marrow. Between the diaphysis and epiphysis is a transition region known as the metaphysis.

Inside the bone and situated on the outside of the medullary canal is the endosteum, made of bone cells designed to assist the bone in remodelling itself. Similarly, but on the outside of the bone is the periosteum, which contains nerves, blood vessels

and lymphatic vessels that serve to keep the bone healthy. Articular cartilage can be found at the joints between bones on the epiphysis.

The various cells in bone do not make up the bulk of bone mass, this is largely made up of both organic and inorganic substances, namely collagen and hydroxyapatite. There are four types of cells found within bone tissue which have a role in maintaining BMD; osteoblasts, osteocytes, osteoclasts and osteogenic cells.

Osteoblasts are formed from osteogenic cells which serve as stem cells and are responsible for forming the bone matrix (19; 20). The role of the osteoblast is to secrete a collagen matrix that calcifies and form the bulk of bone mass.

Osteocytes are formed from osteoblasts which transform into osteocytes as they become trapped within the calcified matrix and continue to secrete enzymes thus maintaining bone mineral concentration. Osteocytes are responsible for maintaining bone tissue and are nourished via canaliculi, channel structures within the bone matrix that allow nutrients to reach the osteocyte (21; 22). Osteocytes and osteoblasts are incapable of mitosis and therefore do not divide or replicate. Instead, they are formed from osteogenic cells that differentiate and divide into osteoblasts. Osteogenic cells can be found in adipose tissue and in bone marrow.

Osteoclasts are cells which break down bone continuously, resorbing bone. Osteoclasts and osteoblasts together form a homeostatic balance, as the bone formation of the osteoblast cells is controlled by the bone resorption activity of the osteoclasts.

Osteoclasts are multinucleated and originate from white blood cells instead of osteogenic cells. This function is dependent on the presence of mesenchymal stem cells that can differentiate into osteoblasts and osteoclasts; these are present in the periosteum and the endosteum part of the bone. The mesenchymal stem cells present in bone marrow form osteoblasts via osteogenic cells or osteoclasts via white blood cells to promote a homeostatic balance, as the bone formation is controlled by the osteoblasts forming new bone and the osteoclasts' bone resorption activity.

Understandably, the macroscopic regions within the bone can have implications regarding the transmission of mechanical forces through the bone, and the role of individual cells on homeostasis is a key contributor to BMD.

2.2 Osteoporosis

When homeostatic balance is interrupted by either reducing the formation of bone via osteoblasts, or increasing bone resorption via osteoclasts, osteoporosis can occur. The loss of bone that results from this can be rapid and severe; the risk of fracture that arises from osteoporosis is a cause of morbidity, loss of mobility, and a decrease in quality of life, all of which contributes to the clinical motivation described in section 1.1. The increase in porosity and fragility is shown in Figure 2 below.

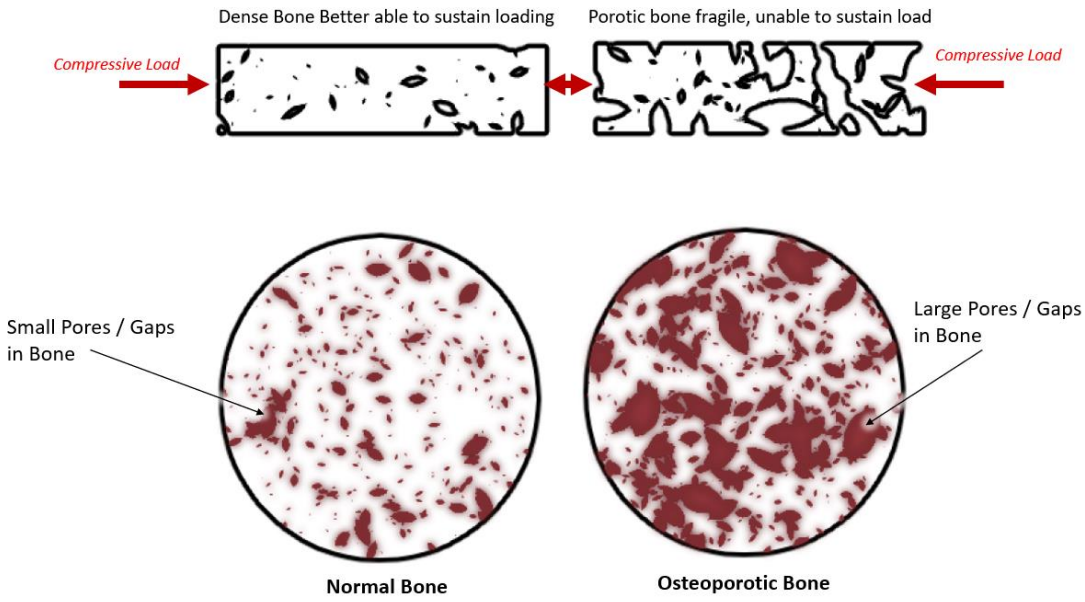

Figure 2: Osteoporotic vs healthy bone diagram

This homeostatic process of resorption and formation is affected predominantly by reductions in mechanical stresses occurring during disuse. As one of the determinants of bone morphology, this reduction of mechanical stress inhibits osteoblast-mediated bone formation and accelerates osteoclast mediated bone resorption (23). In particular, reduction in mechanical stress on the bone is known to inhibit osteoblast-mediated bone formation; as a result, disuse can cause what is known as disuse osteoporosis. Disuse can occur through bed rest (24) and through past applications for fracture treatments (25), which can make treating fractures from osteoporosis especially challenging.

Maintaining healthy bone is a complicated process with a variety of factors that can contribute to a weakening of the bone. These can be due to a failure to develop a strong skeleton, potentially caused by genetic, nutritional, and lifestyle factors

(26). Ageing, particularly in the female population, is also a serious driver of osteoporosis (27), however it is also present in the male population (28; 25).

As described in the Clinical Motivation section of this thesis, the cost of osteoporosis to health services is considerable. Common fractures occur at the wrist, hip, and spine, where trabecular bone makes up the majority of bone volume (26).

2.3 Spinal Cord Injury Osteoporosis

One of the causes of osteoporosis results from suffering a spinal cord injury. This is especially problematic since osteoporosis can develop from the trauma of the injury itself, the disuse that occurs following loss of mobility, as well as neural factors with loss of control over the limbs below the site of injury. All have a negative impact on BMD (29; 11; 12).

Injuries to the spinal cord are often described in terms of their location and their completeness. A ‘complete’ SCI will remove all feeling and ability to control motor function below the site of injury, whereas an incomplete injury will leave some motor and sensory function to varying degrees. In addition, the location of the injury along the spinal column will cause differences in the area affected by paralysis. Paraplegia affects all or part of the trunk, legs, and pelvic organs, whereas tetraplegia also affects the arms and hands. This will depend on what section of the spinal cord is injured; the higher the injury, the more extensive the damage (30). The location of injury has repercussions on the added difficulty for physically demanding treatments, as is discussed in Section 3.4 of this thesis.

In addition to the trauma of suffering a SCI, these patients suffer a rapid and severe loss in bone density in the long bones below the site of injury. In particular, trabecular bone is more affected compared to bone in the cortical region. Severe bone loss affects primarily the regions below the site of injury, interestingly reports of increased bone density in bones above the site of injury have been made (31). Trabecular bone being affected severely renders this region of the bone an attractive region of interest for stimulating the activity of bone-forming cells. What is therefore known based on the above information is:

- SCI causes rapid and severe loss of BMD, rendering patients suffering from SCI injuries particularly important as a group to investigate.
- SCI injuries have severe repercussions on the ability of patients to perform physically demanding treatments, and consideration of these limitations is important for designing a viable wearable device in later sections.

2.4 Assessing Bone Mineral Density

Assessing bone strength is difficult to perform directly; instead, what is done to diagnose osteoporosis is to assess BMD, which is determined to be the density of minerals such as calcium within the bone at a local region of interest, either to determine whether a region of bone is at risk of fracture or to monitor the progression of osteoporosis. In response to this need densitometric techniques are used to assess the degree of BMD loss which is used to characterise the degree of osteoporosis at a target region. The current clinical standard for measuring BMD change is dual x-ray absorptiometry (DXA) or DXRA (32), which provides an areal bone mineral density indication. The methods available to infer bone strength from BMD measurements using the techniques covered in this section form the

available options that are considered as part of the animal trial experiments in Section 3.9.

In DXA, the x-rays used possess enough energy to pass through the body and be detected after transmission. The bone and soft tissues in the target area absorb a degree of the energy carried by these x-rays resulting in a reduction of amplitude or attenuation. The degree of attenuation varies with the density and thickness of the target bone, and the energy of the photons. Attenuation follows a reverse exponential formula (33) and can be described using the Bouger-Lambert-Beer law for a beam through homogeneous material which is described by the formula

$$I = I_0 e^{-\mu t}, \qquad \textit{Equation 1}$$

where I is the measured x-ray intensity at the sensor through a thickness of material t, I_0 is the initial x-ray intensity, μ is the linear attenuation coefficient of the homogeneous medium.

DXA compares the degree of absorption between two x-ray beams at different energy levels, one high and one low. Using this comparison the density of bone in the target area can be calculated, since bone and soft tissues have different absorption characteristics depending on the energy of the beam being used. By repeating DXA scans the changes in BMD can be observed and measured reliably (34). DXA is recommended as a clinical tool for diagnosing osteoporosis as it is non-invasive and established clinically.

An alternative to DXA scanning exists in the form of peripheral quantitative computed tomography (pQCT) (35). In contrast to DXA imaging which provides an areal BMD (aBMD) measurement, pQCT is a volumetric method that can calculate volumetric bone mineral density (vBMD) whilst also using a lower radiation dose compared to DXA. These advantages have enabled QCT scanning to emerge as a viable alternative to DXA when available. A diagram of a typical DXA set-up is shown below.

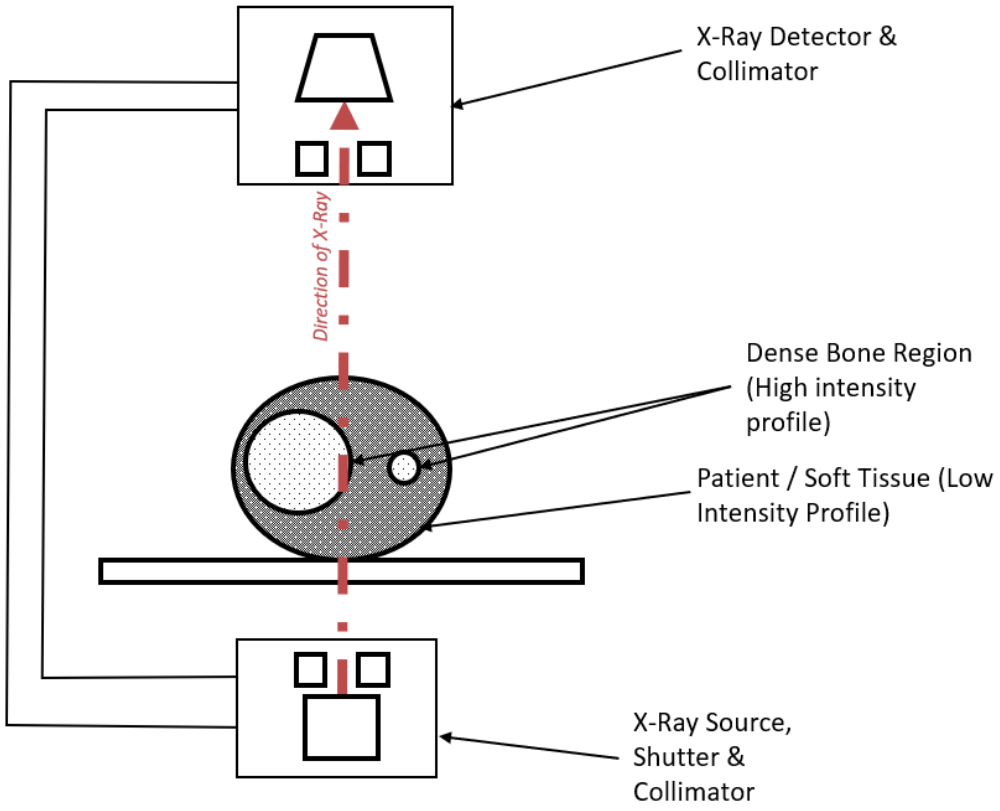

Figure 3: Diagram of DXA setup

Quantitative computed tomography (QCT) may be performed using any CT scanner combined with the use of a calibration phantom of known density in order

to allow the scanned image to be quantified in terms of a bone density measure by comparison against that calibration phantom.

Standard CT scanning involves using x-rays to produce images of a cross-section of the target in thin ‘slices’. Thickness of individual slices can vary depending on the resolution of the CT machine used but typically range between 1-10 millimetres for a standard CT scan. Unlike a fixed-point X-ray, the CT scanner rotates the X-ray 360° around the target, which provides a detailed 3D view of the target region. Unlike for traditional X-rays, a CT scanner utilises specialised digital X-ray detectors instead of a film. Micro-CT scanning is an imaging technique similar to CT scanning but using a scanner with a much higher resolution (36), making it appropriate for imaging smaller geometries. This property renders it ideal for analysing the BMD and vBMD of the animal bones harvested following the animal trials of this study.

CT scanning calculates the attenuation coefficient value corresponding to each voxel in Hounsfield units (HU), where lower HU represents less-dense bone and where higher HU represents denser bone regions (37). The CT scanner by itself is unable to measure the mineral density at each voxel point; in order to estimate the mineral density from the attenuation coefficient values, hydroxyapatite phantoms are provided in order to calibrate the CT scanners or can be included in the image if positioned near the target being measured. This permits the transformation of attenuation coefficients per voxel into volumetric bone mineral content and volumetric mineral density. The operation of the CT scanner is shown in Figure 3 below.

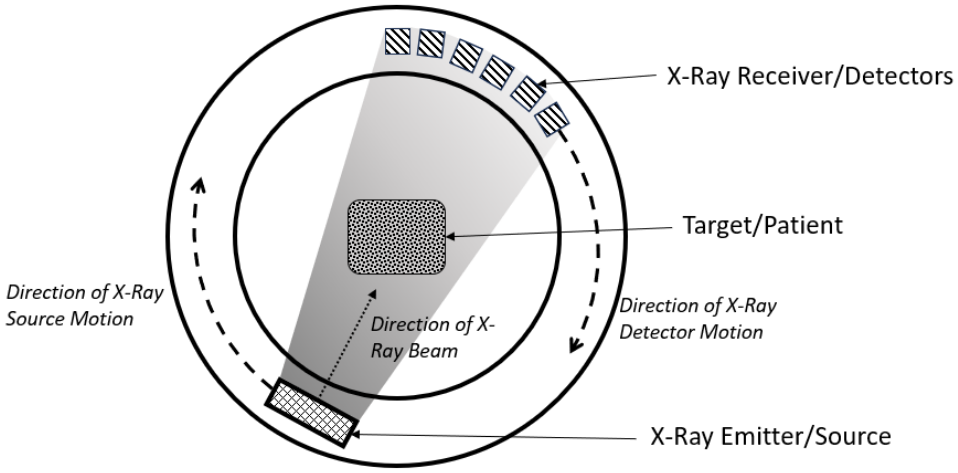

Figure 4: CT Scanning Diagram

QCT can be used to quantify BMD in regions such as the femur, forearm, tibia, and spine, and since a volume of interest (VOI) can be identified during scanning, the trabecular and cortical regions can be differentiated between.

Peripheral quantitative computed tomography (pQCT) in addition to giving information on bone density, also provides information on geometry of the bone, size of the bone, and indications of mechanical bone strength (35) in part due to its capacity to consider changes in BMD across the z-dimension.

The use of CT scanning is an attractive method of assessing BMD following stimulation, and will form the primary method of assessing BMD during the animal trials as discussed later in this thesis due to the ability of micro-CT scanning to image small geometries and to provide indications of vBDM following the harvest of target bones. Standard CT imaging techniques were used by the Spinal Injuries Unit at the Queen Elizabeth Hospital to screen for participants for osteoporosis due to its availability at the clinic in question.

2.5 Osteoporosis Treatment

Current osteoporosis therapies fall into three broad categories:

- Pharmacological
- Physical
- Wave or vibration therapies

The various treatments covered in this section, their limitations, benefits, and drawbacks are important to consider as part of assessing the viability of a potential alternative treatment. Any proposed treatment must be compared against available treatments at the time, and so an awareness of alternative techniques is necessary for discussion of the results of this thesis.

2.5.1 Pharmacological

Pharmacological treatments for osteoporosis are commonly prescribed for the condition. There are several types of pharmacological treatment; anti-resorption agents such as bisphosphonates (38; 39; 40), antibody-based medication such as Denosumab© (41), and sclerostin antibodies (42; 43; 44).

Bisphosphonates are the most commonly prescribed treatments for osteoporosis and have been found to reduce bone resorption through inhibiting osteoclast function and so allowing BMD to be increased. Bisphosphonates are made up of two phosphonic acids joined to a carbon, plus two chains designated R1 and R2. Bisphosphonates bind to hydroxyapatite crystals on the surface of bone, which makes them viable for use in the treatment of metabolic bone diseases. When an active osteoclast begins the process of bone resorption, bisphosphonates are

released from the bone, entering the osteoclast and causing a loss of resorptive function and allowing for BMD to be increased.

Antibody based medication and sclerostin antibodies are another type of pharmacological treatment that both increases new bone formation whilst also reducing bone resorption (42; 43) by targeting the Wnt pathway. The Wnt signalling pathway allows proteins to pass signals from cell to cell or within the same cell. Sclerostin is a natural inhibitor of the Wnt pathway, which is a key element in bone formation. Additionally, the activation of the Wnt pathway causes an inhibition of bone resorption by osteoclasts. Drugs such as Romosozumab© bind to the human form of sclerostin and inhibit its action. For this reason, sclerostin antibodies are being investigated as a potential pharmaceutical drug treatment for osteoporosis.

2.5.2 Physical Therapies

A number of physical therapies to mitigate against osteoporosis have been developed based on the principle of Wolff's law (45), which states that bones in a healthy person will adapt to the loads it is subject to. Loading the limbs is a method in which BMD loss can be reduced, as it provides a stimulus to the bones and surrounding tissue which promotes the production of osteoblasts to increase BMD. It is known that effects such as disuse, extensive bed rest and microgravity (experienced in space travel) have a profoundly negative effect on bone density (21; 46). By performing physical exercise, the bones can be loaded and reduce the effects of disuse on bone density. This loading of limbs can take a variety of forms, since osteoporosis frequently targets older, ageing patients or patients with existing injuries, and can include sling therapy (47), standing training (48), or

weight/resistance training and aerobics (49; 50; 51), among others. Physical therapy is applicable to both osteoporosis from SCI as well as postmenopausal or disuse osteoporosis, though in the case of SCI it can be especially challenging to implement (52).

2.5.3 Therapeutic Vibration

In this section, a selection of vibration therapy techniques will be introduced based on the type of source they use, including ultrasonic vibration therapy and Whole Body Vibration (WBV).

2.5.3.1 Whole Body Vibration

Whole Body Vibration builds on the physical therapies of loading limbs to provide stimulus to improve bone density (53). WBV is a technique used to deliver oscillations through the entire body, as opposed to a specific target region, by placing the patient on a vibrating plate, either standing or sitting as required, which then mechanically loads the limbs compressively.

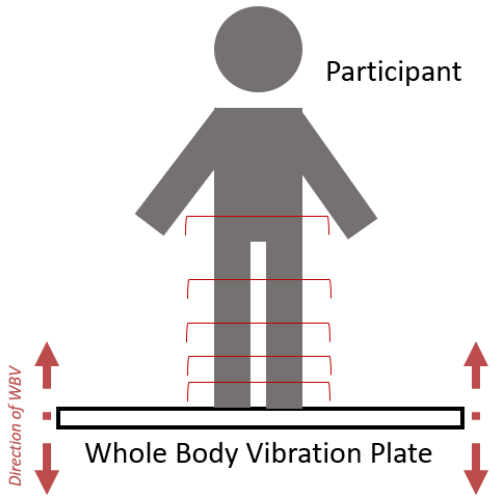

Figure 5: Diagram of whole body vibration (WBV) set-up

This is theorised to have a benefit to bone according to several potential explanations such as Wolff's law (45; 48), mechanostat theorem and mechanotransduction theory, which also relates to the adaptation of bone tissue to the mechanical environment via feedback loops or biochemical response (54; 55).

WBV has been explored as a potential therapy for postmenopausal osteoporosis (56; 57) and has been explored for patients suffering from osteoporosis due to SCI (58; 59; 60). The intent of this therapy is to stimulate bone growth through cyclic loading of the bone as a result of the vibration; according to piezoelectric theory, bone formation can be stimulated by an electrical potential difference caused by pressure applied to the bone. Due to the anisotropic nature of bone, this is direction dependant. For example, a bone under bending motion will accumulate an electrical potential.

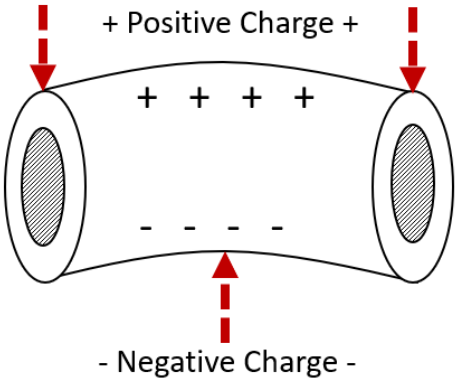

Figure 6: Simplified diagram of a bone generating charge under bending motion

Motion delivered by the vibrating plate can be oscillatory or linear; depending on the type of machine it can be delivered standing or via an inclined bed. It involves maintaining a static position or performing exercises whilst on a vibrating platform

which vibrates at a low frequency, ranging from 12.5 to 90 Hz (61) and high amplitudes.

WBV functions by repeatedly loading the bone by applying an acceleration using the plate; this puts the bone under a compressive stress. This stress is propagated through the body via the skeleton. Due to the complexity of the human body, it can be difficult to predict the transmissibility of compression between regions in the body, such as between the ankle and the knee, or the hip and the spine; these can be affected by posture, muscle activity, weight of individual body segments, and others (62).

Whilst there have been a number of studies exploring WBV, reviews and follow-up studies dispute the efficacy of WBV's effect on BMD and bone architecture (63; 64; 65). As a form of physical therapy is it well-documented as a means to promote muscle activity, however in the context of providing BMD improvements for SCI patients it retains some downsides inherent to physical exercise as a treatment in that it is physically demanding and requires patients to be standing for the duration, and papers disputing the effect of WBV propose that the benefits of WBV in terms of reducing fracture rates may result from WBV training reducing the likelihood of falls, not by directly affecting bone health. Therefore, it may be viewed as a supplement to existing physical therapies rather than an example of mechanical vibration promoting bone activity directly. As a result, the research of alternative techniques remains attractive.

2.5.3.2 Ultrasound Vibration Therapy

Pulsed ultrasound has been investigated as a potential therapy in the prevention and treatment of osteoporosis following SCI (66). Ultrasound is a high-frequency acoustic wave, greater than the maximum frequency audible to humans (approx. 20kHz), travelling through the body. As a diagnostic tool, ultrasonic imaging is incredibly widespread and used throughout the world to image internal organs. As a site-specific therapy technique, ultrasonic vibration can be aimed towards a target region to deliver acoustic energy to a site with the aim of stimulating cell production. Waves are transmitted through a media via compression and rarefaction, and can be visualised using the diagram below.

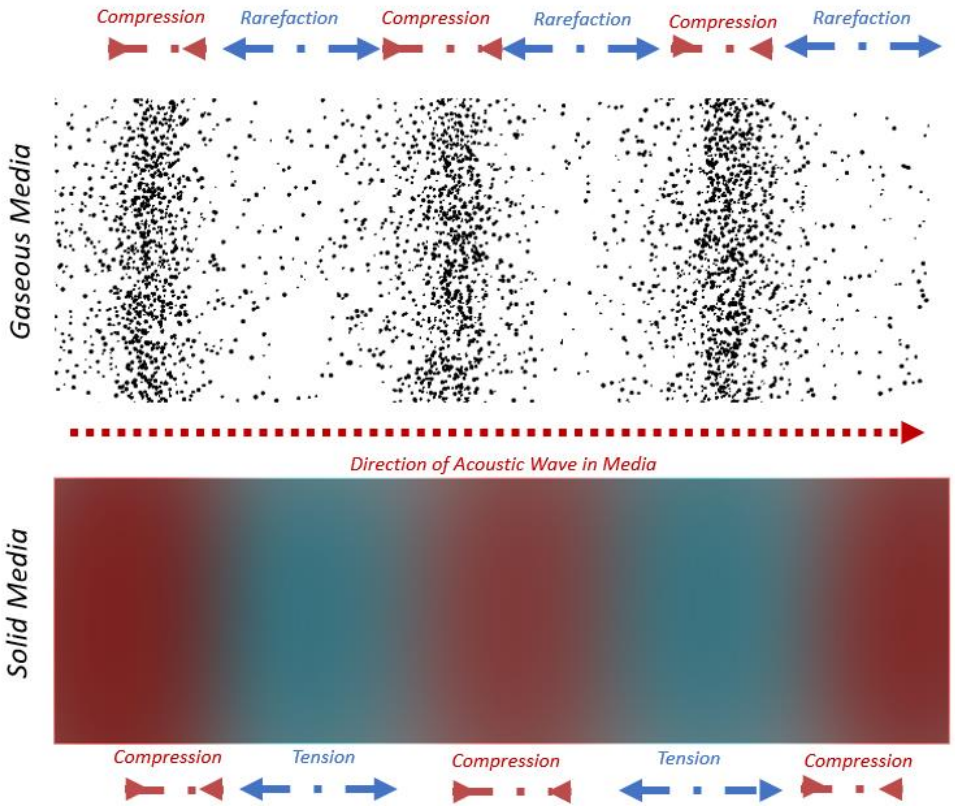

Figure 7: Diagram of acoustic wave compression/rarefaction and compression/tension propagation in a simplified gaseous and simplified solid media

Acoustic waves have a given frequency and wavelength depending on the speed of sound in a media (67; 68; 69).

This relation is described simply as

$$f = \frac{c}{\lambda}, \qquad \textit{Equation 2}$$

where f is the frequency of the wave, given in Hz, c is the speed of sound in a given media, and λ is the wavelength of the wave in the media in metres.

Traditional ultrasound uses single-element transducers applied to a target. The ultrasonic wave travels through the body through alternating compressions and rarefactions in a plane wave. The stresses that are applied to the propagation medium cause elements inside to oscillate and vibrate.

The pressure plane wave can be derived from a combination of Newton's second law and conservation of mass. In three dimensions, Newton's second law can be described according to the following differential equation,

$$\frac{d}{dx}p(x,t) + \rho_0 \frac{d}{dt}u(x,t) = 0 \qquad \textit{Equation 3}$$

The pressure plane wave propagates along a direction *x* according to the following formulae,

$$\frac{d}{dx}p(x,t) + \rho_0 \frac{d}{dt}u(x,t) = 0 \qquad \textit{Equation 3}$$

and

$$\frac{d}{dt}p(x,t) + \frac{1}{k}\frac{d}{dx}u(x,t) = 0, \qquad \textit{Equation 4}$$

where ρ_0 is the mass density of the medium at rest, *p* is the pressure of the wave, *k* is the compressibility of the medium and *u(x, t)* is the particle velocity produced by the wave.

By combining the two formulae, the acoustic wave equation can be obtained. This is given as

$$\frac{d^2}{\delta d}p(x,t) - \frac{1}{{c_s}^2}\frac{d^2}{dt^2}p(x,t) = 0, \qquad \textit{Equation 5}$$

where $c_s = \frac{1}{\sqrt{\rho_0 k}}$ is the speed of sound in the media. A plane wave comprising of a single frequency will have the solution

$$p(x,t) = Pcos(\omega t - kx), \qquad \textit{Equation 6}$$

where P is the wave amplitude, ω is the angular frequency, and k^* is the wave number.

Ultrasound is often described in terms of intensity, which is the power per unit cross-sectional area, also related to pressure. This is shown by

$$I\left(\frac{W}{m^2}\right) = \frac{P^2}{2\rho_0 c}, \qquad \textit{Equation 7}$$

where I is the intensity and W is power. As for all acoustic waves, ultrasonic waves are reflected and transmitted at the boundary between two media. The reflection coefficient is given by the formula

$$R = \frac{Z_2 cos\Theta_i - Z_1 cos\theta_r}{Z_2 cos\Theta_i + Z_1 cos\theta_r}, \qquad \textit{Equation 8}$$

where Z is the acoustic impedance of the plane wave for a given media and is described by the formula

$$Z = \rho_0 c. \qquad \textit{Equation 9}$$

The properties of reflection and attenuation are harnessed in order to produce ultrasonic imaging, but the high-frequency vibration is also delivered as a potential therapy. Because the acoustic wave imparts a vibration, this acts as a mechanical stimulation to the target region, it has been used to promote a response from the bone. The specific vibration characteristics imparted vary depending on the study, often described in terms of intensity.

Intensity of a plane wave decreases with distance in an exponential fashion (72) according to the formula,

$$I_x = I_0 e^{-u(f)x}, \qquad \textit{Equation 10}$$

where the term u(f) is a frequency dependent intensity attenuation coefficient and x is the distance between two points in the direction of propagation. In a material, the amplitude of vibration depends on intensity. In practice, attenuation of vibration is typically referred to as α(f). Stoke's law of sound attenuation describes attenuation in a fluid according to the formula,

$$\alpha = \frac{2\eta(2\pi f)^2}{3\rho {c_s}^3} \qquad \textit{Equation 10}$$

Where η is the dynamic viscosity coefficient of the fluid, ρ is the density of the media, and c_s is the speed of sound in the media. However, absorption, scattering, reflection, diffraction, mode conversion and phase cancellation (70) contribute to the attenuation in biological media. In practice, only the most dominant factors are cited when applicable, though this does not mean the other mechanisms do not contribute.

In terms of vibration amplitude this takes the form of the equation,

$$A = A_0 e^{-\alpha(f)x}. \qquad \textit{Equation 11}$$

Reflection and transmission are understood as a factor of the acoustic impedance of two materials at a boundary, which are also a factor of material density and compressibility. Taking the attenuative properties of the material into account is also often necessary in order to separate the attenuation and transmission effects when measuring a sample.

Using the equations shown above, the attenuation coefficient can be derived from the distance the wave travels and the difference in vibration amplitude measured, however as attenuation is also frequency dependent it is often described in terms of frequency dependency.

Low-intensity pulsed ultrasound (LIPUS) has been used to accelerate fracture healing (71; 72; 73) and involves a period of ultrasound delivery followed by an off period in a repeating fashion. Studies aimed at examining its biological effects have taken place; ultrasound aims to affect the signal transduction mechanisms by introducing a mechanical force. It was shown that LIPUS affects osteoblasts and ossifying cartilage, increasing ossification, affecting chondrocyte proliferation and matrix production, and affecting the permeability of cell membranes (74; 75; 76). It is established that bone cells respond to mechanical forces via signal transduction mechanisms. It has since been additionally investigated for treatment for osteoporosis in rats (77; 78).

Studies into low-intensity pulsed ultrasound are varied and ongoing; a summary of some example studies are collected into the following table to provide an overview of types of LIPUS investigated.

Table 1: Summary of LIPUS Studies on rats, human in-vivo, and in-vitro

Study	Subject (Type, condition)	Pattern (Pulse type, dose)	Outcome
Daniela C. I. Carvalho and Alberto Cliquet, 2004 (78)	Rat, osteopenic	200 us burst, 1.5 MHz repeating at 1kHz (20 min/session per day, 20 day period)	Positive effect
Shuxin Sun et. al., 2020 (77)	Rat, ovariectomized, osteoporosis	1.5 MHz repeating at 1kHz (20 min/session per day)	Partial reduction in bone mass reduction
C. M. Korstjens et. al., 2008 (75)	In-Vitro (cartilage tissue)	1.5 MHz (20 min/session per day, 6 days)	Positive effect
T K Kristiansen et. al., 1997 (72)	Human in-vivo, fracture	200 us, 1.5MHz repeating at 1kHz (20 min/session per day)	Positive effect
Dieter Gebauer et. al., 2005 (79)	Human in-vivo, fracture non-union	200 us burst, 1.5MHz sine wave repeating at 1kHz (20 min/session per day)	Positive effect
S J Warden et. al., 2001 (66)	Human in-vivo, SCI osteoporosis	10 us burst, 1MHz sine wave repeating at 3.3kHz (20 min/day, 5 days/week, 6 week period)	No positive effect detected

As LIPUS is an ongoing area of research, this table is intended to highlight the various applications of LIPUS research on animal models, in-vitro models, and in humans, as well as the potential avenues for therapy this technology might provide.

Prior to this project, nanokicking had not been established as a treatment for osteoporosis; however, should it be developed as a potential treatment, it would be considered a therapeutic vibration similar in concept to LIPUS, however at notably lower frequencies compared to ultrasound delivered continuously, and at lower amplitudes compared to WBV, as performed in in-vitro studies described in more detail in section 2.8.

2.6 Bone Cell Stimulation

In regenerative medicine, using stem cells to reconstruct or differentiate cells into an osteogenic lineage is a major area in the field. Studies performed on osteogenesis in-vitro are performed for a variety of reasons including the study of degenerative diseases such as osteoporosis, to increase understanding of bone development, and potentially provide an alternative to a reliance on donor bone cells.

One avenue for causing osteogenic differentiation of stem cells is by stimulating the cells using a variety of techniques such as electrical fields (80; 81), ultrasound, and mechanical forces (82; 83).

Mechanical systems to stimulate the bone often involve a simulation of the bone loading mechanisms in-vivo. These systems may use bioreactors to apply a stress

on a seeded scaffold (80), deliver strain via stretching (84; 85), bending (86) and using perfusion mechanisms (87).

Using ultrasound, osteogenesis can also be stimulated, and ultrasound has been reported to improve bone regeneration, establishing the use of vibration conceptually as a means to promote osteogenesis as shown in Table 1.

This section will approach a variety of cell stimulation approaches aimed at promoting bone growth.

2.7 Mechanical Stem Cell Stimulation

Given that understanding the relationship between mechanical demands and bone development has been established since Wolff's law, work has been done to relate the behaviour of bone to the behaviour of individual cells as a response to their environment (88; 89). The goal of this research is to better understand how mechanical forces can affect cell behaviour, and so the experiments to provoke a response from bone moved in-vitro to focus on the response mesenchymal stem cells have to various mechanical stimuli.

Stem cell differentiation is shown to occur after mechanical stimulation (90; 89), showing differentiation towards tissue lineages including bone, cartilage, tendons, muscle, and adipose tissue. Studies focussing on osteogenic cell differentiation look at mechanical stimulation as a way of engineering bone tissue or promoting bone growth. Fundamentally, all mechanical stimulation shares the commonality of applying stress in some form to a target cell.

Stress can be applied in a variety of ways. Tensile stress can be applied to two-dimensional cell models by applying the cells on an elastic substrate and stretching

the substrate, causing the cells adhering to the substrate to become strained (101; 102). If the cells are seeded into a three-dimensional scaffold, the scaffold can have stresses applied to it in a multitude of ways (82; 84; 93).

Studies involving the application of hydrostatic compression have been performed to provide stress in order to stimulate cells. This is done by generating pressure by compressing gas within a closed culture chamber. This can be done either intermittently or continuously (88). In-vitro, experiments involving mechanical loading have been carried out to promote osteogenic differentiation. Such experiments involved 3-dimensional models. These showed an increase in alkaline phosphatase activity, bone-specific protein transcript levels (alkaline phosphatase and osteopontin) and mineralised matrix production which is evidence of bone cell reproduction.

Others involved stretching cells subject to cyclical stress-strains (85; 84), showing an effect of strain on prostaglandin and osteoblast proliferation. The stress can be mechanical or fluidic (93). The application of cyclical stress can be compared conceptually to vibration, as vibration through a media involves a pressure (stress) wave propagating through a media in a cyclical, or harmonic, manner.

2.8 Nanokicking & Nanovibration

It is well established that cells respond to their environment through chemical signalling as well as mechanical stimulation. These responses can include changes to cell adhesion, gene expression, migration and morphology. Studies have shown cells respond differently to a variety of surface topologies and recent studies

indicate that mechanical forces have the capacity to generate biological responses (94; 95; 96).

Mesenchymal stem cells are multipotent cells possessing the capacity to differentiate into bone, adipose, reticular, neural, and smooth muscle cells. Evidence shows that cells respond to their mechanical environment, including the surface they are situated on (97; 98), leading to exploration of other mechanical methods to promote mesenchymal stem cell differentiation.

The nanoscale interactions of the cell and its environment is of particular interest (99; 100). This led to the investigation of mechanical vibration stimulation at the nanoscale (2), which involved placing mesenchymal cell cultures on a bioreactor designed to vibrate the culture plates at frequencies between 1 and 1000 Hz, imparting a nanoscale mechano-transductive stimuli to the cells and observing their differentiation into osteoblasts. A simplified diagram of a bioreactor is shown below.

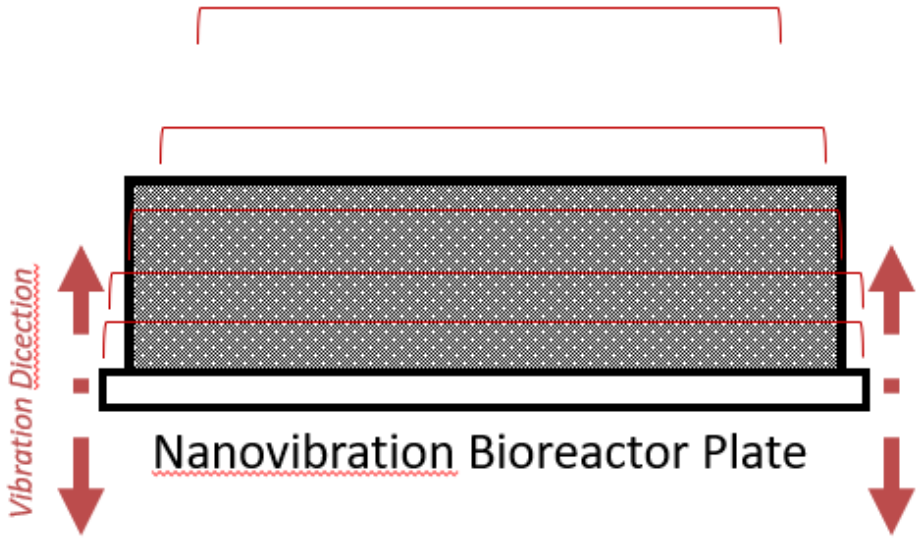

Figure 8: Representation of bioreactor plate transmitting vibration to cell stack

In-vitro, multiple frequencies near 1000 Hz have subsequently been further explored, with frequencies ranging from 150 Hz to 5000 Hz. These vibrations were delivered using bioreactors consisting of a metal plate actuated by an array of piezoelectric transducers, capable of vibrating culture plates attached magnetically to the surface of the bioreactor (13; 4; 3). The vibration is transmitted to the cells uniformly, imparting an acceleration to the individual cells. This acceleration will cause deformations, internal stresses based on the amplitude of vibration delivered. The amplitudes ranged between 5 nm and 40 nm depending on frequency and the average displacement investigated was approximately 30 nm at 1000 Hz used to stimulate osteoblastogenesis.

This technique, dubbed ‘nanokicking’ to refer to nanovibration at low frequencies (also called nanovibration in this thesis) as a means to promote osteoblastogenesis is considered a valuable avenue for further research as it has the potential to be

used in either up-scaled cell growth protocols with the aim of growing osteoblasts to produce bone material or explored in-vivo to determine whether the technique could be applied directly to the mesenchymal stem cells present in bone marrow and adipose tissue as a potential therapeutic intervention.

In-vitro, the cells are vibrated continuously in batches using bioreactors involving a vibrating plate driven by a series of piezoelectric transducers that deliver the nanoscale mechanotransduction to the cells (2; 13). This has the benefit of avoiding using chemicals with potential off-target effects by limiting the stimulus to mechanical activity alone.

Nanovibration is the technique that is proposed for in-vivo use in this thesis. Based on the studies done by Roberston et. al., a frequency of 1000 Hz and a vibration amplitude of 30 nm was targeted for this study based on the positive results observed indicative of osteoblastogenesis. At the stage at which this project was proposed, no in-vivo studies had been performed. Establishing dosages of nanovibration to deliver is based therefore on vibration amplitude that shows promising osteoblastogenic indications in-vitro. Not specified by the in-vitro experimentation at this stage of research was the duration of vibration required in-vivo; these durations would be specified based on practical limitations in subsequent preliminary investigations.

The project therefore relies on the research provided up to the point of the project launching in order to explore the application of the in-vitro technique in-vivo. The goal of this project is to design and investigate the application of nanovibration in-vivo for the target population and comment on its feasibility. This investigation is

based on a challenge and an assumption; the challenge being that the vibrations transmitted via bioreactor to cells in-vitro can be delivered successfully to in live, large bones following vibrational transmission through soft-tissue, cortical and trabecular bone regions, and other connective tissues and the assumption that cells in-vivo will exhibit the same response as in-vitro. It is currently not definitively known what vibration amplitudes may lead to a positive effect on bone health in-vivo using this technique, however from the existent literature it is hypothesized that given the amplitude delivered to mesenchymal stem cells, that comparable vibration amplitudes are sensible as an initial target. This project therefore takes a first step towards demonstrating whether these assumptions are applicable. At the time of beginning this project, a combination of amplitudes between 5 – 40 nm and frequencies of 1000 Hz were considered the most relevant characteristics based on in-vitro work cited above. As the in-vitro work had no limitations on session duration, the duration of the sessions done as part of this work were determined by practical limitations and ergonomical restrictions.

In summary:

- Treatments that exist for osteoporosis can be described primarily as pharmacological, physical, or involving therapeutic vibration.
- Limitations to both pharmacological and physical therapies are known at this stage, and whilst in-vivo experiments using therapeutic vibration are ongoing, they appear promising in many cases.
- Nanokicking has been shown to promote bone-forming cell growth in vitro repeatably; however its use in-vivo remains unexplored and limitations

regarding whether positive effects can be observed within practical durations, or at all, must be demonstrated.

3 Materials and Methods

3.1 Biological Samples & Tissue Phantoms

3.1.1 Biological Samples

Biological samples were used for testing and characterisation of vibration in an organic medium similar to that which would be used with the device in the preliminary clinical evaluation and animal trials. Bones were used due to the complexity of the trabecular structure that would present a challenge to reproduce using synthetic materials (101; 102), existing examples and studies of which require the utilisation of complex mixtures of materials or equipment not readily available for use in this project. Bones of two types were used throughout the course of the project; bones of rat origin, and bovine femurs sourced from cows.

Rat bones were initially used both due to availability and the use of rats in the animal trials associated with this project and were used to help design the wearable prototype device used in the animal trials. Rat bones were delivered to the University of Strathclyde from the University of Glasgow. They originated from Sprague-Dewy rats that were culled following experiments and frozen at -20°C. The effects of freeze-thaw cycles on the decrease of biomechanical properties such as stiffness and strength of biological tissues are not significant (103, 104), however both rat and bovine bones were delivered frozen and were kept frozen until use and underwent a single freeze cycle to reduce any degradation to their structure and properties due to repeated freezing and thawing as much as was practicable.

Bovine femur samples were used as a substitute for human bones due to their availability and size. As the femur used was a large weight-bearing bone, these

were used to characterise in greater detail the vibration amplitudes present within the target region through its cross-section. Additionally, due to the increased size of the bovine femurs, this made it easier to measure a greater number of measurement points using the tools available.

Limitations for both sources of biological samples (rat and bovine) are various; whilst the structure and regions within the bone are qualitatively similar (overall, all bones possess a diaphysis, epiphysis, cortical and trabecular regions, and are surrounded by various soft-tissue types such as cartilage, skin, and muscle when not de-fleshed) the size and mechanical properties of animal bones are expected to vary compared to human bones. Rat bones were therefore used purely as a means to provide initial confidence for the animal studies prior to performing the experiment proper, and bovine samples are expected to require higher driving amplitudes compared to for human limbs due to the differences in mass and size. It is also noteworthy that the bovine samples provided were sourced from healthy animals and would not exhibit signs of osteoporosis. These limitations are accepted as part of the study and are intended to be reviewed alongside the other results taken from investigations and preliminary evaluations on human participants in order to provide an overall thorough assessment of the device performance.

Bovine femurs were sourced from the John Scott Abattoir partially de-fleshed. The bovine femurs were frozen at -20°C upon delivery at the University of Strathclyde.

3.1.2 Synthetic Gels

Synthetic phantom gels were used in addition to bone samples to mimic soft tissue (muscles, fat) in experiments detailed later in this chapter. Two synthetic gel types were used; the #0 and #3 phantom gels sourced from Humimic Medical, LLC (8EX21). The #0 is a stiffer gel designed to simulate muscle stiffness, whereas #3 is designed to simulate softer tissues such as fat. The properties of these gels are described in the following table below based on values from Humimic Medical's website:

Table 2: Synthetic Gel Materials Property Table (Humimic.com)

Gel Type	Young's Modulus (MPa)	Density (Kg/m^3)	Speed of Sound (m/s)
#0	0.57	880.38	1449.30
#3	0.19	981.63	1458.85

Comparing the advertised stiffness of #0 Gel compares it approximately to muscle tissue which is stated by (105) to range between 0.46 and 0.54 MPa (103). At low loads (which is appropriate for low-amplitude nanovibrations) adipose tissue is reported to vary greatly, but as reported by Pirnat (106) ranges from negligeable stiffnesses for the purpose of this work to up to 35 kPa; whilst this is far below the Young's Modulus advertised by the #3 type gel, this is partially accounted for by using thicknesses of gel in excess of what is found at target regions, and serves nonetheless as a means to quantify qualitatively the effect of different tissue stiffnesses on nanovibration transmission.

Both synthetic gels were workable and able to be formed as suited the practical requirements of the study. The gel can be moulded and re-moulded as needed to suit various shapes and sizes.

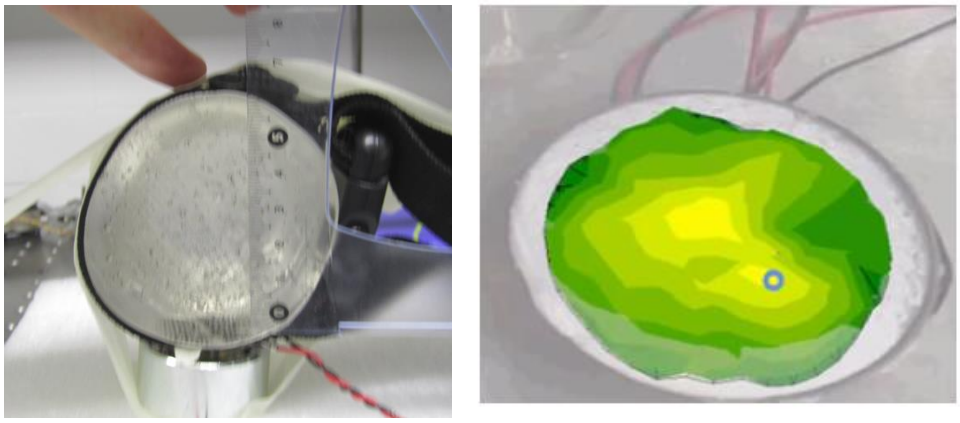

Figure 9: Gel Cylinder with diameter of approx. 6 cm (left) and 6 cm diameter gel moulded to 19 mm thick disc as used during SLI testing (right)

The synthetic gels were cut into small pieces and placed into cylindrical silicone moulds 6 cm in diameter. They were then heated at 123°C for 4 hours until all bubbles were removed. The gel was then allowed to cool for at least 12 hours. In some instances, the gels were then further cut to shape using a scalpel. The gel cylinders were made in a variety of thicknesses; 6mm, 11mm, 15mm, and 19mm. Due to the soft nature of the synthetic tissues and due to difficulties assuring that cuts would be clean and result in consistent thicknesses, instead the samples were poured by weight of the synthetic gel in the moulds and were measured after cooling. This method yielded more consistent thicknesses for the experiments performed within +/- 1 mm.

When applying synthetic gels alongside other samples, typically bovine bone samples, ultrasound gel would be used to improve transmission and contact between the synthetic gel and the bone, particularly in cases of uneven surfaces.

3.2 Electronics Design

An overview of the electronics designed and manufactured by Dr Paul Campsie, at the time a research associate at the Department of Biomedical Engineering at the University of Strathclyde, is given in this section and applies to the prototype devices used in both the animal trials and the preliminary clinical evaluation.

The overall function of the electronics in this project is to supply voltage to the transducer elements used to transmit nanovibration to the target region of bone for both studies, as well as amplify and treat the signal provided by the accelerometers used to measure and provide visual feedback for the studies.

A diagram describing the basic functionality of the electronics for both studies is shown below in Figure 4.

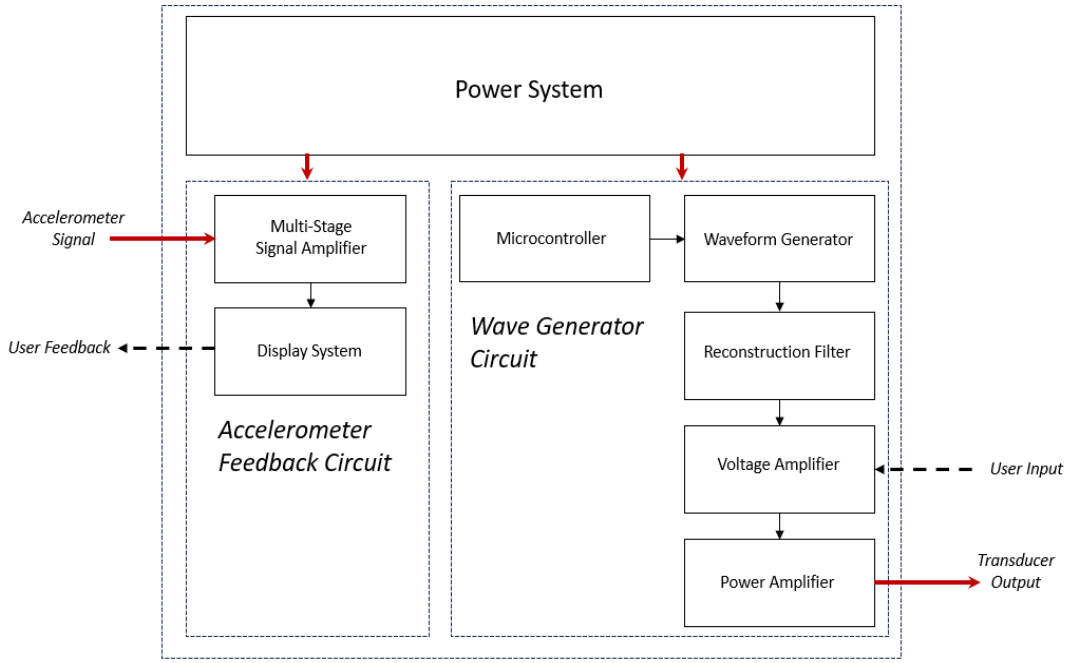

Figure 10: Diagram of the electronics system used in the devices. Shows relation between various components.

The overall electronics design is the same for the device designed for the investigations at the University of Strathclyde, the preliminary clinical evaluations, and the devices used for the animal trials.

The electronics can be divided into the following basic systems.

- Power system
- Wave Generator Circuit, used to generate the nanovibration
- Multi-Stage Signal amplifier, used to amplify the vibration measured by the accelerometer during use
- Display system
- User interface.

The electronics were required to produce a sinusoidal voltage that would then be amplified to power the bone conduction transducer to emit a sinusoidal vibration

within a controlled range. In addition, the device had to pick up the voltage signal from the accelerometer, amplify the voltage, and then allow for this signal to be either displayed or stored. The required functions were achieved by including a wave generator circuit and an accelerometer amplifier circuit, the components of which are described in Appendix 2, as well as an image of the circuit taken for illustrative purposes.

This amplification stage can be manipulated by the user via a potentiometer knob. This gain can be controlled during use of the device by adjusting the potentiometer via a mechanical knob; this knob is part of the user interface of the electronics box. The accelerometer used to detect the vibration utilises an inertial mass on a piezoelectric polymer film to generate a voltage when an acceleration is detected. Due to the nanoscale displacements being measured resulting in very small accelerations that only generate small voltages, an amplification process was used to boost the voltage generated by the accelerometer as part of the amplifier section of the electronics system. This was subdivided into several stages, described in Appendix 2. Once amplified, the electronics system for the preliminary clinical evaluation and the animal trial diverged.

In addition, due to minor variations between each accelerometer, at the ranges of acceleration the accelerometers were subject to, each accelerometer used would be individually calibrated by laser interferometer.

This was done by affixing the accelerometer to a vibrating plate, which would vibrate at 1000 Hz (the vibration frequency accelerometers were to be used at). The laser interferometer would record the vibration amplitude on the top of the

accelerometer for each interval, and the output Peak-Peak (PP) voltage was recorded. This enabled a plot of vibration amplitude vs. PP amplitude to be drawn up per accelerometer. Linearity between accelerometer PP output and vibration amplitude can be established visually, and a linear formula was determined using a best-fit function; as, logically, the intercept between vibration amplitude and PP amplitude was set to be 0 (as under perfect conditions without noise, an absence of vibration would result in an absence of voltage output by the accelerometer), however, due to a noise floor present at low amplitudes, this results in higher errors at amplitudes below 1 nm. For the accelerometers used during investigations involving the wearable device on human participants, Sum of Squared Errors (SSE) for each accelerometer was 0.22 and 0.62; excluding vibration amplitudes under 1 nm reduces SSE per accelerometer to 0.10 and 0.40 respectively. An example calibration plot is given below for an accelerometer used in the Preliminary Clinical Evaluation.

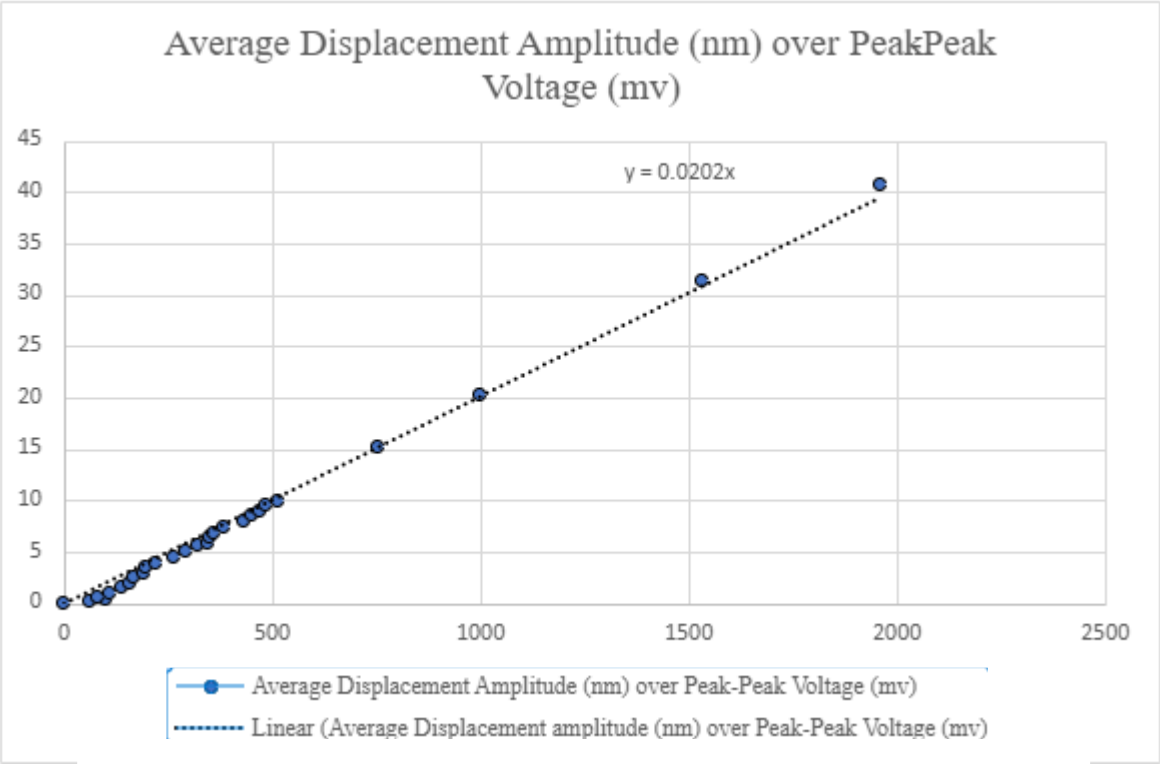

Figure 11: Example calibration plot for an ACH-01 Accelerometer (Accelerometer 1).

This allows for vibration measurements using accelerometers to be done with confidence of accuracy within the requirements of the project, and acknowledges limitations in measurements below 1 nm; this also provides a lower limit for what can be considered measurable vibration using accelerometery.

During use, the signal generated by the accelerometer would undergo some processing; the stages involved are described below. In summary, the analogue sine wave would be converted to a DC signal using the stages described and for the preliminary clinical evaluation a 1 kHz frequency filtered out using default bandpass filters available on the Arduino Nano microcontroller (Arduino, Massachusetts, USA). Further filtering was not found necessary. For the animal trials, a more advanced data acquisition unit was able to perform FFT to the signal

in real-time during the study as for the animal trials, simultaneous live readings were possible and desirable in order to allow the operator to make adjustments during the trial if needed in response to animal behaviour.

In the case of the device used in the preliminary clinical evaluation, it was necessary to store a record of the measured vibration signal on the device, so that the vibration results could be collected and analysed following the evaluation, as it was not practical for researchers or clinicians to be present during every vibration session and to allow the participant to operate the device themselves without needing additional training to interpret, record, or store the results themselves.

Code on the Arduino applies the calibration equation to the measured direct current (DC) voltage to convert it into displacement amplitude then saves the displacement amplitude data in a text file on a micro-secure digital (SD) card. The micro-SD card reader was purchased as a standalone printed circuit board (PCB) (Adafruit Industries, New York, USA). This was to retrieve data stored on the device throughout the experiment for analysis without interrupting the experiment.

The user interface for the electronics system used in the preliminary clinical evaluation was also specific to that device. Based on the amplitude read, the Arduino was programmed to assess whether the amplitude detected was within an acceptable range and would light either a red light-emitting diode (LED) or a green light-emitting diode (LED), present on the outside of the box, depending on this amplitude. If the displacement amplitude was recorded as being between 1.5 nm

and 40 nm, the green LED would be lit, and if the amplitude was outside this range, it would be red.

These values were selected based on early vibration measurements taken on bovine samples, where a vibration was delivered to a bovine femoral head and the vibration on the opposing side of the femoral head was measured via scanning laser interferometer (SLI). Whilst these measurements were be examined in more detail in follow-up experiments on bovine samples after the conclusion of the preliminary clinical evaluation, the lower limit of 1.5 nm was selected to give confidence that a detectable nanovibration was present inside the bone should that vibration amplitude be detectable on the far side. The results for the initial bovine measurements is provided in section 4.4.1.

During the use of the device, this would provide visual feedback to the user of the device. If the light was red, this prompted the user to adjust the amplitude of the device by manipulating the gain knob or by adjusting the position of the device on the knee in order to return the measured amplitude to within the acceptable nanovibration amplitude range indicated by the appearance of the green light.

For the animal trials, it was preferable to have the researcher present at the animal trials observe the data live as it was being recorded in order to allow small adjustments of the experiment in response to animal motion and in response to this visual feedback.

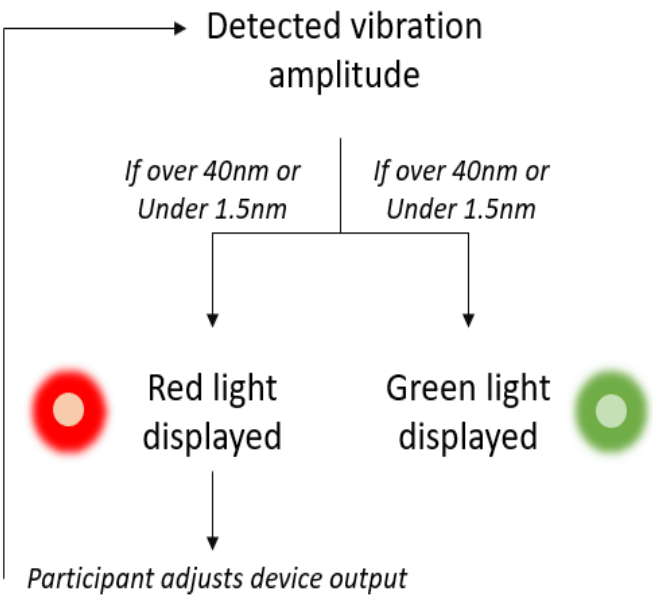

Figure 12: Diagram of the feedback loop for displaying the green or red lights in response to measured vibration amplitude

For the purposes of data acquisition, an A37 OP-AMP was used. The amplified signal was sent to a Cambridge Electronic Design (CED) Micro 1401 data acquisition unit (CED Limited, Cambridge, UK) connected to a personal computer (PC) where all the raw data of the measurement session was recorded by Spike2 software (associated with CED Limited hardware). Depending on the level of vibration measured, the program may also indicate whether an adjustment to the transducer output needed to be performed; if the amplitude was below 10 nm or above 40 nm, a red light was displayed. Between 10 and 40 nm, a green light was displayed.

The circuitry was battery powered using a rechargeable phone charger (Jonkuu, Shenzen, China) with an output of 5 V DC and with a charge of 10000 mAH. The voltage from this source was adjusted to the appropriate levels using boost converters, DC-DC converters, or linear regulators.

The transducer and accelerometers were housed in bespoke 3D printed parts; the design considerations for these housings are detailed in the following sections. The remainder of the electronics was housed in a plain electronics box modified to allow for the power-socket and user interface components.

3.3 CAD and Prototype Manufacture Techniques

In order to manufacture prototype devices throughout the project for investigations at the University of Strathclyde, the preliminary clinical evaluation, animal trials, and wave characterisation experiments as described in later sections, rapid prototyping techniques were employed with particular emphasis on 3D printing. The methods and means of 3D printing were common to many aspects of the project, and are described in this section.

Prototypes were manufactured in-house by rapid prototyping facilities in the University of Strathclyde. 3D printing was used to rapidly manufacture various iterations of prototype devices. This allowed for various pitches to expert consultants at the Scottish Centre for Innovation in Spinal Cord Injury (SCISCI) at the Queen Elizabeth University Hospital, Glasgow and expert researchers at the University of Glasgow (for the preliminary clinical evaluation and animal trials respectively) and potentially alter components quickly to suit specific participants if needed. This flexibility and ability to quickly redesign components in response to suggestions and discoveries from the work done was beneficial for the fast-moving requirements of the project (107).

The 3D printer used for the functional prototypes was an FDM printer (Makerbot Ultimaker 2+ Extended, MakerBot, New York City, USA), which is a Fused

Deposition Modelling (FMD) 3D printer. This means that it applies layers of heated polymer filaments on top of one another in order to create the desired shape of the printed part.

Very early prototype devices were made using a digital light projection printer (EnvisionTec Desktop XL, EnvisionTec, Dearborn, Michigan, USA), which uses digital light projection curing on a photopolymer, which is poured into a bath. This tool was not used beyond the early prototypes as the solid material it resulted in was heavier, took longer to print, and was not considered beneficial to the end result as partially hollow FDM components were considered to be better at reducing unwanted vibration from the vibrating transducers through the device (as opposed to towards the target region) by reducing density (69). Beyond the 2rd prototype, the same FDM printer was used on all prototypes.

Parts were designed in CAD software using Creo 3.0 as .prt components and assemblies and subsequently converted to .stl files in order to be printed by the Makerbot. The Makerbot printer printed the parts in polylactic acid (PLA). All parts were cleaned after printing to remove stray filaments, support material and sharp edges by hand. Layer thickness varied between 0.1 mm and 0.3 mm depending on build. Infill density varied depending on the build between 20% and 50%. These were adjusted depending on the size and shape of the individual prototypes. Prior to printing, the expected parts were previewed, showing regions of thinner walls or significant aliasing artefacts, at which point the print settings were adjusted where possible to ensure a more robust build.

For the animal trials specifically, infill was denser, ranging between 40% and 50%, as the smaller size components were believed to be more fragile and to prevent breaks a denser build was preferred; this was balanced against trying to reduce infill in order to prevent vibration from transmitting through the device to the accelerometer, thereby rendering accelerometer measurements less meaningful. In addition, during later animal trials, 3D printed parts were also sourced from SGD.com with the following settings; 0.2 mm resolution, 70% infill and also printed in PLA, as a result of COVID-19 restrictions during the project.

The printed parts were cleaned up using knives, scissors, and files to remove sharp edges that could cut or injure participants, animals, or users during use, and where necessary were filed down to handle tolerance issues with bought-in components.

3.4 Design Considerations - Preliminary Clinical Evaluation and Investigations

This section covers the techniques and materials used when designing the prototype wearable device included in the preliminary clinical evaluation and the investigations at the University of Strathclyde. At this stage of the device, the dose of nanovibration, that is to say the 5 – 40 nm vibration delivered to the target region was intended to be applied for the duration of up to 4 hours, based on previously discussed expectations of limited durations of application. At the stage at which the design began, the focus was on designing a device that could demonstrate the feasibility of delivering repeatable nanovibration to a target region over the duration of a hypothetical treatment; the degree to which attenuation of the delivered nanovibration would affect the output inside the bone was as yet unestablished. Therefore, outcomes for these investigations and tests are focussed

on achieving a measurable degree of vibration amplitude in a manner not overly affected by variation between applications. The effect of the vibration amplitude delivered to the target region, as specified in earlier sections, is examined in repeatable animal trials described in later sections.

The objective of the investigation and preliminary clinical evaluation was to design and build a wearable clinical prototype device to apply adjustable and measurable nanovibrations to a selected area of bone. The ergonomic design of the device was determined by iteratively building 3D printed models to be worn at an osteoporotic region on the lower limb in order to deliver the vibration directly to an area prone to fracture. The upper knee joint, lower knee joint, and ankle were explored as potential targets due to the trabecular bone at these regions suffering from low bone density that severely compromises the mechanical properties of the bone due to bone loss following SCI (29; 11; 12). These areas were also considered to be comparatively easy to measure using pQCT in a repeatable manner by the clinical staff, should a sufficient number of participants be recruited to the preliminary clinical evaluation to warrant bone density measurements. The duration of application was determined to be 4 hours, based on input from experts within the SCISCI at the Queen Elizabeth University Hospital and expectations based on what the maximum tolerance for wearing a device of any kind would be for patients without incurring risk of pressure sores or other discomfort.

Input from experts within the SCISCI at the Queen Elizabeth University Hospital, Glasgow informed the design process and its practical application. Following initial investigations at the University of Strathclyde, the upper knee joint was selected as the target region for the preliminary clinical evaluation, and the final

device design comprised a transducer, transducer housing, two removable arms, an accelerometer, an accelerometer housing, two knee support straps and an elasticated strap.

The iterations of the wearable device design cover the following experiments:

- Initial Investigation at the University of Strathclyde
- Secondary Investigation at the University of Strathclyde
- Preliminary Clinical Evaluation

These investigations are detailed in later sections of this thesis.

At each stage of the device development process, feedback from users and expert opinions were fed back into the design for later stages in response to challenges, additional requirements, and improvements. The overall requirements of the device are as follows:

- Deliver a consistent vibration to the target region of bone
- Measure/record a received vibration signal on the opposite side of the target bone region
- Be able to be worn by a participant comfortably

The target regions were regions of bone prone to fracture, specifically the upper knee joint (proximal femur condyle), lower knee joint (proximal tibia condyle) and ankle (distal tibia malleolus) shown in Figure 6 below. The results for the preliminary clinical evaluation are given in section 4.1.

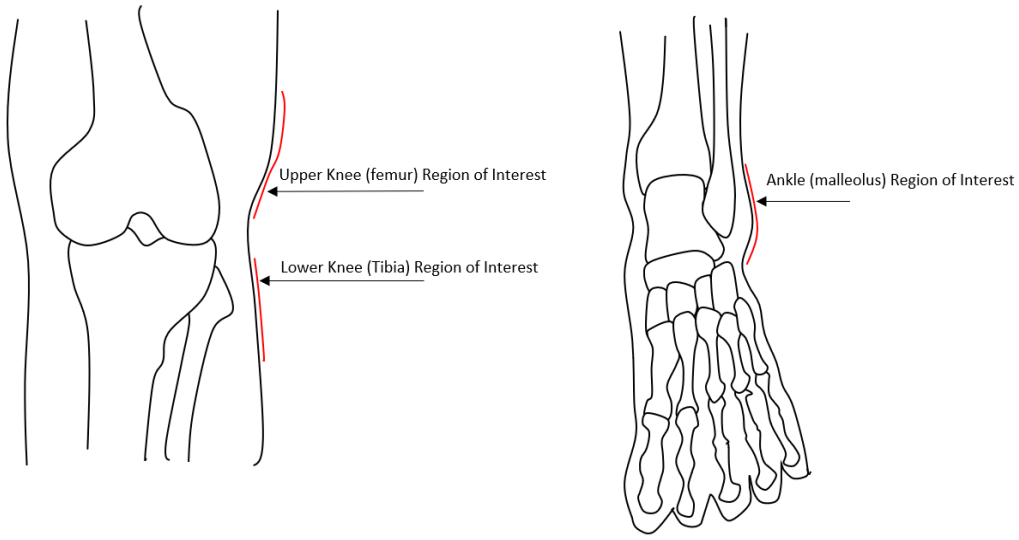

Figure 13: Diagram of the target regions on the knee joint and ankle

3.4.1 Overview of Components

The components that make up this design throughout its design and development process are as follows:

- Transducer & Transducer Housing
- Accelerometer & Accelerometer Housing
- Straps
- Modular Arms
- Wiring

3.4.1.1 Transducer

The component responsible for emitting the required vibration to the target region of bone was the transducer. The transducer used for this prototype was an LB07 large surface transducer with a transducer surface size of 44 mm diameter. A commercially available transducer with a large surface area was chosen for the initial design due to its ability to apply a vibration to a wider area of skin, spreading

the pressure and allowing for a larger surface to be vibrated. An image of this component is shown below.

Figure 14: Image of LB07 Transducer sourced from LB07 Datasheet; see Appendix 2

Due to its size and weight, owing to it being the only solid metal component of the overall design, the transducer was the most cumbersome part of the device. Distributing its weight comfortably was a priority during the design of the wearable device prototype.

The transducer's surface was placed directly on the participant's skin in order to obtain the best connection and most consistent nanovibration. In order to prevent pressure sores and discomfort due to the cold metal on skin, the participant wore a tubigrip bandage on the leg (108). This provided protection for the participants' skin. An illustration of an early device design is shown in the image below.

Figure 15: Photo of early wearable device prototype applied to the knee with hook & loop sling and elasticated strap, unpowered featuring tubigrip sock padding

To avoid having a larger component of the device take up space between the legs of a patient, the section containing the transducer was positioned on the lateral side (outside) of the joint; this would be important in instances where a patient in a wheelchair would have their knees pressed close together.

The transducer housing was made using CAD and 3D printing to hold the transducer in place and allow space for the electronics to be connected to the battery source. It needed to be robust but also thin enough to minimise size and weight. An illustration of the transducer housing is shown in Figure 16 below.

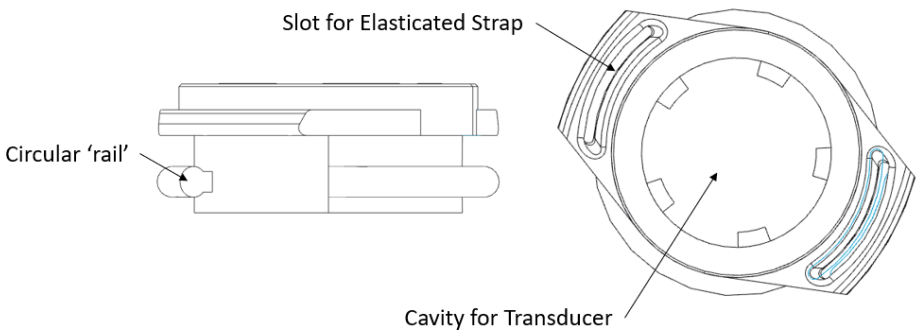

Figure 16: Representation from CAD models of transducer housing component with annotated features

3.4.1.2 Accelerometer

To assist the wearer and other clinicians in varying the output of the device to ensure a measurable output on the medial side (inside) of the joint, a separate section containing the accelerometer (described in the electronics section) was positioned on the medial side of the joint opposite the transducer.

The accelerometer measures the nanovibration transmitted to the opposite side of the leg after it has passed through the target area of bone. This reading allows the nanovibration to be adjusted to meet the parameters of the trial. An illustration is shown of the ACH-01 accelerometer from the datasheet in Figure 17 below, displaying the critical dimensions of the accelerometer by itself.

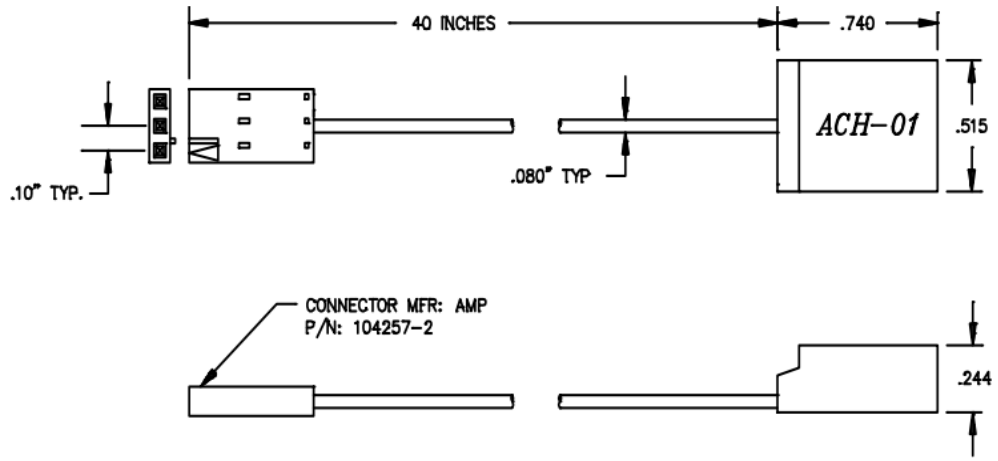

Figure 17: Diagram of ACH-01 dimensions sourced from ACH-01 datasheet, see Appendix 1. All measurements in inches.

3.4.1.3 Modular Arms

In order to minimise movement of the device on the leg and to maintain a consistent contact with the skin to allow a steady measurement of nanovibration, arms were added to the transducer housing. These arms protruded in an L shape, aligned with the direction of the upper and lower joint, and were held in place via two straps, one above and one below the joint attached to the transducer housing section. The device was held in place at the joint, whether the leg was flexed into a sitting position or extended as in a lying down position. The ability of the arms to align to the direction of the leg was achieved by making the arms capable of rotating about the centre of the transducer housing, enabling a degree of customisation and adaptability to different flexions at the knee, as shown in Figure 18 on the following page.

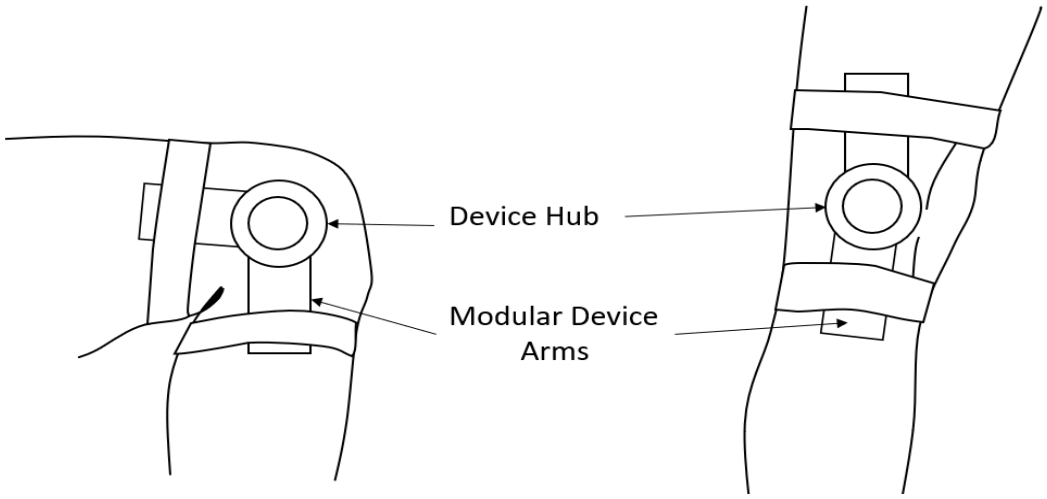

Figure 18: Diagram depicting modular arm orientation as applied to knee joint region

3.4.1.4 Straps

Both the transducer housing and accelerometer housing were held in place using straps, which served to hold both the accelerometer housing and transducer housing in place relative to one another at the target site.

The transducer and transducer housing, as the largest component of the device, required larger, less elastic straps that wrapped around the leg above and below its centre of gravity. These straps used hook & loop material and were firmly affixed to the modular arms described in the above section. Due to the modular arms' ability to rotate as described in the above section, these straps would be wrapped on either side of the joint.

In order to hold the lighter and smaller accelerometer housing in place, as well as apply a constant, gentle compressive force on the accelerometer housing and transducer housing, an elasticated strap was used. The elastic strap wrapped around the joint, and connected the accelerometer housing to the transducer housing on the opposite side of the target site.

3.4.2 Evolution of the Wearable Device Design

The design of the device changed as a result of design feedback provided by both the participants of the investigations and the researchers applying the device. The feedback provided resulted in the following changes to the device.

In early designs, a tubigrip sock bandage was included to protect the wearer from the flat metal surface of the transducer plate during use but was found to make the wearer become too hot and made wearing the device for the short investigations uncomfortable, leading to its removal. This was replaced by a layer of protective technogel padding 9 mm thick on the surfaces of the device in contact with the participant's skin. The technogel padding took over the role of protective padding material and acted as a cushion between the transducer plate and the skin.

Technogel is a material used for padding in orthotics and prosthetics. Here, it was placed on the transducer surface to act as a soft interface between the rigid surface of the transducer plate (made of stainless steel) and the target area soft tissue region on the participant. This prevented any hard edges and surfaces on the transducer from pressing into the skin. The compliant nature of the padding also enabled better contact with the skin as the technogel could conform to the irregular geometry of the joint where a rigid material could not. This padding was also added to the accelerometer surface in contact with the skin for similar reasons.

The earliest version of the device did not feature a bespoke housing for the accelerometer, this was added following the initial investigation at the University of Strathclyde to reduce the manual intervention required to position the accelerometer correctly opposite the transducer and provide protection from

potential shocks and drops during application. An illustration is shown below in Figure 19.

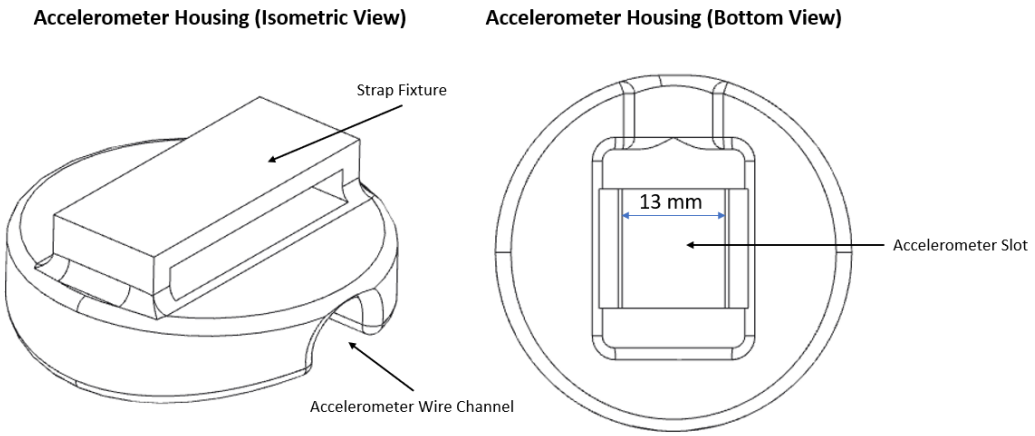

Figure 19: Representation from CAD of the accelerometer housing

The initial investigation highlighted design issues in applying the early prototype device at the distal tibia (ankle), as the device was prone to wobbling over the malleolus which caused difficulties in applying the device both reliably and comfortably. It was also noted that at the ankle the transducer surface did not appear to conform well to the ankle malleolus, resulting in only a small region of the malleolus in contact with the transducer surface.

Other design details raised were that the device straps were cumbersome to attach to the leg using the long hook-and-loop strap that would wrap over the arms of the device. A need for a dedicated accelerometer housing was established, as positioning the accelerometer by the investigator was difficult, which involved inserting the accelerometer between the leg and the bandage.

The transducer housing, accelerometer housing and modular arms were all redesigned and reprinted over the course of the project to avoid flat surfaces where

the surface of the device may come into contact with the user and provoke pressure sores if pressed against the skin, which was a priority consideration considering the duration of time the device was anticipated to be worn and the potential for mis-application by the participant in the preliminary clinical evaluation.

The arms of the wearable device were adapted to include a curved concave surface on the inside to help the Technogel padding and straps conform to the shape of the leg. Wearer-facing edges were rounded or chamfered to at least a diameter of 1mm to prevent sharp edges that could present a cutting risk during handling and wear, with large rounded surfaces being preferred where the geometry of the device allowed them to be easily implemented using FDM printing. An image of the CAD model of the device is shown in Figure 20 below to illustrate the rounding and curved surfaces as they appear on the final model.

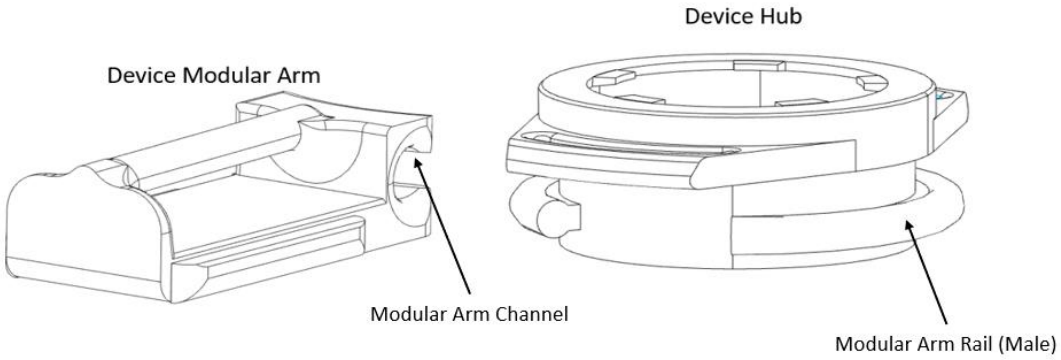

Figure 20: Representation of the transducer housing and the modular arm

The design was also amended to accommodate the device being used with the leg fully extended to allow the arms connected to each strap to be removed. This

means that in order to make additional space, one arm can be taken off the device to allow for greater comfort whilst lying down.

The rail that was used to guide the modular arm around the central hub was changed from a T-shape to a circular shape partway through the device development. This was done to further remove any right-angle edges and to provide a larger, more tactile area to assemble the modular arms onto. A comparison is shown below in Figure 21.

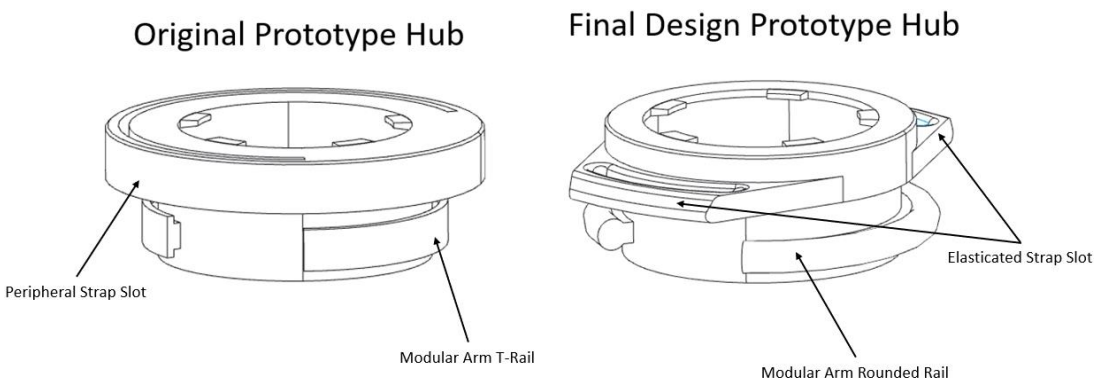

Figure 21: CAD representation of an early vs. final transducer housing design for comparison

In the initial stages of development, the person attaching the device (patient or helper) wrapped the straps around the upper and lower sections of the knee joint. The straps were fed through a slot, tightened, and then fixed in place using hook and loop material that was used to hold the strap in place throughout the duration of the vibration delivery. The elasticated strap was then wrapped around the leg and the accelerometer housing pressed gently against the opposite side of the knee joint; the position of the accelerometer housing shifted until appropriate positioning was achieved. The elasticated strap was then held in place using hook and loop material.

The intention was that as the elasticated strap would be approximately stretched to comparable amounts each application, this would standardise the compressive force applied by the strap between applications. Whilst it is still subject to variations in application from use to use, it is nonetheless more difficult to over-tighten or under-tighten compared to the bought-in straps used.

Later versions of the elasticated strap removed the need to pass the elasticated strap through a slot, and instead were directly sewn onto the transducer housing for ease of application by the participant.

The straps were originally made of hook & loop material of the sort used in medical slings, in order to minimise skin irritation and discomfort during extended use (planned for up to 4 hours per day). Medical slings are worn continuously, for long periods of time, so this material choice was considered safe as a breathable and comfortable option. These straps could be adjusted to fit different shapes and sizes by wrapping them around the leg until the hook and loop effect could secure them in place.

The hook and loop straps proved cumbersome to apply and prone to slippage over time, and were replaced by bought-in sports type straps (CAMBIVO Patella Tendon Knee Strap) after the investigations at the University of Strathclyde. These straps assisted in the application of the device and held it in place in a more secure manner for the up to 4-hour duration of each nanovibration session. Figure 22 below shows both the original strapping arrangements and the revised sport straps with the knee in the flexed position.

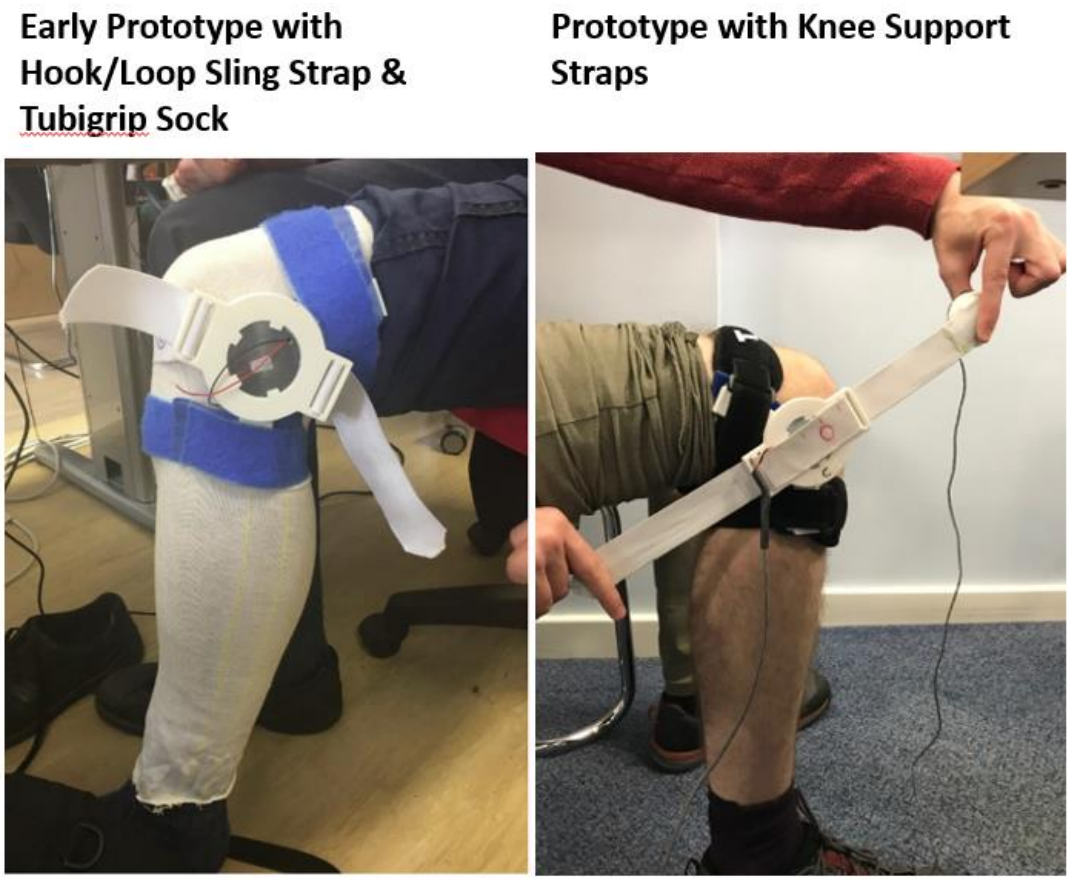

Figure 22: Photograph of the early straps used (hook & loop sling) vs. knee straps as applied to the knee region

The support straps are used on the lateral side to allow for access and to allow for adjustment during the therapy if needed. The knee support straps were not fully elasticated to provide greater support and stability to the transducer component of the device.

The combination of the new support straps and the light elasticated strap allowed for the light accelerometer component to be pressed gently into the target region on the bone, whereas the non-elastic knee support straps were better suited to supporting the heavier transducer components, prevent shifting of the device during use, and to accommodate the knee shape; this was the combination used in

the final iteration of the prototype device used in the latter part of the preliminary clinical evaluation.

The device required wiring to link the transducer and the accelerometer to the battery power source. This was achieved in the initial design by a simple soldered wiring connection. This provided power but the fixed connection was inflexible and prone to accidental damage. Due to wear on the wire and solder joint leading to damage and failures, a taller hub was designed that allowed for the use of a mono audio jack port to be installed. This meant that rather than the wire becoming damaged by frequent bending and wear, it was able to be removed and quickly replaced as well as facilitating device storage when not in use. In other regards the device was functionally identical. The upgraded hub design is shown in Figure 23 below.

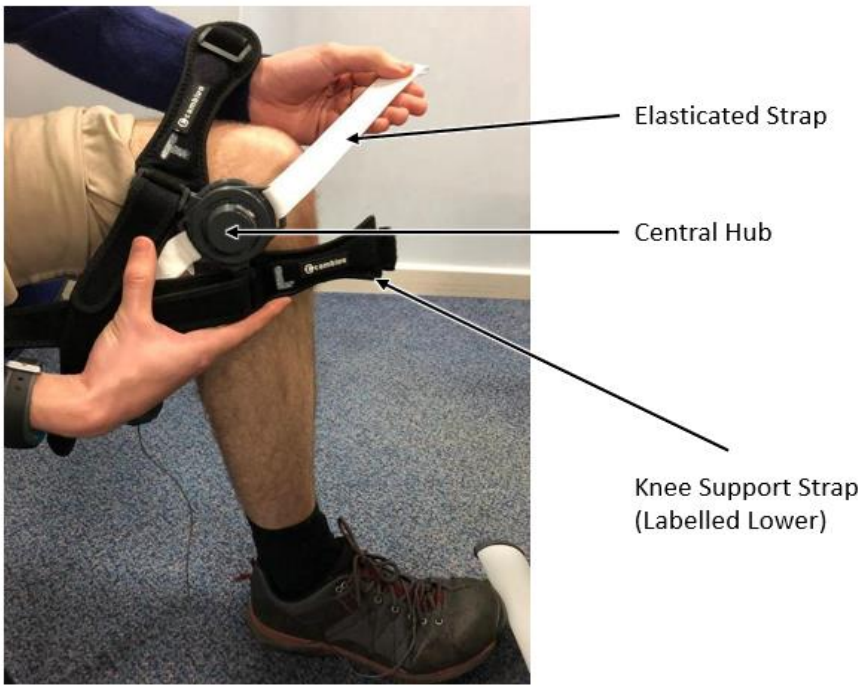

Figure 23: Wearable nanovibration prototype as used in the preliminary clinical evaluation

A user manual was provided with the device informing the participant and any other persons using the device as to the proper method of applying it (Appendix 3). The participant was also given instruction on the application of the device on receipt to ensure they were comfortable with its usage prior to the preliminary clinical evaluation. This was not required for the investigations, as a researcher would be present for those shorter sessions to apply and remove the device.

Due to the complexity of the ankle joint, specifically with variations in the position, prominence, and symmetry of the malleolus (109), which varied widely from user to user in the investigations at the University of Strathclyde, there were difficulties in making the device fit the varying shape of the ankle joint comfortably whilst applying a consistent vibration. This resulted in discounting a device designed to apply nanovibration to the ankle after the investigation phase described in section 3.6 and this was therefore not used on spinal injuries patients. Figure 24 below shows this device from both sides at the point the design process was discontinued.

Figure 24: Photo of the wearable ankle device as used during the 2nd investigation at the University of Strathclyde

In addition to difficulties in applying a consistent vibration at the ankle, the prototype ankle device was not used in order to avoid the potential development of pressure sores which was a concern throughout the design of the device.

In summary; the device underwent significant redesigns from the initial concepts proposed at the start of the project. These were:

- The design began as a single-piece 3D printed housing to a multi-component hub with two modular arms that could rotate about the central hub, enabling a greater variety of leg positions for the user.
- The location of application was determined to be the knee, with the transducer applying the vibration to the lateral side of the distal femur.
- The means of holding the device in place evolved from a hook-and-loop repurposed sling to modified knee-support straps better suited to the knee geometry and less cumbersome to apply.
- A tubigrip ‘sock’ was replaced with 9 mm technogel padding on the transducer and accelerometer in order to help prevent both overheating and the development of pressure sores during use.
- Redesigns to the hub wire to feature a jack, reducing wire wear during use.
- Use of an elastic strap distinct from the knee support straps to hold in place the accelerometer in order to enable a more repeatable application of the accelerometer against the medial knee joint.

3.5 Design Investigation at the University of Strathclyde

The design of the prototype wearable device was based on information obtained during an investigation at the University of Strathclyde, for which ethical approval

was sought and approved from the Departmental Ethics Committee (DEC). The investigation was carried out in two phases, an initial investigation and a follow up to assess the evolution of the device in order to use it as part of the clinical trials. The design investigation had three objectives:

- Measure the amplitude and consistency of transmission using the device
- Obtain feedback to improve the design of the device
- Select a target area of bone to use in the clinical investigation

The device was tested at the proximal tibia condyle (knee), distal femur condyle (knee) and distal tibia (malleolus of the ankle) areas of the leg. The three regions were assessed for amplitude and consistency of vibration by applying the early prototype of the wearable device on the lateral side of each of these target regions. The investigation did not assess the effects of nanovibration as an intervention to stimulate bone formation, but instead to compare the device fit and effective nanovibration transmission at different bony points in the lower limbs across different individuals.

The investigation recruited nine volunteer participants from the University of Strathclyde (n = 12). Potential participants were excluded if they were under 18 years of age, had a disability that prevented them from wearing the device without significant discomfort (e.g. an existing diagnosed musculoskeletal disorder such as fractures or damage to soft tissues in the lower limbs), if they had an inflammatory joint disease (e.g. rheumatoid arthritis), an implant in the knee and ankle region, an inflammatory skin condition, (e.g. dermatitis), if they were pregnant, or if they had undergone recent surgery in the lower limb.

The initial prototype used in the design investigation at the University of Strathclyde is described in section 3.4. The prototype was powered directly by a wave signal generator delivering a 20 V Peak-Peak (PP) sine voltage to generate the vibration from the transducer. In this iteration the arms were fixed in place and did not rotate about the transducer element.

During the experiment, the participant sat down and exposed their knee and ankle. The investigator located the most suitable position around the joints to apply the device by palpation. The device was then attached to the target site using a hook-and-loop splint bandage, with the vibrating element in position against the bony protrusions at each site. On the opposite side, the accelerometer was held in place against the skin surface. During the experiment the participant was required to sit still and minimise movement in the lower limb. A photograph showing the device as used in this investigation is shown in Figure 25 below:

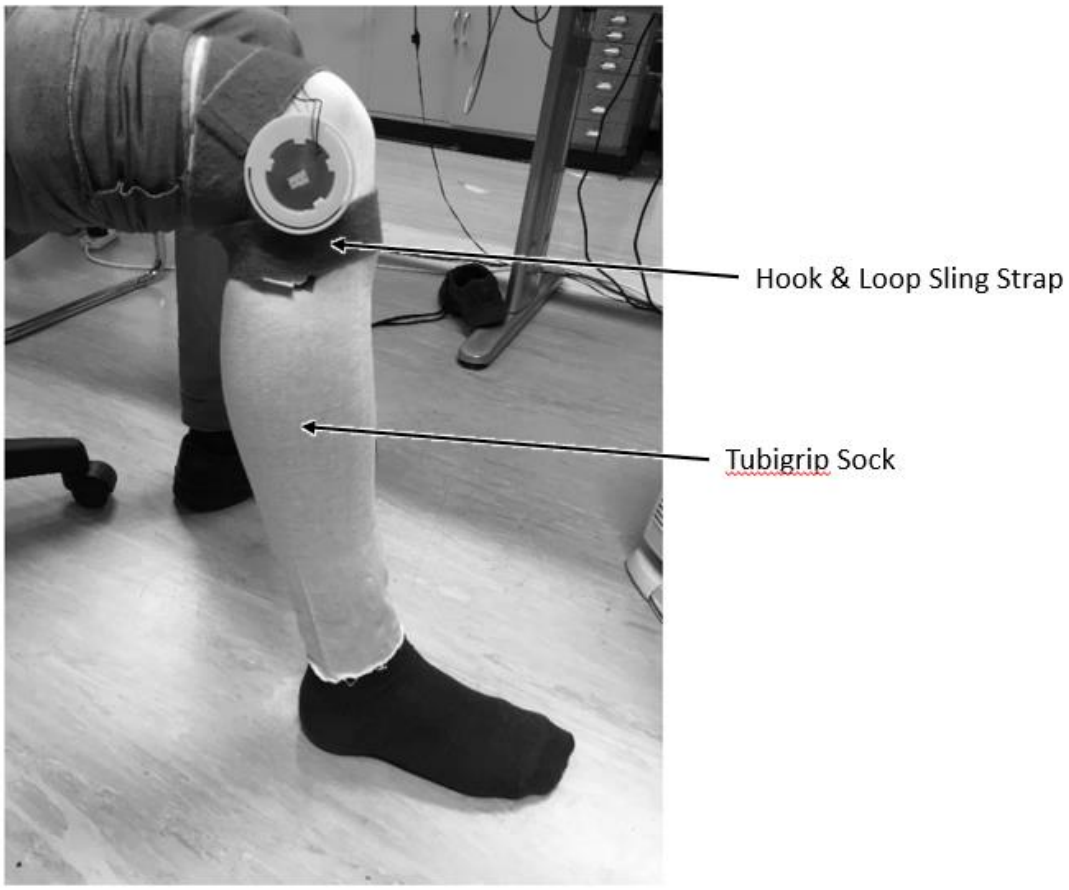

Figure 25: Wearable nanovibration device as used in the investigation at the University of Strathclyde featuring the hook & loop strap from a medical sling and tubigrip compression sock

In the above image, a compression sock (referred to as a tubigrip sock) was used to prevent direct contact with the skin by the harness during the earliest stages of prototyping, wires, or any other hard surface. This was subsequently removed due to concerns of the participant overheating and as sturdier wiring as well as more streamlined transducer housing shapes were implemented, as well as confidence in hard surfaces of the device not coming into contact with the exposed skin was reinforced.

No personal information was collected from the participants and they were each assigned a subject number. Nanovibrations were delivered for no more than 5

minutes per site of interest. The vibration amplitude at each site as measured by the accelerometer was recorded against the subject number. The investigation returned vibration amplitude results for each target region of bone as measured by the accelerometer.

Design feedback was provided by the participants and the researcher applying the device, which would inform future prototype devices used in the follow-up investigation and the clinical investigation.

The vibration amplitudes at each site were averaged in order to determine the mean vibration amplitude across the participants, and the standard deviation for each site was calculated based on the sample of average peak-peak amplitudes to gain information regarding the expected range of vibrations measurable. Normality is assumed for these measurements.

There were 12 participants in the initial investigation. The overall average at each site as well as the standard deviation and expected maximum and minimum range of vibration (95% confidence, excluding negative values assuming symmetrical normal distribution, calculated by adding and subtracting the standard deviation multiplied by 2 from the average) are shown below in Table 6 in section 4.1.1. below. The standard error was calculated by dividing the standard deviation by the square root of the count. The vibration amplitude used for this set of results was 1000 Hz.

In the instance of the lower confidence limit falling below 0, as it is not possible to have a negative amplitude, this is assumed to be 0. In parenthesis is the calculated lower confidence limit.

The means of vibration amplitude at each area were compared via two-sample t-test assuming unequal variances and using ANOVA.

After the initial investigation, there were indications that the distal tibia proved problematic regarding the variation in the size and accessibility of this area. This gave inconsistent results and required more input regarding fitting and maintaining the device in place. The results from the distal tibia were therefore regarded closely in the follow up investigation.

3.6 Follow-up Investigation at the University of Strathclyde

Following the initial investigation, a secondary investigation, for which ethical approval was sought and granted by the DEC at the University of Strathclyde, was performed in order to finalise design changes to the device. For the follow-up investigation, 9 healthy participants were recruited (n = 9), sourced from the University of Strathclyde. The same exclusion criteria as for the previous investigation in 3.5 were used.

The prototype device was applied to the same regions as for the initial investigation; at the distal femur, proximal tibia, and distal tibia in the same manner as described in section 3.5. In this investigation the device had been modified to accommodate the design feedback in the initial investigation. The accelerometer was housed in its own dedicated 3D printed compartment and was pressed against the regions of interest using an elasticated strap. At the distal tibia (ankle), a special housing was designed to better accommodate the shape of the ankle to reduce variation observed from the initial investigation in order to

improve repeatable transmission of vibration. The updated designs are shown in Figure 26 below.

Figure 26: Wearable knee & ankle nanovibration device as used in the follow-up investigation at the University of Strathclyde

No other aspect of the investigation was changed from the investigation detailed in 3.5.

The investigation returned vibration amplitudes measured by the accelerometer at the target regions. This information was used to select target regions for future studies as well as supply design feedback as provided by the participants and researcher applying the device. As for the previous investigation, means were compared first by ANOVA and then by subsequent paired t-tests assuming unequal variances. Normality is assumed for these results.

Due to the complexity of the distal tibia at the ankle joint or malleolus as discussed earlier, there were difficulties in making the device fit comfortably and with stability due to it being a bony protuberance with a wide variety of shapes and sizes, as well as difficulties maintaining contact and applying a consistent controlled level of vibration to this area of bone. This resulted in the design process for this zone of interest being discontinued and was therefore not used in the preliminary clinical investigation on SCI participants.

3.7 Preliminary Clinical Evaluation

This section describes the planned preliminary clinical evaluation. This includes a section on the participants, followed by a description of the experimental setup including the scanning protocol used and image analysis. Ethical approval for this preliminary clinical evaluation was sought and granted. Feedback relating to the design of the wearable device was incorporated into the final design used in the preliminary clinical evaluation. Clinical results were obtained by the hospital and are not able to be reproduced as part of this thesis.

3.7.1 Participants

Participants were recruited as volunteers anonymously from the Queen Elizabeth National Spinal Injuries Unit (Southern General Hospital, Glasgow, UK). Potential participants, to be eligible, had motor-complete SCI at neurological levels C4 and below (grades A or B on the American Spinal Injuries Association Impairment Scale (ASIA). Participants were excluded from the evaluation if they were below 16 years of age, dependent on ventilators at 5 weeks post-injury, had suffered recent (within the previous 10 years) concurrent bilateral fractures in bone to be scanned, were unable to provide informed consent, or were undergoing a

previous diagnosis and/or treatment for osteoporosis. Candidates who agreed to take part in the preliminary clinical evaluation provided informed consent prior to participation, and ethical approval for the study was obtained from the NHS Greater Glasgow and Clyde.

Candidates participating in the evaluation were either paraplegic or tetraplegic. Following their injury, BMD readings were taken at target sites on the leg in order to assess if the candidate could be characterised as having rapid bone loss (11; 12) in the lower limbs. If this was the case, the candidate would be eligible to take part in the evaluation as a participant. Candidates could drop out during the evaluation if they requested to do so or if the evaluation was causing harm to them. Participants were not referred to by name and personal details regarding the participants were not shared.

Over the course of the Preliminary Clinical Evaluation, whilst exact participation rates would be dependent on participant availability, it was assumed that a small number of participants of up to 6 might be made available, subject to the nature of the bone loss they experienced, whether they were willing and able to participate, and whether they were able to successfully complete the study.

If sufficient participants were recruited, bone density analysis techniques would be used to assess any effect from the device. Scans were to be performed using a peripheral Quantitative Computer Tomography (pQCT) scan (XCT 3000, Stratec Medizintechnik, Pforzheim, Germany) and carried out by a single operator within 5 weeks post-injury, and repeated at 4, 8, and 12 months post-injury, which informed the duration of the preliminary clinical evaluation.

Unfortunately, due to low turn-out limited to two participants, only one of which completed the experiment, the preliminary clinical evaluation was unable to draw significant conclusions regarding the nanovibration's effect on BMD. The outcomes of this study were therefore used only to assess the viability of the method of application and overall usability, not contribute to the assessment of any kind of effect on BMD.

3.7.2 Experimental Setup

The setup for the preliminary clinical evaluation was informed by the results from the Investigation at the University of Strathclyde and the Follow-up Investigation at the University of Strathclyde detailed in sections 3.5 and 3.6. From those investigations it was observed that in terms of achieving a repeatable and consistent measurement between participants, targeting the proximal tibia and distal femur (i.e., the knee joint) was preferable to targeting the ankle; whilst the ankle achieved much higher amplitudes depending on the method of application of the device, the inconsistency and difficulty of application rendered it unsuitable as a target region for participants with reduced mobility. Therefore, the ankle was not considered as a target site for the preliminary clinical evaluation. Of the two knee joint target sites, the distal femur was selected due to a combination of ease of application (the distal femur is easier to reach for a sitting participant compared to the proximal tibia) and displaying higher vibration amplitudes during the Investigations (as described in sections 4.1.1 and 4.1.2), allowing for easier application at the target vibration amplitude.

Upon beginning the evaluation the participant was required to wear the device for a number of sessions lasting up to 4 hours per session. The participant began

wearing the device for 15 minutes in the initial session to help get used to the device, then 30 minutes for the second session, then 60 minutes for the third, then 90 minutes, then 120, until the session duration would reach 4 hours. 4 hour was selected as an anticipated maximum session duration that participants would be comfortable performing, however in practice it was not feasible for the participant to wear the device for the full duration of the 4 hour session.

The participant was instructed to complete a log including the duration of the session and any notes associated with the session, such as forgetting to record the session, or if the session had to be abandoned partway through, in order to provide additional feedback to the conductors of the evaluation. When reporting the session duration, the completed sessions are included in the tables provided in section 4.1.4, with gaps included in Figure 40 (both planned over the week-end as well as impromptu due to participant availability).

The device was worn on the right leg, with the transducer plate resting on the distal femur on the lateral side. The left leg was not subject to vibration, serving as a control. After the completion of the experiment, both legs would be scanned for BMD in order to assess any changes caused by the vibration sessions.

During the first session the participant was given instruction on how to operate the device to ensure that the participant was able to apply the device safely by themselves. The participant was able to contact the conductors of the evaluation in case of the device failing, becoming damaged, or other concerns. Additionally, the participant was given a manual detailing the use of the device (see Appendix 3).

The accelerometer recorded the vibration amplitudes during each session. The participant was instructed to maintain the vibration amplitude above 1 nm and below 3 nm and was given instruction on how to either adjust the positioning or tightness of the device or adjust the output voltage of the wave generator box issued with the device. In addition to the recorded amplitudes logged by the accelerometer.

The device used is described in section 3.4. When the participant pressed a button on the electronics box, the accelerometer logged the vibration amplitude recorded, and allowed the conductors of the experiment to plot vibration amplitudes over the duration of the session, assess how much the vibration amplitude might vary throughout a session, and determine the average vibration amplitude per session. In summary, the preliminary clinical evaluation returned a log of the vibration amplitude during each session, the session duration, the dates for each session, and feedback from participants regarding the device and is described in section 4.1.4.

3.8 Design of the of Animal Trial Prototypes

This section covers the design of the animal trial prototype device used to deliver nanovibration to the hindlimb long bones of lightly restrained paralysed rats. The nanovibration delivered was for this device intended to be not only measurable and repeatable, but of the same amplitude and frequency as for the intended dose (that is to say, 1000 Hz frequency vibration delivered to the bone at an amplitude of at minimum 30 nm and at maximum 100 nm) for the same duration as applied during the investigations involving human participants (up to 4 hours).

A prototype device was designed for use in animal trials which aimed to investigate the use of nanovibration as specified above specifically to investigate the effect of the dose as a means to induce a positive effect on BMD following SCI for the prevention/reversal of bone loss following complete spinal cord transection in rats. The animal trials were conducted by Prof. John Riddell and Dr Jonathan Williams and are described in section 3.9.

The design of the device was informed by discussions with Prof. John Riddell and Dr. Jonathan Williams for use in a preclinical study. The final design was the result of many iterations, which were initially optimised on rat cadavers, before further optimisation and validation in both naïve and spinal cord injured rats. The intervention to test the efficacy of nanovibration against spinal cord injury-induced osteoporosis was not started until the design optimisation was complete as well as characterisation of the transducers (see section 3.8.1.1).

The requirements of the animal trial device are as follows:

- Deliver a consistent vibration at the target region of the animal leg.
- Display the measured vibration to the investigator and record data.
- Prevent undue irritation to the animals during the study.

3.8.1 Overview of Components

The components that make up this design throughout its design and development process are as follows:

- Transducer
- Accelerometer
- Animal harness prototype
- Straps
- Wiring

3.8.1.1 Transducer

The bone conduction transducers used in the animal trials needed to be as small as realistically possible whilst delivering a required level of vibration to the target region of the animal hindlimb. This was achieved by sourcing significantly smaller transducers than those used in the human wearable device. The transducer used was an Adafruit bone conductor transducer (Adafruit, New York City). An image of the smaller transducer (sourced from Adafruit) prior to assembly in the 3D printed housings, is shown below. These transducers were sourced due to their availability and their reduced size.

The dimensions of this transducer were 21.5 mm long; a limiting factor of the design was that the length of the transducer needed to be smaller in length than a rat hindlimb bone. Due to their small size, they were considerably more delicate

and required to be carefully mounted within the 3D printed parts. An image of the transducer is shown in Figure 27 below:

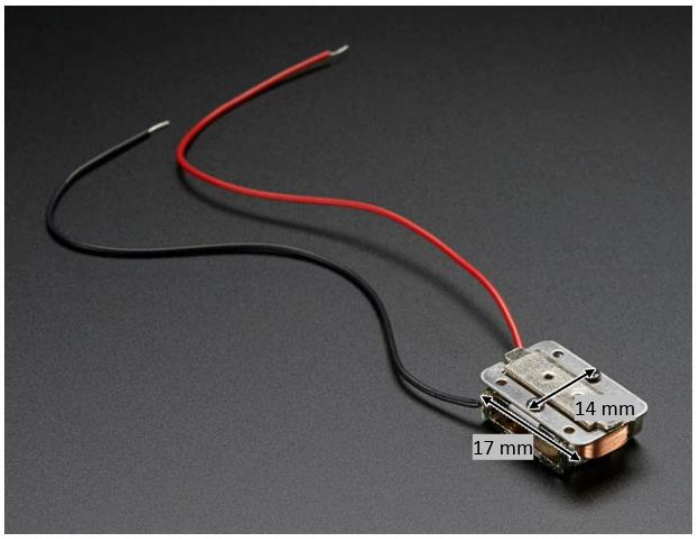

Figure 27: Photo of an Adafruit bone conduction transducer

The transducer was positioned on the lateral side of the hindlimb to allow for easier access; despite the reduced size of the transducer, combined with its housing it was still the largest component used in the overall assembly, and so it was therefore preferable to keep it on the outside to avoid it interfering with the rat.

3.8.1.2 Accelerometer

The accelerometer used was an ACH-01 accelerometer. To ensure a measurable output on the medial side (inside) of the joint, a separate section containing the accelerometer (described in the section 3.4.1.2) was positioned on the medial side of the joint opposite the transducer. Due to its small size, unobtrusive profile, and low weight, it was considered an acceptable transducer for the requirements. A

diagram of the accelerometer dimensions (in inches) can be found in section 3.4.1.2.

The accelerometer measures the nanovibration transmitted to it via the target area. This reading allows the nanovibration to be adjusted to meet the parameters of the trial.

3.8.1.3 Animal Harness Prototype

The transducer and accelerometer were required to be held in a fixed position with the target area of bone to be vibrated between them. Due to ease of access, the target area of rat bone was the tibia which is a delicate, narrow bone in a rat. To facilitate steady nanovibrations to the bone, an animal harness prototype was designed to contain the transducer and accelerometer in a fixed position opposite each other with the rat bone held securely between them.

This housing was manufactured as two components, each intended to house the transducer and accelerometer respectively, connected by a bridge of material. Due to the small size of the individual components, the harness was made as one connected part for ease of application.

3.8.2 Evolution of the Animal Trial Prototype

The initial prototype design was made using rat cadavers to establish parameters of size and approximate shape. The initial prototypes were early explorations of a means of applying a vibration to the leg and varied in approach.

Initially, the intention was to allow the rats free movement in the cages during the trial. The device used in the animal trials was designed to be as small as was practical in order to not be uncomfortable for the rats and cause them to move, which would affect the readings and the vibration transmission; it was noted that small movements would have a large effect on the vibration readings recorded by the accelerometer.

Whilst the size requirement to keep the device as small and unobtrusive as realistically feasible remained, it proved impractical to allow the rats free movement in the cages as this broke the connection between the power source and the electronics, as well as the transfer of information from the electronics to the data storage. Allowing the rats free mobility also gave them the opportunity to remove or damage the device which they would attempt to do. Eventually the device that was designed works only for restrained rats that have paralysed hindlimbs.

The transducer and accelerometer components were both initially selected as being small and less obtrusive alternatives were not discovered during the design process that were considered viable. Effort was instead made to optimise their housing harness component.

Early harness designs involved a screw device that could be easily tightened by an investigator during the trial, however this idea was abandoned for two reasons. The screw knobs were difficult to grip due to the small diameter, and the rigidity of the components was deemed potentially harmful to the animals if improperly applied. Instead, elasticated straps were used, which took up less space, were lighter, and by sewing hook & loop material to their ends, were quick and easy to apply and adjust by the investigator. The straps were 1 cm wide.

The two parts of the housing harness, one for the transducer and one for the accelerometer, were connected using a foam 'bridge' made of a soft, flexible material, Poron Vive (Rogers Corporation, Arizona, USA), which is used as a padding material in ergonomic soles. This material was selected in order to reduce the transmission of vibrations travelling from the transducer to the accelerometer through the device itself instead of through the rat hindlimb, which was considered a downside of connecting the transducer and accelerometer housing directly. The use of Poron Vive reduced the potential for unwanted vibrations that could travel

through a rigid, 3D printed bridge which would be captured by the accelerometer and alter the results of the experiment.

Poron Vive is also soft and pliable, which helped it conform to the shape of the rat leg and made it easier to fit to the rat as opposed to a hard, rigid connection. A small cavity was included in the 3D printed parts to assist in the assembly of the parts; this meant that as the bridge was assembled to the two 3D printed components via adhesive, there was a physical guide to help with positioning.

The design allowed for the accelerometer to be held in place using a resistance fit, achieved by accommodating the size of the accelerometer by 0.1 mm - 0.5 mm and using filing to remove excess material included as part of the printing process. A hole was made on the other side of the slot for the accelerometer so that the accelerometer could be easily removed by inserting a thin rod through the hole and pushing the accelerometer back out.

The transducers used in the animal trials were inserted into a slot on one of the 3D printed parts, and the wires of the transducer slid through a channel where they could be held in place using adhesive. An image of the CAD model prototype is shown below in Figure 28, along with a diagram of the overall assembly in Figure 29.

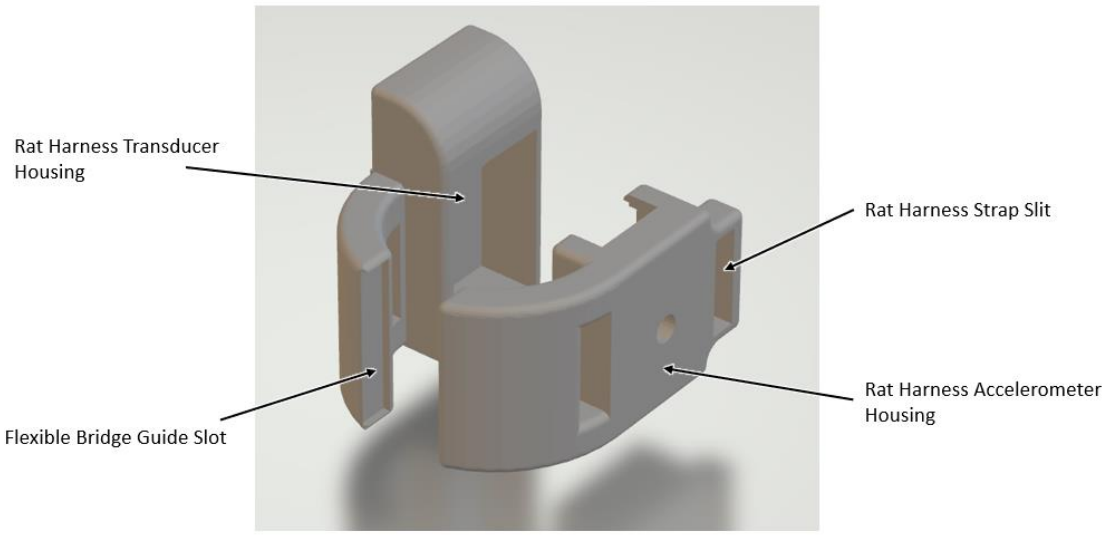

Figure 28: CAD representation of the 3D printed components of the animal harness prototype including the transducer housing (left) and the accelerometer housing (right)

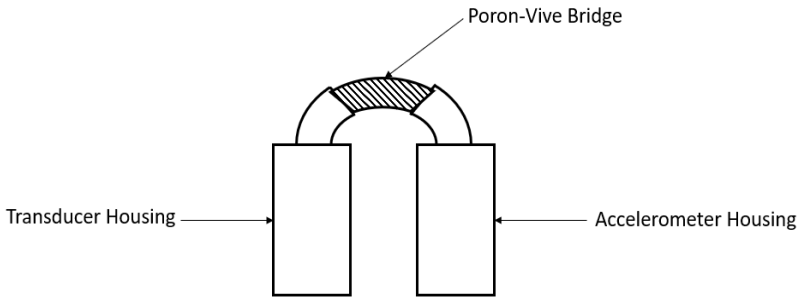

Figure 29: Diagram of the animal harness identifying the major components, annotated

To prevent harm to the rats, which could include pressure sores as described in earlier sections to do with the human participants, as well as inadvertent pinching or cuts, thin layers of Technogel (approx. 3 mm - 5 mm thick) were applied to the metal vibrating plate of the transducer to prevent direct contact of this hard part with the rat hindlimb and remove the chance of fur getting caught in the metal.

This was not done on the accelerometer side as the components on that side were all plastic and smooth and was considered less harmful.

By the end of the design process, the number of components used in the assembly were reduced to the transducer housing, the accelerometer housing, the accelerometer and transducers themselves, the Poron-Vive bridge, the Technogel padding, and the adjustable strap. In use, only the strap required adjustment. Figure 30 below shows the device in use.

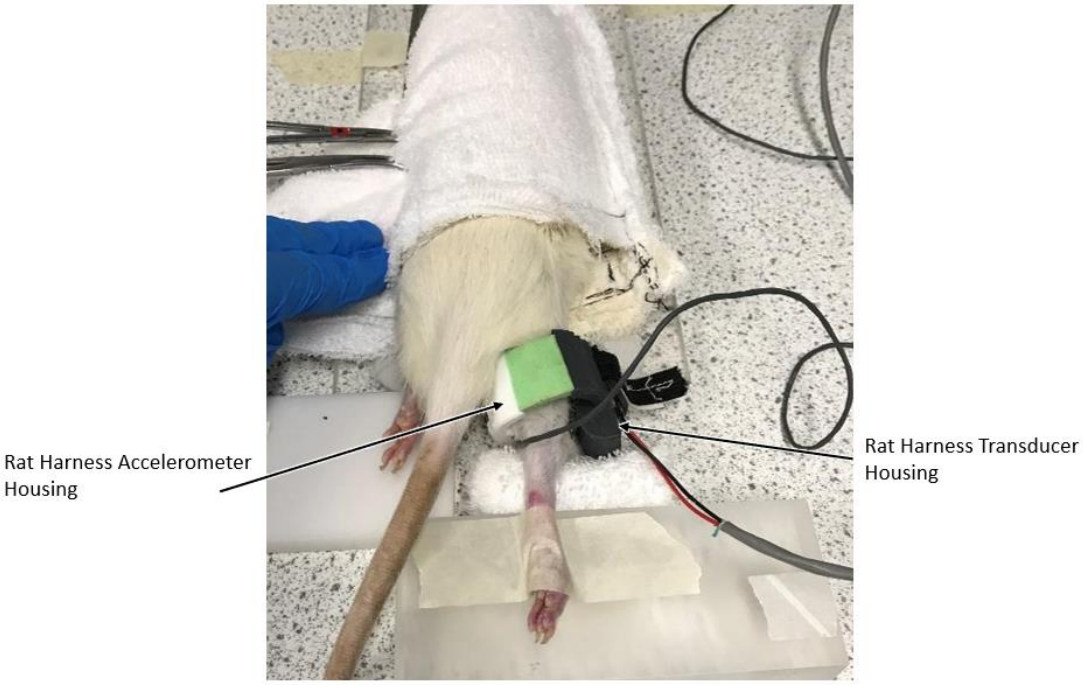

Figure 30: Animal trial device in use on restrained rat

3.8.3 Transducer Characterisation & Wave Generation

Characterising the transducer was done using a wave generator powering the various transducers used and a single-point laser interferometer aimed at the vibrating plate of the transducer.

The transducers were characterised over a range of peak-peak voltages at 1000 Hz, since this was the vibration frequency at which the devices would run. The vibration amplitude at 1000 Hz was then recorded over Peak-Peak voltage in order to obtain the calibration curve for that transducer.

For the animal trial devices, it was necessary to calibrate each transducer individually, as it was discovered there was a considerable degree of variation in vibration amplitude for each transducer. For the transducers used in the preliminary clinical evaluation, there was less vibration variation between transducers. Each transducer, upon being selected to be used in an animal device, was installed into their 3D printed housing and had a reflective tape applied to the vibrating element. They were then characterised at a series of peak voltage amplitudes delivered by a wave generator and the resulting vibration amplitudes were measured using a laser interferometer and recorded in a spreadsheet. Each transducer was labelled with a letter in order to keep track of each transducer. Throughout the experiment the transducers capable of delivering the highest

vibration were typically used, since this would mean that during the experiment it would be easier to deliver a vibration at the required level; due to variations in animal size, it was simpler to reduce the vibration output of a transducer that could output a higher degree of vibration than adjust the positioning of a transducer that struggled to deliver the required amount.

3.9 Animal Trials

This section describes the animal trials undertaken in Glasgow University with the aim of assessing the effect of nanovibration on BMD. All experimental procedures were approved by the Ethical Review Panel of the University of Glasgow and carried out in accordance with the Animals (Scientific Procedures) Act of 1986.

The animal trials were conducted with the assistance of Dr. Jonathan Williams and Prof John Riddell who have kindly allowed the trials to be summarised here as well presenting the results of the trials in section 4.2. In particular, the organisation of the trials, access to the animals and ensuring ethical approval could be achieved was done with the help of Prof. John Riddel. The vibration sessions themselves were conducted by Dr. Jonathan Williams who was able to retrieve the data from during the animal trials themselves as well as perform the micro-CT scans presented in section 4.2.2 and 4.2.3.

The trials utilise the bespoke designed nanovibration device as described above in section 3.8 to apply nanovibrations to the target region of bone and to record measurements. The animal trial is described shown in the following sections:

- Animal preparation and considerations.

- Experimental set up and conducting the experiments.
- Bone density measurement and analysis techniques.

The results for the animal trial experiments can be found in section 4.2.

3.9.1 Animal Preparation & Experimental Design

The animal trial used twenty-six Sprague-Dawley rats acquired from Charles Rivers Laboratories, Kent, United Kingdom. These animals were weighed (201 g - 225 g) and housed in pairs in a temperature-controlled room under a 12-hour light-dark cycle and ad libitum access to food and water for 1 week of acclimatisation.

In order to assess the impact of the nanovibration on bone subject to osteoporosis as a result of spinal injury, after the week's acclimatisation the rats were anaesthetised and given a spinal transection in order to perform a laminectomy at the T9-T10 level of the spine to generate a spinal cord injury.

The rats were separated into two groups. 20 were given spinal cord surgery (SCI rats) at the T9-T10 level. Once exposed, a small hole was made in the dura and the spinal cord was cut transversely at two locations 1mm apart. Six rats were given sham surgery. In this case, after exposure of the spinal cord, the wound was closed again immediately without further action.

Three days after the spinal cord surgery, the SCI rats were prepared in advance for the nanovibration treatment by training the rats prior to the treatment delivery.

3.9.2 Conducting the Experiments

The original intention was to allow the rats to move about the cages freely. However, the rats' movement adversely affected the nanovibration and damaged the nanovibration device. For this reason, the rats were restrained in towel-like pouches and the session duration limited to what the rats would comfortably allow; during the experiment, the rat's hind-leg would be taped in place to prevent excessive movement from spasticity, which occurred during the trial. It should be noted that by reducing spastic action, this logically results in lower bone loading due to muscle movement than if spasticity was allowed; however as the effect of this on BMD was unknown at the time of initiating the experiment, the test proceeded.

Whilst the restriction of motion would be necessary or desirable in any human population, thereby rendering an ergonomic comparison to the human-centred experiments, by ensuring that BMD reduction was repeatable and consistent, the effect of nanovibration on BMD would be more readily measured if present.

Three days after the spinal cord surgery, the SCI rats were prepared in advance for the nanovibration treatment by training the rats prior to the treatment delivery.

This training involved the rats being placed within soft towel pouches with the edges folded and clipped to lightly tighten the pouch around the rat to restrain them, forming a pocket the rats could be inserted into comfortably and where they remained for up to the duration of a vibration session. The rats were placed in the pouches for increasing durations, starting with 15 minutes a session for the first week of training, then 30 minutes the second week, 60 minutes the third week,

then 120 minutes for the following three weeks. From the second week onwards, a deactivated prototype device would also be applied to the right hindlimb to acclimatise the rat to wearing the device during the intervention, as the device alters the position of the hindlimb. Tape was applied to hold the leg steady and to ensure the leg would be fully extended during the vibration sessions.

This training also allowed for rats most suitable to undergo the treatment to be identified. Only rats that were calm for extended amounts of time were selected. The hindlimbs were exposed at the end of the pouch to allow the device to be applied to the hindlimb and easily adjusted. The setup is shown in Figure 31 below, showing the pouch, the extended leg, and the vibrating device as applied to the right hindlimb.

Figure 31: Animal Trial experimental set-up showing rat pouch, vibration device on hindleg, during vibration session

Following the pouch training, 10 out of the 20 rats in the SCI group were selected to be subject to the intervention whilst the remainder would serve as controls. The rats selected for the intervention were split into two groups, referred to as N40 and N100. For the N40 group, the measured vibration amplitude at the hindlimb was 40 nm, and for the N100 group the measured vibration amplitude was 100 nm, in order to compare any effects from varying vibration amplitudes.

These vibration amplitudes were selected in order to be consistent with previous literature on nanovibration used in-vitro as discussed in section 2.8. In previous literature, vibration amplitudes were applied to cells in-vitro up to 40 nm, and so

this amplitude was selected to enable some comparison with in-vitro studies. 100 nm was selected to account for possible attenuative effects in the bone and in case a greater amplitude of nanovibration was required for in-vivo samples compared to in-vitro.

The vibration was measured during the experiment by the accelerometer part of the prototype device (shown in the above image on the left/medial side of the vibrating device on the right hindlimb). If the measured amplitude was not within a specified threshold (35 - 45 nm or 90 - 110 nm, depending on group) then the vibration output was adjusted by either changing the wave generator power by adjusting the gain knob, tightening the strap manually or adjusting the position of the device on the leg to improve contact between the transducer surface and the hindlimb.

The daily vibration sessions took place over a period of 6 weeks, with 2 sessions 7 days a week, each session lasting up to 2 hours. A vibration session consisted of securing the rat in a pouch, attaching the vibration device to the target area on the hindlimb whilst the accelerometer monitored the vibration displacement amplitude. All devices were monitored individually and adjusted to maintain a measured vibration amplitude at the accelerometer between the two target amplitudes; 40 nm and 100 nm. The accelerometer stored a vibration amplitude reading once per minute, taking the average of the last 60 second readings of the peak displacement. This provided a record of the vibration amplitude measured by the accelerometer for each individual rat per session. The vibration information combined with results from bone mineral density analysis (method outlined below) is shown and analysed in the results section 4.2.

In summary, the experiment featured the following groups of animals out of the 26 in total:

- 2 rat groups given vibration delivery sessions at amplitudes of 40 nm and 100 nm, comprising 6 animals in group N40 and 4 in group N100
- 10 control animals
- 6 animals given SHAM surgery

Groups N40 and N100 were subjected to vibration delivery for up to 4 hours a day, for a total of up to 110 hours over the course of the study depending on animal tolerance. In practice, the average total hours subjected to the therapy was 79.22 hours, ranging from 28.8 to the full duration of 110 hours.

After completion of the experiment the rats were euthanized by anaesthetic overdose.

3.9.3 Bone Mineral Density Analysis Technique

The BMD results of the study were compared using statistical analysis between the different animal groups. Normality was assessed using the Shapiro-Wilk test on residues as well as by visual inspection. Following this, a paired t-test was performed if the data could be normally distributed; otherwise, a paired Wilcoxon test was used. The techniques used for generating the BMD data are as follows, as performed by Dr. Jonathan Williams.

Both tibiae and femora from the hindlimbs were μCT scanned using a Bruker SkyScan 1172 scanner (Kontich, Belgium) at 10 μm isotropic voxel size. All scans were performed in oversize mode at 70 kVp X-ray tube voltage, 100 μA X-ray tube current, 470 ms integration time, 10 μm voxel size with 2k camera resolution

and 0.4° rotation step for a total of 180° with a 0.5 mm aluminium filter to reduce beam hardening artefacts. Projection images were reconstructed using SkyScan NRecon software (Version 1.6.9.18, Kontich, Belgium) into 8-bit grey level cross-sectional images, with the following reconstruction parameters: ring-artefact correction = 13, beam hardening correction = 40%, smoothing = 2.

A representative μCT dataset was selected from each group and used as a reference dataset. These reference datasets were manually adjusted to standardise the alignment, such that the long axis of the femoral shaft is the Z-axis of the dataset using DataViewer (Version 1.5.6.2, Kontich, Belgium). All remaining datasets within each group were rigidly rotated to the alignment of the reference dataset in an automated fashion, again using DataViewer.

Four VOI were selected from the tibiae and femora for morphometric analysis. These were the entire proximal epiphyseal trabecular region enclosed by the growth plate, the proximal metaphyseal trabecular region, determined as being between an offset of 2/5% of the bone length from the growth plate to 5% of the bone length, the proximal metaphyseal cortical region, and mid-diaphyseal cortical bone region determined as being between 57.5% and 62.5% of the bone length from the proximal end for the tibiae. For the femora the VOI were the distal epiphyseal trabecular, distal metaphyseal trabecular, distal metaphyseal cortical, and mid-diaphyseal cortical bone regions.

For comparisons between groups, only the hindlimb subjected to vibration was included due to the pairwise analyses indicating differences between left and right comparisons in both control groups. For multiple group comparisons, normality

was assessed in the same manner as for the paired tests. Homogeneity of variances was tested using Levene's Test. Normally distributed data with homogeneous variances were tested using one-way analysis of variance (ANOVA) with Tukey's HSD. In cases of normally distributed data but with non-homogeneous variances ANOVA was performed with Games Howell post-hoc test. Data assumed to not be normally distributed was tested with independent samples Kruskal-Wallis test for multiple groups with Dunn's post-hoc test

3.10 Modelling Vibration Transmission via Finite Element Analysis (FEA)

In order to understand and visualise the behaviour of nanovibration through a bone region, computer modelling techniques were deemed valuable to complement the experiments described in earlier sections to describe the vibration behaviour within the bone media. This section details the finite element analysis (FEA) used to do this. The advantage of FEA over direct measurements is that the measurement tools available on physical models and samples are only able to provide vibration information at a given point or series of points on or in the sample, whereas FEA can provide a more complete visualisation of the vibration across the whole sample in a simplified form.

FEA was used prior to laboratory-based experiments detailed in later sections as an early means to gain a basic understanding of vibration behaviour prior to committing to a laborious experiment, as well as inform upcoming experimental design.

The aims of this section are as follows:

- Describe a simplified model made for simulating the transmission of low-frequency vibration through bone
- Describe the Finite Element Analysis setup for simulating vibration amplitude through via harmonic response analysis

This section shows the simplified models of bone designed using CAD used in the FEA as well as the setup of the FEA to visually represent the vibration amplitude through the models. The results for the FEA modelling sections can be found in section 4.3.

3.10.1 Modelling Bone via CAD Models

Bone is complex in nature, particularly bone in the trabecular region as targeted in this research, as it is formed of different structures with different densities and behaviours. A series of CAD models were designed to help visually represent how the vibration from a transducer source would affect the body as a whole. The initial CAD model addressed the issue presented by the small dimension of individual trabeculae in relation to the wavelength of the nanovibration to be applied by modelling the material as bulk media, simplifying out the complexity as a starting point. This had the advantage of showing how the transducer transmitted a wave through the bulk material. However, this block shape had the disadvantage of oversimplifying the complex differences of material from hard cortical bone through softer trabecular bone and back out through hard cortical bone again. In order to gain a stronger understanding of the effects of geometry on vibration behaviour through bone, several CAD models were designed with increasing levels of complexity as follows:

- A simple cube
- A cube with an ‘arm’ designed to represent the femoral shaft
- A femur model

For each level of the three levels of shape complexity the CAD model was designed in Creo 3.0 as a solid part.

Meshing was done under the assumption that the wavelength will exceed the dimensions of the sample under test. The effects from small features such as trabeculae were not modelled, as there was an inability to measure and confirm the vibration amplitude on such small geometrical features; individual elements were set to a maximum dimension of 1 mm in a grid pattern in order to aid in producing successful harmonic simulations. Automatic optimisation performed by Ansys Workbench 17.0 was avoided to enable better control of resolution should it be necessary. When designing the femur model, a chord length of 1 mm was set when converting the CAD model in Creo 3.0 to a filetype accepted by Ansys Workbench 17.0. These values were selected due to limitations in measurements on the proxy media models; as 1 mm was the realistic limit that dimensions such as depth and thickness could be drilled/cut to, higher resolution was not deemed necessary.

As the primary regions of interest were distant from the edges and concentration regions of the model, a uniform mesh was selected initially. In the event that a complex behaviour was observed, or that unusual behaviour observed in later vibration tests done on proxy media was inconsistent with results seen as part of the FEA modelling, non-homogeneous mesh approaches were to be considered

based on measurements taken on the bone surface and best judgement; however this was not considered necessary following the gathering of results, as the FEA modelling was determined to be adequate for visualisation purposes and overall comprehension of the vibration behaviour in the bone.

The three models are shown below in Table 3.

Table 3: Table of Simulation model shapes and an illustration of their 3D shapes

Simulation Model Shape	**Illustration**
Block Model, Single Material	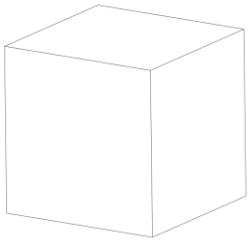
Block Model, Composite Material	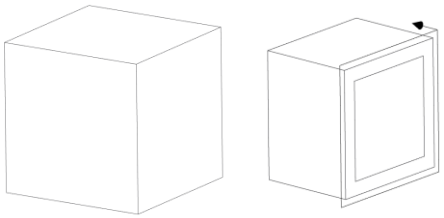
Block Model, Single Material, Transducer Model Only	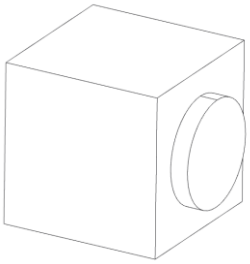

Armed Block Model, Single Material, Transducer Model Only	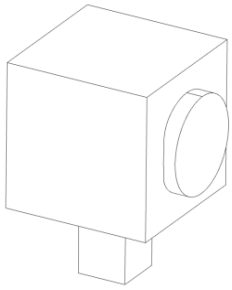
Armed Block Model, Composite Material, Transducer Model Only	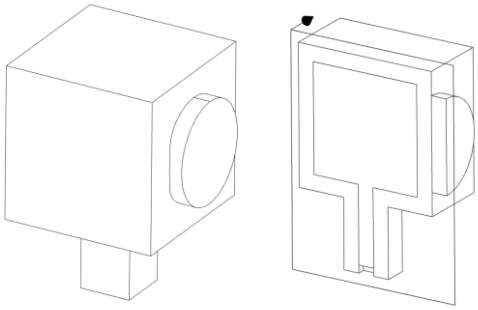
Femur Model, Single Material, Transducer Model Only	
Femur Model, Composite Material, Transducer Model Only	

Block Model, Composite Material, Transducer & Soft Tissue Model	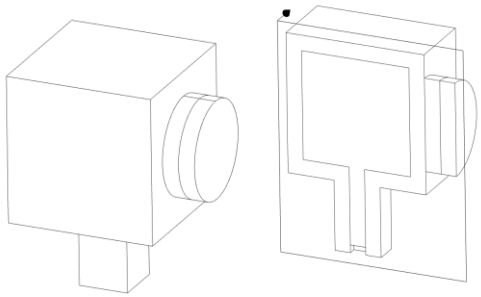
Femur Model, Single Material, Transducer & Soft Tissue Model	
Femur Model, Composite Material, Transducer & Soft Tissue Model	

To further replicate the distinct cortical and trabecular regions of realistic bone samples, a second set of CAD models was drawn using the same outer dimensions as those above, but hollow. An assembly model was then constructed using the hollow CAD model and a separate internal region that could then be given separate material properties to the outer hollow component, creating a composite model. This added the further assembly models:

- A composite simple cube
- A composite armed cube

- A composite femur model

For each model, the large cuboid element was set to have a width of 90mm. This dimension was selected to be close to the width of a femoral head. The width of the arm had a width of 30 mm and protruded from one of the cuboid faces.

In order to represent the physical transducer element, a CAD model of a simple disc was made which could then be included in the assembly model and given its own material properties. This disc model was made to be 30 mm in diameter, consistent with the diameter of the bone conducting transducer used in the wearable prototype devices described in earlier sections.

Finally, a large disc was also drawn to represent a layer of soft tissue for the nanovibration to traverse before reaching the simulated bone. In order to be consistent with Scanning Laser Interferometry (SLI) measurements performed on synthetic soft-tissue analogues, the disc was made to be 10 mm thick and 60 mm in diameter shown below in Table 4.

Boundary conditions for each region are described in section 3.10.2.

Table 4: Table of Disc Models used in FEA; Transducer Disc Simplified Model (left) and Synthetic Tissue Disc (right)

Disc model	Synthetic tissue disc
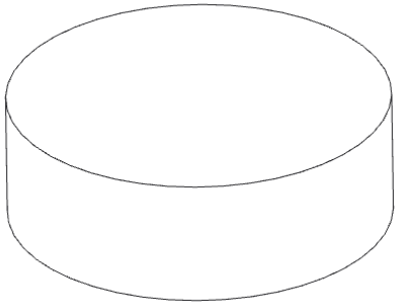	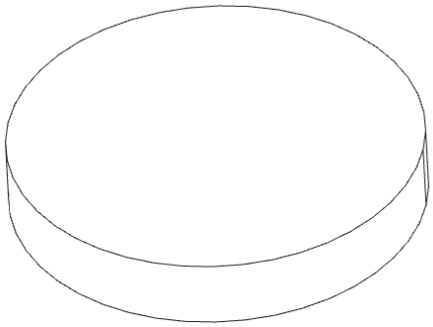

By combining these individual models into different assemblies, the effects of low-amplitude vibration could be observed with increasing levels of verisimilitude. Each model representing the femur (both single-material and composite) would either be used solo, with a transducer disc, or with a transducer disc & soft-tissue disc. This resulted in 18 separate models simulated. The simulations were used to inform the design of the transmission devices to maximise the transmission effectiveness and contact with the target area. Evaluation of the FEA analysis was enhanced by visual representation. The results from the simulation are shown in the results section 4.3.

As the FEA models used in this section are scaled to bovine femurs in approximate size, direct comparison is intended between the results from FEA experiments to the experiments detailed in section 3.11; however, as overall behaviour in a qualitative sense is not expected to be conceptually different between bone types (as most bones have a cortical and trabecular region, are surrounded by soft tissue, and are vibrated using a similar transducer plate), should the FEA be found to be

representative of vibration transmission behaviour, the behaviour of vibration within bones can be estimated.

3.10.2 FEA Setup - Harmonic Response

As the goal of using FEA for this purpose is inherently to simplify a complex environment in a manageable way, the FEA has several key limitations that were imposed in the Ansys Workbench 17.0 models used. These were the following:

- All materials are assumed to operate in a linear elastic manner over the displacements used.
- Tissue regions were simplified to bulk media regions of homogeneous material as described in section 3.10.1.
- Boundary layers between tissues were assumed to be bonded; boundary layers between tissues and transducer elements were non-bonded.
- For models representing a bone clamped in place, the 'arm' face was considered constrained in all axes.

As a means of identifying the primary contributing factors affecting vibration amplitude through the bone, these limitations were considered acceptable; as only vibration amplitude was considered, as opposed to waveform shape (which would be expected to display more complexity in response to the various changes in density and elasticity within the region) , linear elastic materials were deemed sufficient for the small vibration amplitudes measured. Homogeneous materials were similarly considered an acceptable simplification with the understanding that small changes within the bone microstructure would not be represented. Boundary

layers and constraints used were selected based on understanding of the model at the time.

Each model as described above was used in an Ansys Workbench 17.0 harmonic response simulation. In each instance the vibration frequencies simulated were 500 Hz, 1000 Hz, 2000 Hz, 4000 Hz, and 5000 Hz. These frequencies were selected to observe areas where no vibration was experienced, potentially as a result of standing waves, if there were any in the simulation as well as their location.

The simulations were designed to assume a vibration displacement of 1×10^{-6} m. This amplitude was chosen to account for losses in vibration amplitude through the material.

Where an arm was included in the model, the base of the arm was set to have a static constraint. This was to represent the cortical shaft of the bone being clamped firmly during later experiments on bone samples. Where a transducer element was included, the displacement at 1×10^{-6} m was set on the exposed surface of that element.

The boundaries between the transducer element and the bone model, whether it was composite or including a layer of soft tissue, were set to allow a sliding motion representative of the lack of bonding present between the transducers and the target areas in practice. As it was assumed that there would be less or no sliding motion between internal layers, in the case of boundaries between the outer shell and the inner core there was a bonded boundary, as for the boundary between the outer shell and the soft tissue layer. A diagram representing these boundaries is shown in Figure 32.

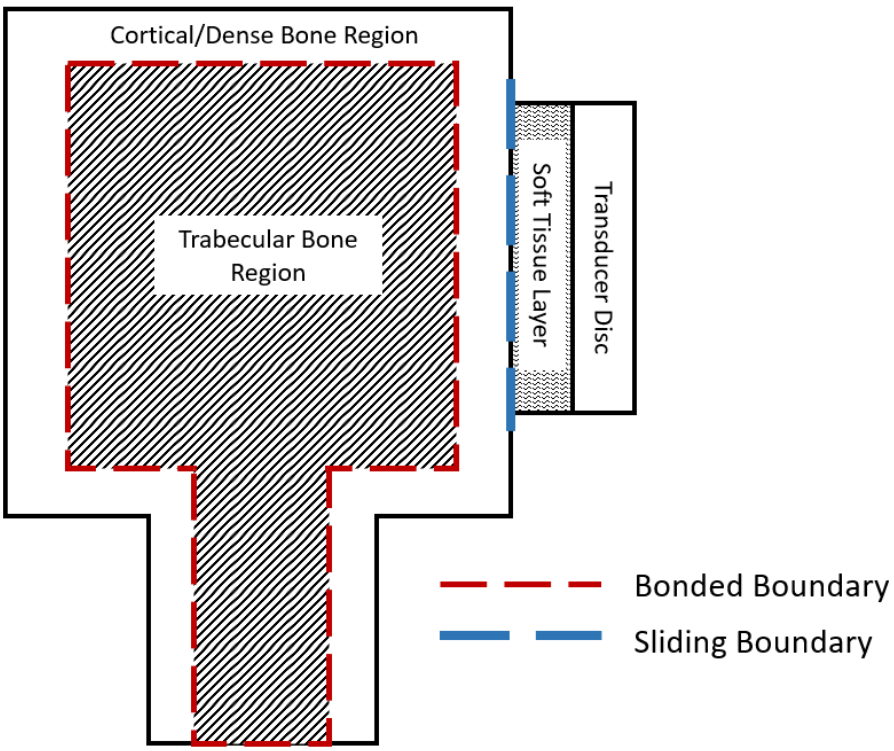

Figure 32: Diagram of regions represented in FEA simulations in Ansys, with boundary types

The simulations returned a representation of vibration amplitude throughout the middle cross-section of the bone model as well as a one-dimensional measurement of vibration amplitude through the centreline of the vibration wave in order to display the peak amplitude through the bone in a graphical form and a measurement of peak vibration on the opposing surface of the bone. This one-dimensional measurement allowed for a visualisation of the waveform shape through the centre of the material being measured, a heat-map view of vibration amplitude across the cross-section, and the vibration amplitude on the side of the bone that were measured by an accelerometer were the device to be applied to a joint.

In order to account for the variations in bone which are not readily represented in the FEA simulations planned, the model designed was aimed to be primarily qualitative in nature, and the exact material properties of the samples studied in later bovine vibration experiments were not used due to practical difficulties in measuring them. Technical estimates determined to be realistic were chosen in order to return interpretable results. These values were input where needed into Ansys to represent the various regions in the simulations and are shown in Table 5: Table of material properties as used in the FEA Ansys simulations.

Table 5: Table of material properties as used in the FEA Ansys simulations

Material	Density (kg/m^3)	Speed of Sound (m/s)	Stiffness (GPa)	Source
Steel (Structural)	7900	5790	200	N/A
Tissue	1585	1060	N/A	Humimic.com
Bone (Dense)	1908	N/A	19.8	itis.swiss, X. K. Wang, 2007
Bone (Trabecular)	1178	N/A	10.9	itis.swiss, Ashman and Rho, 1988

Where needed, the stiffness was approximated from the speed of sound using the formula

$$E = \sqrt{\frac{c^2}{\rho}}. \qquad \textit{Equation 13}$$

A table summarising the results from these simulations is shown in the results section 4.3, and the FEA representations of the vibrations were used to help visualise how the vibration was expected to behave in the bone region.

The results from this FEA experiment can serve to help predict the overall behaviour of vibration amplitude through bone based on a measurement on the bone surface; for example, should transmission/reflection be determined to be the primary factor in vibration amplitude reduction through the bone, if 40 nm is measured on a rat bone the bone surface via laser interferometry, the assumption can therefore be made that 40 nm of vibration is present inside the bone with negligeable losses. This will be visible in cross-sectional views of the FEA model as shown in section 4.3.2 and supported by physical experiments on bovine samples in section 4.4.2, acknowledging limitations of both experiments.

3.11 Vibration Measurement on Proxy Media

The transmission and measurement of vibration through bone and tissue is fundamental to this thesis. The FEA analysis provided a simplified computer-based model of how vibration could be expected to travel through bone and tissue. The clinical wearable device showed that vibration passed through the target area of bone in both human and animal trials. However, due to the nature of live trials, the vibration amplitude could not be measured at intermediate points between the transducer and accelerometer. To further characterise the vibration amplitude present within bone and soft tissue media during a nanovibrational intervention, laboratory-based experiments using proxy samples were designed to measure vibration amplitude within the bone, at boundaries between soft media and bone, and on the surface of bone or other media of interest. This was done to provide information on a wide range of engineering and scientific questions as to how the vibration behaved upon application to a zone of interest.

All vibration characterisation experiments on physical media are located in section 4.4.

3.11.1 Vibration Measurement Techniques

Vibration transmission throughout the laboratory experiments was measured by accelerometery and interferometry. These laboratory-based experiments were carried out before, during and after the individual experiments using the wearable device in order to characterise vibration properties through various tissue samples. This section outlines the major methods of vibration measurement used that will be referenced through later sections.

3.11.1.1 Accelerometery

The accelerometers used for both the animal trial devices and the wearable device used in the preliminary clinical evaluation were ACH-01 accelerometers (TE Connectivity, Shaffhausen, Switzerland), as described earlier in the section 3.4.1.2. These accelerometers were calibrated over the expected range of vibration amplitude (0 nm - 30 nm) on vibrating plates designed and built in-house at the University of Strathclyde. Each accelerometer was calibrated individually on the vibrating plates by magnetically affixing the accelerometer to the vibrating plate and delivering a precise nanovibration using the vibrating plate at the desired frequency of 1 kHz. Confidence in the vibration amplitude measured on the plate was gained by measuring the vibration at a location adjacent to the accelerometer using a single-point laser interferometer. The vibration on the surface of the ACH-01 accelerometer was then also measured using the single-point laser interferometer. The peak voltage generated by the accelerometer for each vibration amplitude was recorded over a range of 1 - 30 nm. Using this data, a linear

conversion formula was generated using a best-fit method and each accelerometer was marked by giving it a number corresponding to its recorded conversion formula. If during the experiment an accelerometer was damaged, it was replaced with a matching accelerometer without it affecting the vibration measurements taken during the experiments.

3.11.1.2 Interferometry

Throughout the experiments, two types of interferometers were used:

- Single Point Laser Interferometer, which performs measurements at a single location determined by where the laser spot is located. The single-point interferometer used was a SP-S Laserinterferometric Vibrometer (SIOS Meßtechnik GmbH, Germany).
- Scanning laser interferometer (SLI) which can perform measurements at multiple locations and show the surface vibration over a predefined region. The SLI used was a PSV-500-H (Polytec, Germany).

Both interferometers were calibrated by their respective manufacturers. Due to the limited time available to use the SLI, the single-point laser interferometer was used for repeated measurements on large numbers of samples, whereas the SLI was used to demonstrate specific vibration amplitude behaviour across the surface of a smaller targeted number of samples.

The SLI, provided by Polytec, was aimed at the opposite side of the sample (bovine bone or synthetic gel) being vibrated. Each time a measurement was taken, the SLI was individually set up to measure a region of exposed bone.

The process of preparing the SLI for use is as follows:

- calibrate each surface to be measured (the exposed surface) by moving the laser spot to different locations on the bone surface and selecting a pattern of positions on the SLI camera. This was done until the laser moved reliably through the pattern of cursor points on the camera, at which point the SLI's camera and laser spot were calibrated for that surface.
- define the coordinate system by selecting 3 separate points on a reference plane visible to the SLI camera. This was done in this experiment by setting up a flat board directly behind the bone sample with three pieces of reflective tape attached in order to ensure the laser spot would be able to reflect with enough intensity back to the SLI.
- determine the predefined path for the laser spot to determine the path, the conductor of the experiment defined the geometry of the region to be scanned and the density of spots inside that geometry, and their pattern. These were determined based on the shape and size of the sample, as well as the positioning of the straps. In order to avoid artefacts due to the curvature of the bone, the edges of the bone surface were avoided, as were any regions of loose flesh remaining on the bone as well as the straps used to attach the vibrating device to the bone. The SLI then automatically determined its focus at several points within the target geometry.
- set the acquisition settings. The bandwidth was set at over 2.5 kHz to ensure that its Nyquist frequency included the target 1 kHz vibration. This was the last phase prior to running the experiment.

The SLI returned a series of amplitude values for each given point measured, which has an associated x and y coordinate. Using this data, a heat map was

constructed using Matlab, to show the vibration amplitude over the measured surface as a polygon mesh. Using this data, the peak vibration amplitude on the measured surface as well as the amplitude drop from the peak can be shown. An example series of points is given in x-y coordinates in the results section 4.4.1.1.

3.11.2 Characterising Vibration through Proxy Media using SLI and Accelerometery

The purpose of this set of experiments is to see how the vibration amplitude spreads across the surface of the bone, soft tissue phantoms, and the transducer surface itself as it would be used in investigations and preliminary clinical evaluations, as well as to provide initial confidence that the vibration is present and measurable inside the trabecular bone region.

The aim of this set of experiments was to:

- assess whether nanovibration would be transmitted through a body of tissue using synthetic gel and the transducer element of the prototype nanovibration device.
- quantify the impact of the Technogel padding layer on vibration amplitude introduced to the clinical wearable device in order to minimise potential skin damage.
- show via surface measurements on the bone whether any notable behaviour was present with regards to vibration spread, and how much of a region might be targeted by vibration.
- construct an early model showing the vibration decrease after transmitting through soft tissue, into the bone, and through the bone to the far surface.

This section will include the samples used, the measuring techniques used, and the experimental setups.

3.11.2.1 Bovine & Gel Samples

Due to their size and accessibility, bovine femurs were used to investigate the vibration amplitude present in the bone during application of nanovibration intervention. These bones were sourced fresh from the John Scott Abattoir and delivered to the University of Strathclyde. They were stored at -20°C in a freezer. The femur (bovine) was selected as the target for this experiment as during the preliminary clinical evaluation the nanovibration was applied to the femur of spinal cord injured patients. The synthetic tissue phantoms, described in section 3.1.2, were moulded into discs 19 mm thick using silicone moulds 4 inches (10.16 cm) in diameter. The gel type used was type #0.

3.11.2.2 Measuring Techniques

Levels of nanovibration through the soft tissue proxy alone were measured using SLI. Levels of nanovibration through combinations of Technogel, soft tissue proxy and bone proxy were measured using a combination of SLI and accelerometery to provide both surface measurement and vibration measurement within the bone.

During this experiment, two techniques to measure the vibration amplitude both inside and on the surface of the bone were used. Firstly, SLI was used to measure vibration on the bone surface and secondly accelerometers of the same type as used in the prototype nanovibration device were inserted inside the bone to measure the vibration present inside the bone.

The accelerometer was inserted into the bone via slots created by using drilling tools and files. The accelerometer was pushed into the slot until the entirety of its casing was inside the bone. The accelerometer displayed the peak-peak voltage on an oscilloscope which was converted into a displacement reading based on the conversion formula for that accelerometer. The conversion formula used was a linear conversion formula based on the calibration data for each ACH-01 accelerometer.

The SLI was targeted at the exposed surface of bone on the side opposite to the transducer. Due to the geometry of the bone sample used it was difficult to ensure the SLI was directed axially to the transducer, however a best attempt was made given the sloping shape of the bone condyle.

3.11.2.3 Bovine Femur Proxy Experiment Setup

Prior to taking the measurements, the accelerometer slot was drilled in the centre of the condyle in a position best suited for work with the drill and milling tools 5-6 cm deep. The slot was also made in such a way that the accelerometer, once inserted, was aligned with the direction of vibration once the vibration device was applied.

The prepared bone sample was then clamped in place on a table in front of a static panel used for defining the SLI coordinate system as described in section 3.11.1.2. Once clamped in place, the vibrating device was positioned on the bone condyle so that the direction of vibration faced towards the SLI. The SLI surface measurements on the bone were subsequently used to create surface heat maps

giving a visual representation of how the vibration spread over the bone surface, and how much of a region might be targeted by vibration.

The vibrating device was activated at a peak-peak voltage of 10 V using the SLI's generator so that the SLI could phase correctly during its reading. The device emitted a 1000 Hz vibration during the experiment and the peak-peak voltage output by the accelerometer was recorded.

This experiment was repeated with an additional 19 mm layer of #0 humimic.com gel inserted between the vibrating device and the bone to serve as a repeatable substitute for soft tissue. The experiment was repeated twice with a different bone sample each time (n = 2). The accelerometer data from the experiments was compiled to construct an early model showing the vibration decrease as it passed through soft tissue, into the bone, and through the bone to the far surface. This basic model was expanded in the next set of experiments which look at transmission of vibration through progressive areas of bone proxy.

3.11.2.4 Vibration Transmission through Synthetic Gel Experiment

An additional measurement with the SLI was performed on layers of #0 humimic.com gel without them being attached to the bone as an intermediary layer. This was done to gain images illustrating the distribution of vibration amplitude across the surface of the gel alone to compare the amplitude of vibration between two gels of different thickness. The aim of the measurements was to describe the vibration decrease from the transducer source as it passed through the different soft tissue media proxies, the results of which are shown in section 4.4.1.3.

This experiment was carried out to provide additional understanding regarding the behaviour of the gels in isolation, gain a qualitative understanding of their reduction over a surface for context in earlier and later experiments, and observe the reduction of vibration amplitude from the central axis of the vibration transmission 'beam' rather than be used to predict a realistic level of vibration amplitude through a hypothetical real-world soft tissue layer; experiments done on realistic media samples in a more readily comparable set-up are described in section 3.11.3.

To perform this experiment, a layer of 9 mm thick technogel was placed on the surface of the transducer used as described in earlier sections. Using the SLI, a heat map of vibration amplitude across the surface of the technogel was taken. Subsequently, a layer of 19 mm thick #0 humimic.com gel was applied to the surface of the technogel, and then another SLI measurement series on the surface of the gel was taken in order to compare the vibration amplitude directly on the surface of the technogel padding and on the surface of the gel. Then, a second layer of 19 mm thick gel was stacked on top of the first, resulting in a 38 mm thick gel layer to further compare the vibration amplitude through gels of varying levels of thickness.

3.11.3 Bovine Sample Vibration Transmission Experiment

This section details the final set of experiments aimed at characterising the vibration amplitude at multiple points through a larger sample size of bones. This follows from the previous SLI experiments which examined the surface spread of nanovibration to focus more on the vibration on the inside of the bone at multiple frequencies. The aim of this set of experiments was to:

- Provide data on vibration presence in bone through experiments on bovine bone samples with an increased level of detail and resolution compared to previously described experiments on bovine samples.
- Strengthen understanding of bone transmission through soft tissue and bone to inform wearable device design.
- Gain visual and graphical information on low-frequency vibration on the surface of and inside the trabecular region of bone in graphical form.
- Identify by measuring vibration amplitude on the transducer surface during vibration delivery the proportion of vibration amplitude transmitted from the transducer to the bone during use.
- Compare the performance of spring coil transducers against piezoelectric transducers to inform future device design.

This section outlines the methodology surrounding the experiment designed to characterise the vibration amplitude through bone, including a section on the bovine samples used, the vibration generation, and the procedure by which measurement points were acquired through the bone.

3.11.3.1 Bovine Bone Samples

Bovine femurs were used as a proxy for this set of experiments. These were procured and prepared as detailed in section 3.11.2 above. These bones were sourced fresh from the John Scott Abattoir and were limited to one freeze/thaw cycle at -20°C prior to and during work to prevent changes to the tissue's mechanical behaviour due to freezing cycles. For ease of clamping and working, only the knee joint end of the bone was kept for this experiment. Excess bone was removed prior to work via sawing once excess soft tissue was removed using a

combination of scalpel tools and butchery knives, and the proximal end of the femur was disposed of. At least 5 cm of cortical bone was left in order to provide room for the bone to be clamped in place and for the vibrating device to have enough bone shaft to be secured onto. Seven (n = 7) bones were acquired for this experiment.

After being processed, each bone was weighed by weigh scale. On average, the bovine samples weighed 1.28 kg, with a standard deviation of 0.24 kg.

3.11.3.2 Vibration Transmission Experiment Through Bovine Samples

The following experiment serves to measure the vibration amplitude at 1 cm depth increments within the trabecular bone region.

3.11.3.2.1 Experimental Equipment

The nanovibration delivery device used was the same as the one used for the preliminary clinical evaluation as described in earlier sections with the following adjustments; the accelerometer housing was removed to provide an exposed surface for the interferometry measurement and the modular arms and straps were removed for this experiment. Only the central elasticated strap adapted for the size and geometry of the bovine femur was used to attach the vibration device to the bone surface as the bone was clamped to eliminate movement.

The transducer was the same as used in the preliminary clinical investigation and as described in electronics section 3.4.1.2. It was powered by a signal wave generator running at 20 V peak-peak at the range of frequencies 500 Hz, 1000 Hz, 2000 Hz, 4000 Hz, and 5000 Hz to provide comparison data to the FEA analysis

at the same frequency range and to enable the potential visualisation of standing waveforms.

The SP-S Laserinterferometric Vibrometer (SIOS Meßtechnik GmbH, Germany) single point laser interferometer was used as the number of measurements to be taken made use of the PSV-500-H (Polytec, Germany) SLI less practical for reasons of cost and flexibility.

A flat 1 cm diameter drill bit was used to drill through the bone and enable measurements to be taken inside the trabecular region. The 1 cm diameter was a compromise between using a narrower drill hole to avoid compromising the bone behaviour but also allow a large enough diameter to insert the reflective tape and to prevent the laser spot from being interfered with by the walls of the drilled hole. The drill bit was marked along its length in 1 cm increments to facilitate depth measurement.

Reflective tape was applied to the surface of the bone to permit the measurement using a single point laser interferometer.

3.11.3.2.2 Experimental Setup

The nanovibration delivery device was applied to the distal condyle of the femur using elasticated straps and delivered vibrations at frequencies of 500, 1000, 2000, 4000, and 5000 Hz. Higher frequencies than the vibration amplitude of 1000 Hz used in both the animal trials and in the preliminary clinical evaluation were investigated in order to observe any potential waveform effects and to observe a vibration effect other than pistoning, should any exist.

The femur was then clamped with the opposing side of the condyle facing towards the single-point laser interferometer in order to take the measurement as shown in Figure 33 below.

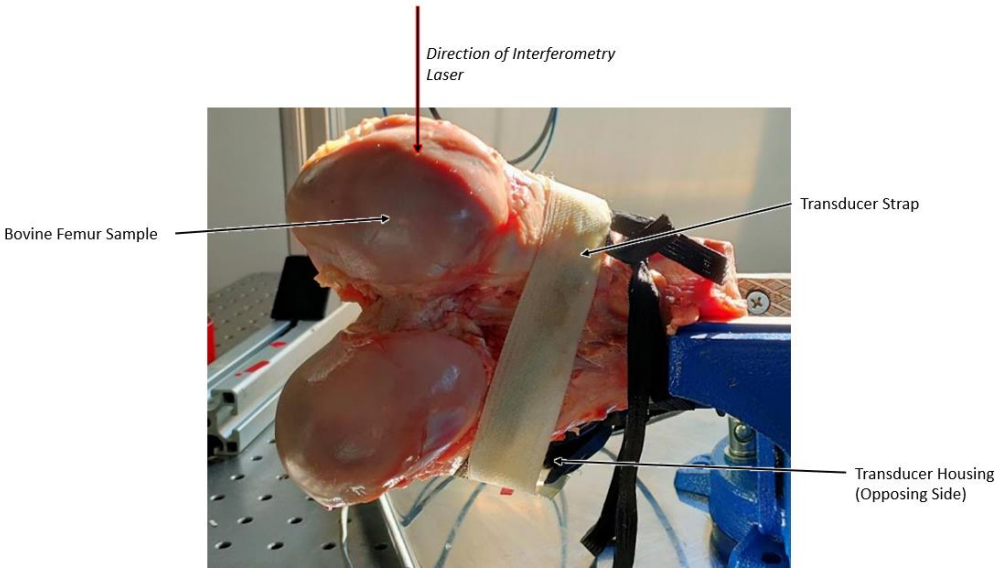

Figure 33: Bovine Femur Sample, clamped, during interferometry

After measurement on the surface of the bone at the specified frequencies, the location at which the measurement was taken was drilled using a 1 cm diameter drill bit.

At each 1 cm increment of depth, the bovine femur was once again mounted in the clamp as above and the nanovibration device applied to it.

Reflective tape was inserted into the drilled hole permitting the measurement of vibration at the given depth.

The measurement using the single point laser interferometer was taken at the specified depth. This was repeated in 1 cm increments until the bone was completely drilled through.

A final vibration measurement was taken on the surface of the transducer whilst it was in use on the bone. This measurement was used to normalise the vibration amplitude inside the bone against the vibration amplitude on the transducer surface as a means to determine what proportion of vibration amplitude was transmitted into the bone and what proportion was lost.

To provide additional confidence in the measurements, a second surface measurement was performed on the bone surface near the transducer, adjacent to the transducer plate.

Each measurement, both inside the bone and on the surface of the bone and the transducer, was repeated five times and averaged to reduce the effect of potential spikes due to noise or artefacts which can occur due to placement of the reflective tape, shocks to the bench from outside forces, and other potential sources of inaccuracies.

During the experiment, the percentage difference of a given measurement compared to the average returned by the 5 total measurements was found to be 2 E-15 % for measurements done on the surface of the bone. For measurements done inside the bone the percentage difference of a given measurement compared to the average of the 5 selected points was similar (8.5 E-16 % at a depth of –6 cm, as an example). These are negligeable differences and are not expected to alter the conclusions drawn from the measurements in any way.

The results are shown in section 4.4.2.

3.11.3.3 Technogel Padding Comparison

Using the equipment described above, the following experiment was performed to provide additional information to inform the engineering decisions taken whilst designing the prototype device, specifically with regards to the Technogel layer used to reduce the chance of pressure sores developing.

The effect of the Technogel padding used was assessed by taking the measurements with and without the layer of Technogel padding for five bovine samples (n = 5) as part of the measurements described in section 3.13.3.2. The means of the vibration measured could then be compared directly for significant differences.

These measurements were complemented by measuring the effect of Technogel on a single bovine bone sample selected from the experiment, which also served as a method to assess the effect of repeat applications of the device on vibration amplitude measured. For this reason, an experiment on a single bone featuring multiple separate device applications (n = 6) with and without Technogel was also performed only taking measurements on the surface of the bone. The results for these measurements are shown in section 4.4.2.4.

3.11.3.4 Spring Coil vs. Piezoblock Vibration Comparison

Lastly, an experiment intended to compare different commonly available methods of delivering vibration was performed by applying vibration to a single bovine sample using two types of vibrating transducer. The first was the same voice-coil transducer type used in the wearable devices in this study, and the other was a

piezo-block transducer that uses piezoelectric transducers to provide motion in three axes.

Both types of transducers were oriented upwards with the bone sample resting on top in such a way that the weight of the bone sample would be distributed onto the active element of the transducer. This was done so that the same compressive force would be applied to each transducer despite their differences in size and shape. Measurements were taken on the opposing surface of the bone, in order to measure the vibration transmitted through the bovine sample at the knee condyle; as well as after the sample had been drilled through, in order to measure the vibration amplitude of the transducer when under compression from the bovine sample. By measuring both on the surface of the transducer during use and on the surface of the bone, a normalised vibration amplitude could be determined. This experiment was repeated 6 times on the same bovine femur sample. A diagram of the setup is shown in Figure 34 below.

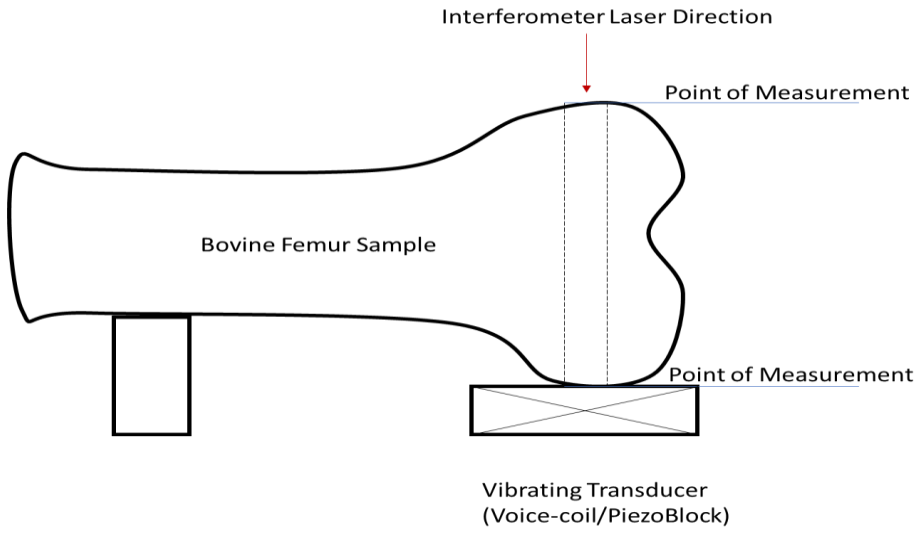

Figure 34: Diagram of the bovine femur as measured during the single point laser interferometer

4 Results

This section covers results gathered from:

- The Investigations done at the University of Strathclyde, made to inform the design of the device and feasibility of vibration delivery to participants
- The Preliminary Clinical Evaluation, made to assess feasibility of vibration delivery and limitations
- The animal trials, done to assess the positive effect of nanovibration delivery on BMD, if any
- FEA modelling work to qualify vibration behaviour through a target region in preparation for vibration transmission experiments on bovine samples
- Vibration characterisation done on synthetic and bovine samples to describe vibration behaviour measured inside the bone region directly to provide confidence of vibration delivery for other studies

No therapeutic effect was observed either in animals or in humans. Successful vibration transmission was observed in all studies.

This section outlines the results gathered throughout the course of the project. This incorporates the results relating to the wearable nanovibration device as used during the initial and follow-up investigations at the University of Strathclyde and the preliminary clinical evaluation. Following this are the results from the animal trials relating to the viability of nanovibration as a treatment for osteoporosis. Lastly, results relating to the overall behaviour of vibration through bone at the desired frequencies are covered through FEA results followed by characterisation experiments.

4.1 Clinical wearable device results

4.1.1 Initial Investigation results at the University of Strathclyde

The initial and follow-up investigations at the University of Strathclyde were designed to meet the following objectives:

- Test the suitability of the initial wearable device to measure the vibration amplitude transmission through the target area of bone on healthy volunteers and provide a baseline of expected vibration amplitudes at target areas of bone.
- Provide design feedback for follow-up studies and assess overall feasibility of design with regards to positioning of the device and delivery/measurement of vibration prior to preliminary clinical evaluation.
- Select one target area of bone from three options namely the distal femur condyle on the medial side, the proximal tibial condyle on the medial side, and the distal tibia at the ankle malleolus on the medial side.

4.1.1.1 Vibration amplitude results

Vibration amplitude at each target area of bone was recorded during the investigations as described in the methodology section (see 3.5 and 3.6) to assess suitability for measurement.

Table 6: Summary of vibration amplitude through target regions University of Strathclyde investigation 1 showing average displacement for each region, standard deviation, error, and upper and lower limits within CI intervals (95% confidence)

Investigation 1	Distal Femur (n = 12)	Proximal Tibia (n = 12)	Distal Tibia (Ankle) (n = 12)
Average Displacement (nm)	**3**	**3**	**15**
Standard Deviation (nm)	0.2	0.8	12.5
Upper Limit (95%)	*3.4*	*4.8*	*39.6*
Lower Limit (95%)	*2.5*	*1.5*	*0 (-10.5)*
Standard Error	0.1	0.2	3.6

This permits a comparison between the vibration amplitudes measured with each application at the sites of interest. The average displacement results highlight the distal tibia as having the highest vibration amplitude, assumed to be due to the ankle bone having little soft tissue between the transducer, the bone and the accelerometer taking the reading. The distal tibia, however, also had the most notable standard deviation, the ankle joint being difficult to maintain an effective contact due to the shape of the malleolus.

The difference in amplitude measured between the distal femur and the proximal tibia was small, as were their standard deviations.

This was encouraging and it indicated that the geometry at the knee both above and below the joint was easier to apply the device to in a more repeatable fashion due to its flatter surface and the presence of more cushioning soft tissue compared to the ankle.

The amplitudes measured at each region are compiled into the graph in Figure 35:

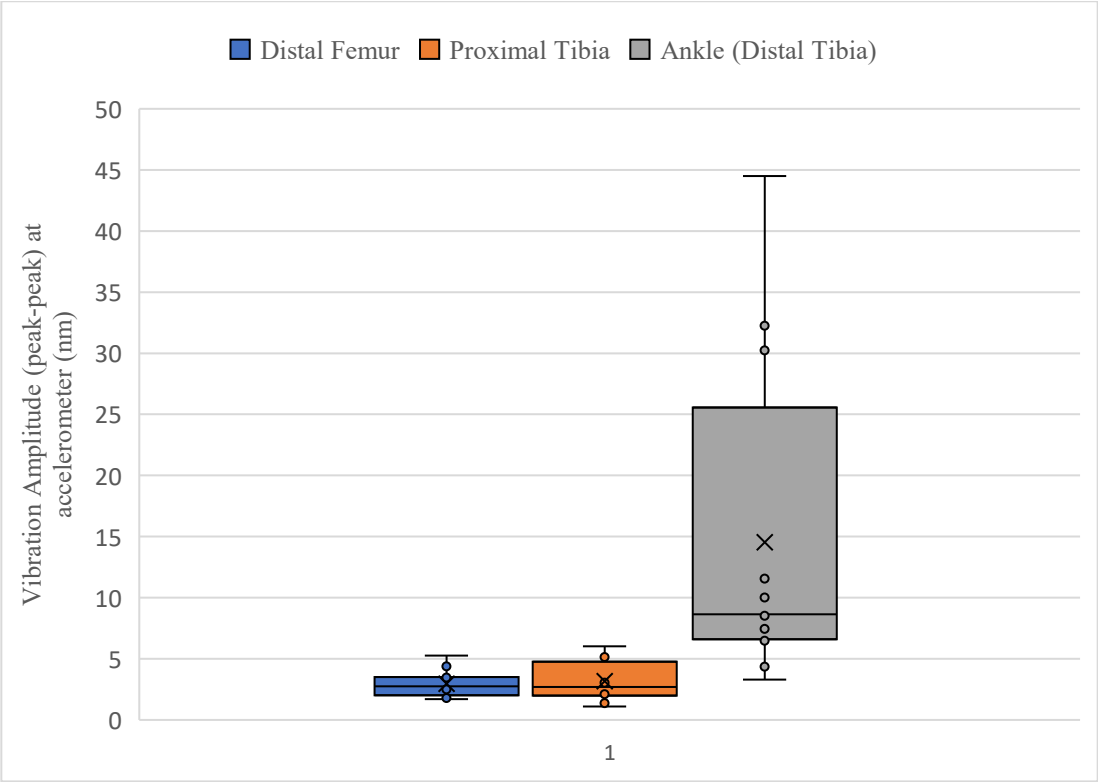

Figure 35: Investigation 1 vibration amplitudes at the distal femur, proximal tibia, and ankle (distal tibia) (nm) with standard deviation bars (n=12) displaying the data points, mean marker (cross), median and interquartile ranges

As can be seen in the graph, the vibration amplitude measured varies with location, particularly between the knee and the ankle which is likely due to a combination of the differences in size and mass of each region as well as the geometry of the surface.

Repeat application experiments showed the device is susceptible to varying ranges of vibration depending on minor changes in application position and surface contact. With regards to the measurements at the ankle, the vibration amplitude varied significantly with each participant, resulting in a wide spread of results. This stemmed from the very complex and angular geometry around the ankle, as well as the awkwardness of being able to apply the chosen transducer element onto the ankle malleolus comfortably.

This resulted in some measurements that were markedly high, whereas others were very low. By comparison, the average transmitted vibration amplitude did not vary significantly between the measurements taken on the distal femur and the proximal tibia ($p = 0.70 > 0.05$). An ANOVA test reveals that the mean at the ankle is significantly different from the other datasets ($p = 0.0009 < 0.05$).

4.1.1.2 Initial design findings of the device – Initial Investigation at the University of Strathclyde

The initial investigation highlighted the following design issues:

- Difficulties in applying the early prototype device at the ankle.
- At the ankle the transducer surface did not appear to conform well to the ankle malleolus.
- The knee device strap used in early stages was cumbersome to attach.
- Positioning the accelerometer without a dedicated accelerometer housing by the investigator was difficult. This involved inserting the accelerometer between the leg and the bandage at the right place and keeping it there.

No difficulties were observed in taking measurements at any location, nor did participants describe discomfort at any given location over the duration of the investigation.

Following the study design changes were implemented, as described in sections 3.3, 3.5, and 3.6 in order to address the noted issues and incorporate possible solutions in a revised design for the follow up investigation.

4.1.2 Follow up Investigation at the University of Strathclyde

4.1.2.1 Refined design of the wearable device

The follow-up investigation shared the objectives from the first Investigation, performed after adjustments to the design; also performed on healthy volunteers to inform the design and feasibility of the study prior to the Preliminary Clinical Evaluation.

The follow-up investigation featured the following changes as described in the methodology section of this thesis. These were:

- A bespoke accelerometer housing
- Adapted knee-support straps
- More rounded edges on 3D printed parts
- Overall shape redesign

4.1.2.2 Vibration amplitude measurements

The follow-up investigation followed the same procedure as the initial investigation.

All participants had a vibration measurement taken at each site of interest. A summary table of the vibration amplitudes, standard deviations and standard error calculated in the same way as in Investigation 1 is shown below in Table 7. The stability of each location was taken by normalising the standard deviation against the mean vibration amplitude at that region; a smaller number represented a narrower relative range. The vibration amplitude used for this set of results was 1000 Hz

Table 7: Summary of vibration amplitude through target regions University of Strathclyde follow-up investigation 2 showing average displacement for each region, standard deviation, error, and upper and lower limits within CI intervals (95% confidence)

Investigation 2	Distal Femur (n = 9)	Proximal Tibia (n = 9)	Distal Tibia (Ankle) (n = 9)
Average Displacement (nm)	2.4	1.0	0.5
Standard Deviation (nm)	0.7	0.6	0.6
Upper Limit (95%)	*3.9*	*2.3*	*1.6*
Lower Limit (95%)	*1.0*	*0 (-0.3)*	*0 (-0.7)*
Standard Error	0.1	0.1	0.1

The investigations found a change in the range of vibration amplitudes measured by the accelerometer compared to investigation 1, and the overall reduced standard deviations permitted the observance of significant differences between the means of each dataset.

Whilst the vibration amplitude on average decreased for each location measured, the vibration deviation narrowed noticeably in terms of standard deviation and standard error.

An ANOVA test performed on the datasets reveals that there was a significant deviation from the mean ($p = 0.0014 < 0.05$). Subsequent paired t-tests reveals that there was a significant difference in the results measured at the distal femur and proximal tibia ($p = 0.039 < 0.05$), a significant difference between the distal femur and ankle ($p= 0.007 < 0.05$) and no significant difference between the proximal tibia measurements and the ankle ($p = 0.08 > 0.05$).

The results from the second investigation show that the vibration amplitude for each region decreased, whilst the standard deviations at each region also narrowed.

This is believed to be due to the application of the device being more streamlined, resulting in less variation in measurements between each application.

Between the initial and follow-up investigation, the redesigned ankle harness was altered to more rigidly constrain the transducer and accelerometer in place as described in section 3.4.2 in order to reduce the variability in measurements at the ankle. However, whilst variation was reduced, there was also considerably lower vibration transmission measured than in the initial investigation. This is thought to be due to an inability to secure a proper contact region between the transducer and the malleolus due to the redesigned harness. As the harness was designed to help ensure a repeatable application compared to the initial investigation, it was as a result more rigid, which restricted its ability to deform in response to the shape of the malleolus and made it less accommodating to varying geometries of the ankle and foot. Whilst this helped apply the device in a more repeatable fashion, it exacerbated the problem of getting a poor contact region between the malleolus and the ankle, thus resulting in vibration amplitudes that were considerably lower than what they otherwise could have been.

The follow-up investigation graph of results, for which the peak-peak amplitudes were also averaged at each site and standard deviation bars added, is shown below in Figure 36. Outlier points are included for reference.

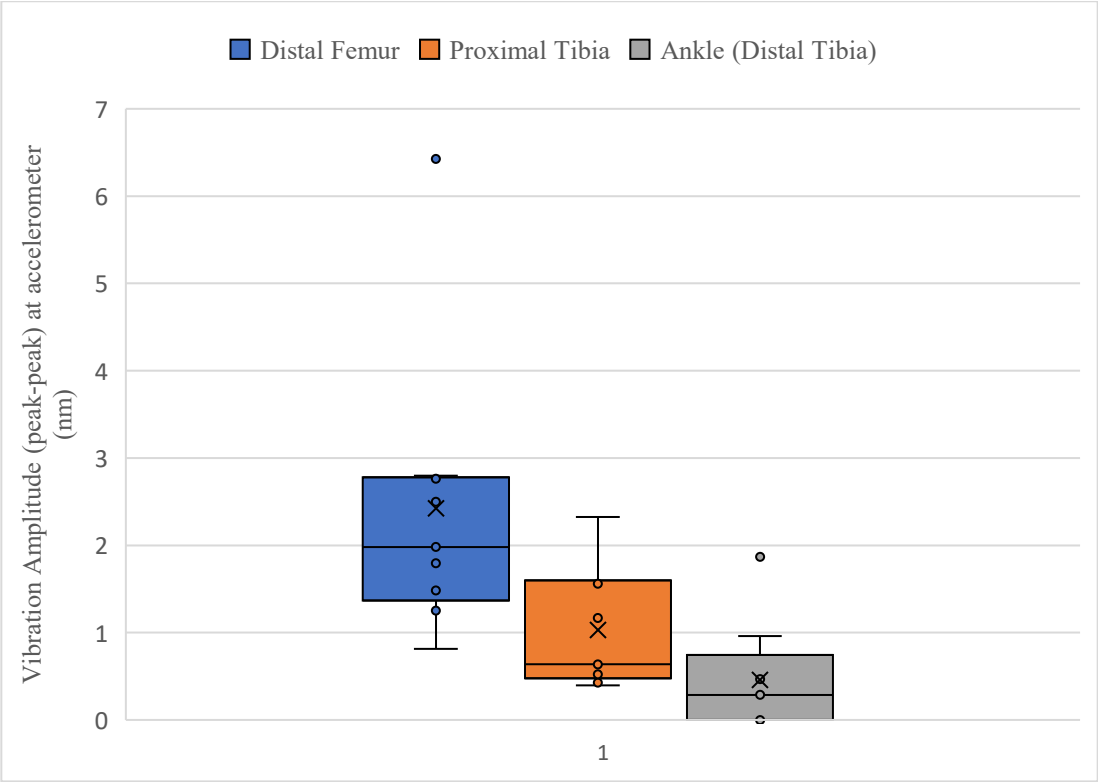

Figure 36: Follow-up investigation vibration amplitude at distal femur, proximal tibia, and ankle (distal tibia) with standard deviation bars (n = 9) displaying the data points, mean marker (cross), median and interquartile ranges

4.1.2.3 Follow up design results

The follow-up investigation highlighted the following design issues:

- It was found to be easier to apply the device to the knee and ankle repeatably due to the improvements in design.
- The rigid 3D printed ankle harness was not as successful as the more flexible harness in delivering comparable levels of nanovibration to the ankle region, likely due to improper contact between the transducer and the malleolus geometry.
- The accelerometer housing rendered it much easier to get consistent nanovibration measurements during the investigation.

These design findings were used to inform further design changes to the device as it was used during the Preliminary Clinical Evaluation.

4.1.3 Summary of Investigation Results

The initial and follow-up investigations at the University of Strathclyde investigated the following results:

- Test the initial wearable device to measure the vibration amplitude transmission through the target area of bone and provide a baseline of expected vibration amplitudes at target areas of bone.
- Provide design feedback for follow-up studies.
- Select one target area of bone from the distal femur condyle on the medial side, the proximal tibial condyle on the medial side, and the distal tibia at the ankle malleolus on the medial side.

This section details the results pertaining to the early investigations at the University of Strathclyde to include the vibration amplitude readings from the original and follow-up investigations as well as comments on the design that were used when altering the shape and applicability of the device.

4.1.3.1 Vibration Amplitude

To provide a comparison of the vibration amplitudes, the initiation investigation and the follow-up investigation results have been compiled side by side below in Table 8. The vibration amplitude used for this set of results was 1000 Hz.

Table 8: Summary of results from the initial and follow-up investigations, showing the highest vibration region and most stable amplitude region for each investigation

Finding	Initial Investigation	Follow-up Investigation
Highest vibration amplitude region (average)	Distal tibia (14.5 nm)	Distal Femur (2.4 nm)
Most Stable (lowest standard error)	Distal Femur (0.0)	Distal tibia (0.1)

The stability of each location was taken by normalising the standard deviation against the mean vibration amplitude at that region. In order to assess how effectively the device was able to deliver a consistent vibration at each site of interest, the standard error and average vibration amplitude were evaluated. It was considered advantageous for the vibration amplitude to be higher at the measured position, as well as having less variation between measurements on a given site; a smaller number would represent a narrower relative range and a site more conducive to a repeatable application. All vibration values measured at the accelerometer are below those used in in-vitro experiments (30 nm on average as described in section 2.8); at the stage of device development at which the Investigations took place, it was believed that vibration within the bone region would be higher within the bone than at the accelerometer surface due to losses from transmission/reflection and attenuation. However, as the priority for the human-wearable device was to establish a repeatable and stable vibration that was measurable during use, this was considered acceptable for the objectives of the study.

The most noticeable result is the reduction in vibration amplitude in the distal tibia as well as the increased stability of this measurement.

Whilst the vibration amplitude observed at the distal tibia during the first investigation appears substantially higher, the unpredictable nature of the vibration amplitude between applications rendered it unsuitable compared to more stable regions, and following redesign in order to assist repeatability was also described by participants as being uncomfortable for short durations of application. Irrespective of vibration amplitude, this target region was deemed unsuitable for further investigation.

Following redesign, the distal femur exhibited higher amplitudes in a comparatively repeatable manner to the proximal tibia and was therefore determined to be a valid compromise between vibration amplitude and repeatable applications and measurements. No negative feedback relating to comfort was supplied at this stage.

4.1.3.2 Design Considerations

Following the investigations, it was clearly viable to design a wearable device that could deliver, at the proximal tibia and distal femur regions, a repeatable vibration on the nanometre scale that could be measured at the opposite side of the target area of bone using an accelerometer during the application. The device needed to be applied carefully, as it remained susceptible to application variation, but using a custom-made housing the device was able to be applied to the leg comfortably and without irritation over the investigation duration, which built confidence in a device capable of delivering nanovibration for longer periods.

It was considered that redesigning the ankle harness with a material less stiff and rigid (which would necessitate moving away from the 3D printed prototyping technology available at the University of Strathclyde Biomedical Engineering Department) or designing each ankle harness around the geometry of each individual participant might be avenues to explore in terms of adapting the device to suit the ankle, however for the purposes of the project the ankle was abandoned as a possible application zone. It was decided to focus primarily on the distal femur condyle as a target region.

The accelerometer housing was incorporated in the later prototypes (as described in section 3.4.2) in order to provide information about the vibration amplitude being delivered. Given that the vibration present in the limb was determined by the consistency of application and the contact between the transducer surface and the limb, the accelerometer provided a feedback system to adjust either the position of the device or the output of the transducer, increasing or lowering the vibration amplitude.

Based on the measured vibration amplitudes during the investigations, it was decided that 2 nm was an achievable target value to use in the subsequent preliminary clinical evaluations due to expectations that it would be repeatably measurable, thereby serving as an acceptable target for users to aim for in order to gather information regarding the feasibility of delivering vibration at consistent levels for extended durations.

The final modifications as a result of these investigations were:

- a detachable mono cable that would power the transducer at the 1000 Hz frequency
- the straps were labelled to help the device be consistently correctly oriented
- a custom-build electric box was issued with the device to supply the transducer with power and read the accelerometery data, store it, and adjust the vibration amplitude
- an indicator of whether the vibration amplitude was close to the target amplitude (2 nm) was also present on the box, displaying a red light if the device was out of range and a green light if it was between 1.5 nm and 2.5 nm and consequently requiring adjustment.

This was the set-up of the device issued to a participant during a preliminary clinical evaluation at the Queen Elizabeth University Hospital Glasgow, Spinal Injuries Unit as described in section 3.7, the results of which are presented below.

4.1.4 Preliminary Clinical Evaluation Results

Sections 4.1.4.1 shows the vibration amplitude results from the preliminary clinical evaluation and the outcomes for the design and development of the prototype device. Accelerometry data was collected over 60 sessions lasting up to two hours per session.

At the start of the study, two participants were recruited, however only one participant successfully completed the clinical trial due to several factors. For this reason, only feasibility of use and stability of vibration amplitude delivery can be assessed; clinical efficacy cannot be determined from this study.

Limitations in recruitment were considered to be partly due to the narrow criteria for the selection of potential participants as they were required to be recent SCI patients and significantly due to the intervention of COVID 19 arresting all patient contact.

4.1.4.1 Vibration measurement

The accelerometery data collected during the 60 sessions is shown in the following graphs. The aims of the sessions were to:

- confirm that vibration was transmitted effectively through the target area of bone from the transducer to be measured on the opposite side of the bone via the accelerometer and recorded for subsequent analysis.
- determine the consistency of the vibration delivered to the target area of bone during the sessions and aggregated over all sessions
- validate the viability of using a wearable device for delivery of therapeutic vibration.

As stated in the methodology section, BMD results were not collected as part of the preliminary clinical evaluation due to low participant turn-out. The results presented in this section are used to assess the feasibility of the device as a potential nanovibration delivery device only.

In summary, the vibration sessions performed by the participant can be seen in the following table.

Table 9: Summary of animal trial session characteristics

Number of Sessions:	60 Sessions
Mean Session Duration (Standard Deviation) (hours/min):	1 hour 57 minutes (37 minutes)
Total Device Use (hours):	119 hours
Mean Vibration Amplitude Measured (Standard Deviation) (nm):	2.1 nm (0.5 nm)

The results are shown in the following graphs to visualise the specific data recorded over the course of the study. The first graph below in Figure 37 shows the session duration for each session; as can be seen, the participant was unable to perform the sessions for the anticipated length of four hours, and was limited to using the device for up to 2 hours for the majority of the sessions. This is consistent with the participant data log.

On average, the session duration was 117.4 minutes long (1 hours and 57.4 minutes), and had a standard deviation across all sessions of 34 minutes. This was notably below the initial target of 4 hours; following session 19 it was agreed to let the participant limit the use to 2 hours per session to accommodate their ability to participate in the study.

It should also be noted that this is far below the durations of vibration delivered to cells in-vitro (which is done continuously); it should be expected that, were

BMD effects measured as part of the preliminary clinical evaluation, there would be a reduced effect compared to that which is observed in-vitro.

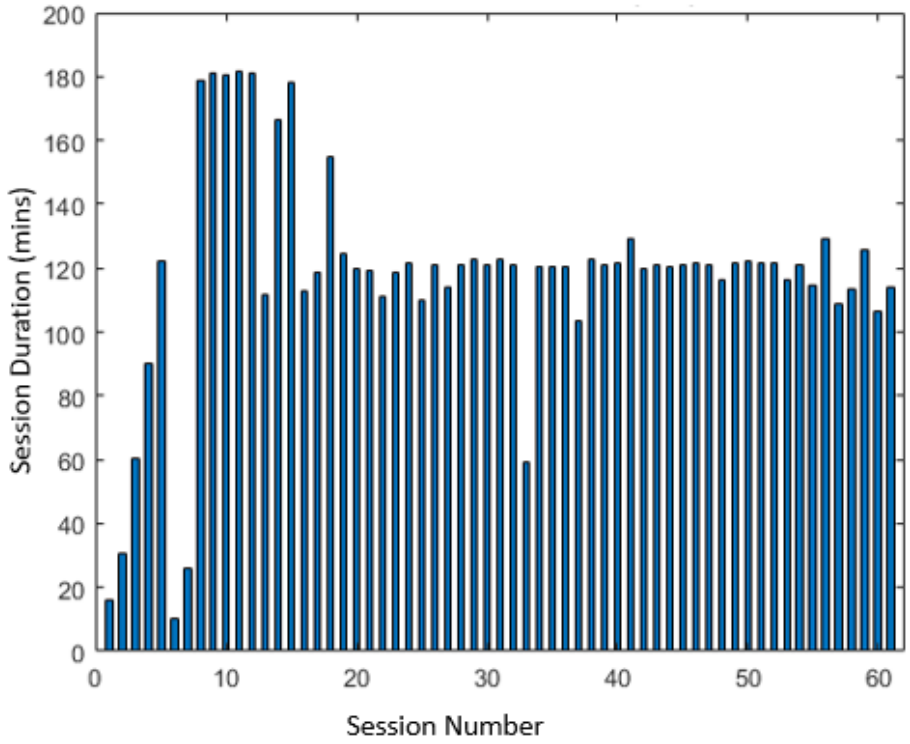

Figure 37: Graph displaying the session duration in minutes for each session recorded during the preliminary clinical evaluation, drawn in Matlab

Following the initial and follow up investigations at University of Strathclyde, 2 nm was established as the target amplitude range for the preliminary clinical investigation. In order to assess the results over the 60 sessions, an average of the recorded amplitudes was taken. This provides a basis for assessment despite the differing lengths of individual sessions. A summary graph of the average recorded amplitude for each session number with the corresponding standard deviation bar is shown below in Figure 38. The overall mean and standard deviations are represented by the red line and black lines, respectively.

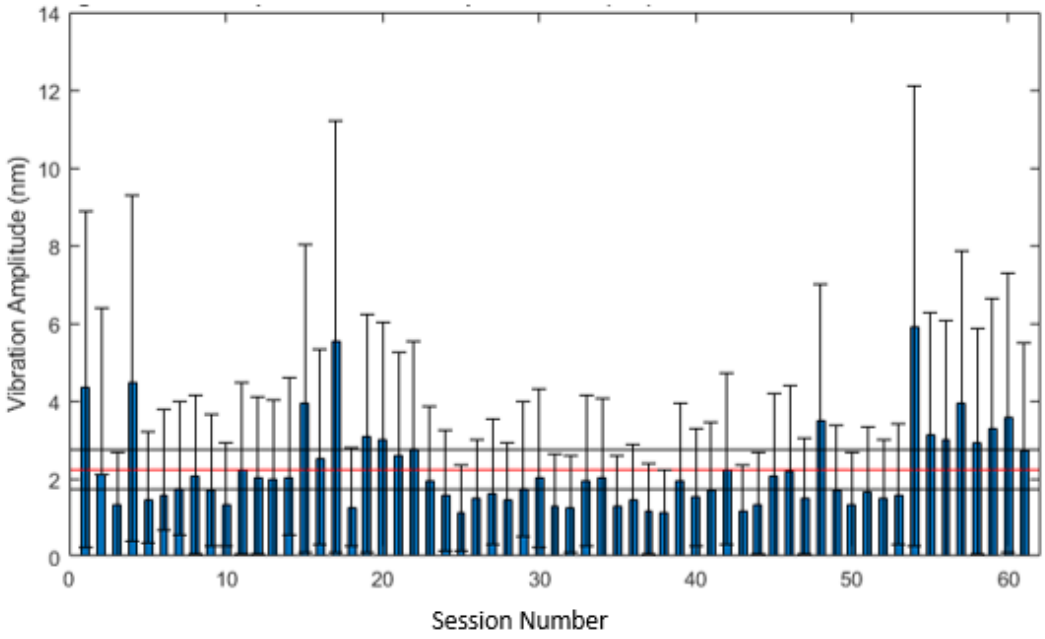

Figure 38: Average vibration amplitude recorded per session (nm) with standard deviation bars. The overall mean and standard deviations are represented by the red line and black lines, respectively, drawn in Matlab

As shown above most sessions recorded a vibration amplitude within the target range (1.5 nm to 2.5 nm). Some sessions recorded a notably higher amount than the average. On average, the overall sessions were on-target, though from the standard deviation per session it can be seen that there was variation in measured amplitude during a session.

The graph in Figure 39 below shows the average recorded vibration amplitude over the session duration, averaged across all sessions at each time-point (black). Also included are the upper and lower standard error boundaries (red). This shows a largely consistent vibration amplitude with significant spikes near the end of the session. The spikes are consistent with the process of increasing the pressure of the device against the skin as the device is detached before tailing off as the device is removed. The vibration passes effectively from the transducer through the bone

to be measured by the accelerometer and the standard error lines (depicted by the black lines above and below the red vibration amplitude line) show a strong degree of consistency in the vibration experienced throughout the session.

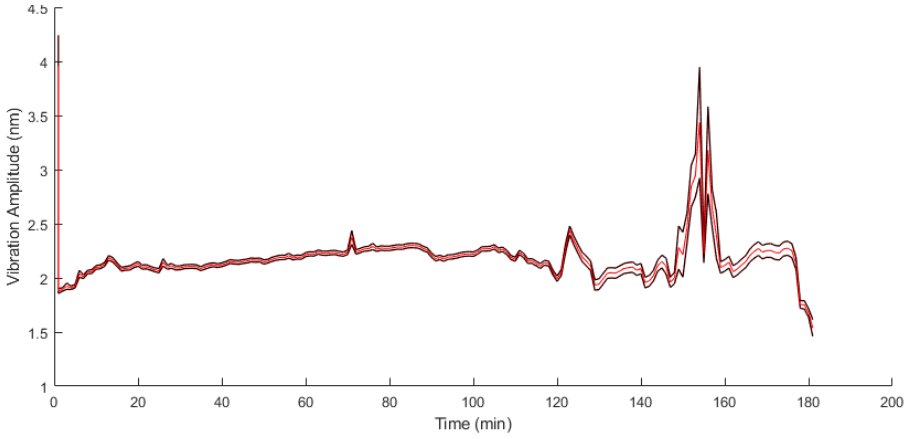

Figure 39: Average vibration amplitude (nm) of all sessions over time during session (min) with standard error, drawn in Matlab

As the participant logged the days on which they used the device, it was also possible to show the overall session duration over time accounting for gaps in

which the participant was not able to perform a session. This plot is shown below in Figure 40.

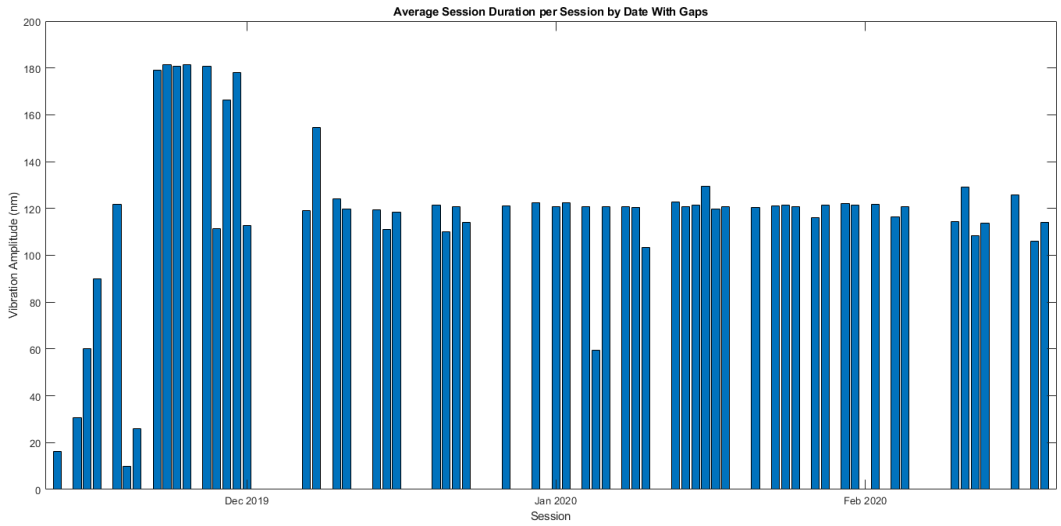

Figure 40: Graph displaying the session duration for each session over time, including gaps between sessions, drawn in Matlab

The results from the preliminary clinical evaluation show that the device transmits from the transducer and is measured by the accelerometer on the opposite side of the target area of bone (in accordance with current understanding of acoustic wave propagation as described in section 2.5.3.2). In order to further establish how the vibration travels through the bone and what effect this may have, results obtained from laboratory-based experiments on bovine bone acting as a proxy for human bone are shown below in section 4.4.

4.1.4.2 Preliminary Clinical Evaluation Design Feedback

Following the preliminary clinical evaluation, valuable design feedback was also acquired regarding the practicality and comfort of the device.

- Applying the device was overall achievable but that the device needed to be adjusted as over the course of hours it would gradually slip or movement would cause it to require re-adjustment.
- The low hum produced by the device made it awkward to use during conversations or around other people which limited both the duration of its use as well as when it could be worn during the day by the participant.
- As the device was attached to a box measuring the transmissions, it was difficult to move around with the device making it difficult and inconvenient to wear for extended periods of time whilst remaining active.
- The size of the electronics box was noted as a factor in limiting use, as it was difficult to carry around whilst in a wheelchair, and that the device was too bulky to wear underneath trousers.
- The device at times was used when lying down with the leg extended. This was achieved by removing one of the modular arms to allow for the leg to extend. This was achieved successfully without issue for the participant.

In general, the device was described as being usable and able to be handled without significant difficulty by the participant, but that over the course of the initial 4 hour session duration it would restrict activity in its current form. See section 5.1 for further discussion regarding the device design.

4.2 Animal Trial Results

The animal trials results are shown in three sections: device design, nanovibration measurement results and bone mineral density measurement results.

The device design and manufacture was part of this thesis project with the aim of providing a piece of equipment to:

- Provide consistent and controllable vibration for use in the animal experiments.
- Deliver a constant output of vibration to the animal subjects by using the measurement of vibration as a feedback system.
- Observe the effects of vibration delivery on BMD/bone mass.

The nanovibration measurement and bone mineral measurement results were gathered by Dr. Jonathan Williams, who performed the work on the animals using the bespoke nanovibration devices and gave permission for the inclusion of measurement data in this thesis to help demonstrate any potential effect of the nanovibration on bone density.

Overall the study covered the following groups.

Table 10: Summary of animals used in the animal trials per group

Groups:	**Number of animals (n)**	**Vibration Amplitude (nm)**
N40	6	40 nm
N100	4	100 nm
SHAM	6	None
Control	10	None
Average Total Time Duration (h):	79.22 hours	

Not included in the above table are 3 animals lost due to complications related to the SCI surgery, and 1 that experienced a burst bladder. These animals were euthanised and therefore not included in the results.

All twenty-six rats were male and weighed 201 – 225 grams.

Overall no positive effect on BMD and bone health indicators was observed; for the N40 group a significant decrease in bone mass was observed of 3-4% wet mass. This suggests that at the doses delivered there was no beneficial impact, and potentially may cause harm to bone health; this is discussed further in section 5.2.

If any other effect was present following the vibration sessions, it was too small to be detected by this study, which was not powered to detect such small differences.

4.2.1 Design and manufacture results

The device for the animal trials was designed and manufactured as shown in section 3.8, methodology, figure 28 and 29. Feedback relating to the device design was received as follows:

The device fitted closely to the rat hindlimb and was able to be applied and adjusted, fulfilling the design criteria. The intervention required to apply the small device was described as fiddly due to the small size of the straps and the number of applications which were required throughout the trial.

Applying the device could provoke a spastic reaction from the rat when applied similar to hyperflexia which could shift the device away from the target bone area. This necessitated multiple adjustments and care when applying, neither of which were conducive to the smooth application of nanovibration during the trial. This

was resolved by taping the rat hindlimb to the hard surface as shown in Figure 41 below.

Figure 41: Photograph of the Rat Hindlimb, restrained, during the animal trial

4.2.2 Vibration Measurement results

Nanovibration was applied in a controlled and consistent manner as shown in the production of nanovibration measurement results below. By viewing the vibration amplitude during the vibration session, a consistent vibration was delivered successfully as part of the study; the effect of which is described in section 4.2.3.

4.2.2.1 Ability of the device to be used for nanovibration

Nanovibration was applied to the rats in two groups, one using a low amplitude (40 nm) transducer and the second using a high amplitude transducer (100 nm).

The graph below in Figure 42 shows the amount of time spent receiving the nanovibration stimulation for each rat as represented by a number (RXXXX) in a cumulative plot. The cumulative plot was used as rats were replaced if they began to show signs of restlessness.

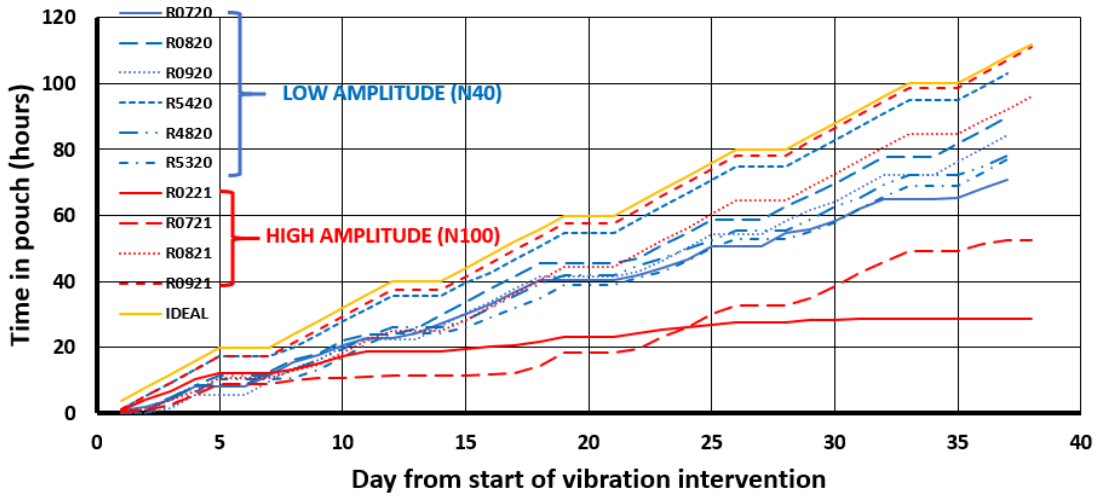

Figure 42: Cumulative time in pouch spent per rat, reproduced with permission from Dr. Jonathan Williams

The designed device was able to be used for up to 4 hours per day. The ideal length of time envisioned is shown by the yellow ideal line on the graph. This proved to be an overestimation of the tolerance for the animals to remain still whilst being measured, which was necessary as the requirement for the vibrations to be measured using an attached accelerometer meant that wire attachments were needed which limited the rat's movement.

4.2.2.2 Effectiveness of the device in applying vibration

Vibration measurements performed on exposed rat bones were performed at the surface of the bone by the interferometer and at the opposite side at the conjunction

of flesh and bone via the accelerometer. These results are shown for each rat in Figure 43 below. These measurements show that the vibration measured at the surface and through the bone at the opposite side correspond, for rats R4720 and R0921 in an almost 1:1 ratio, giving confidence that the vibration was transmitted effectively from the transducer through the bone to be measured by the accelerometer. This is consistent with our understanding that, unless there is a confounding factor not observed in this experiment, that the measurements taken by the accelerometer would be proportional to those observed by laser interferometer.

There were 2 electronics boxes used in this experiment, the use of each box noted with the number 1 or 2 in parentheses on the graph. The second box was capable of outputting a higher degree of voltage amplitude, which was expected to result in a higher transducer vibration amplitude during use. In the case of R0921 (3), this represented an additional repeat measurement after removing and reapplying the device using the higher output electronics box.

Both R1200 and R0920 only used the lower amplitude box.

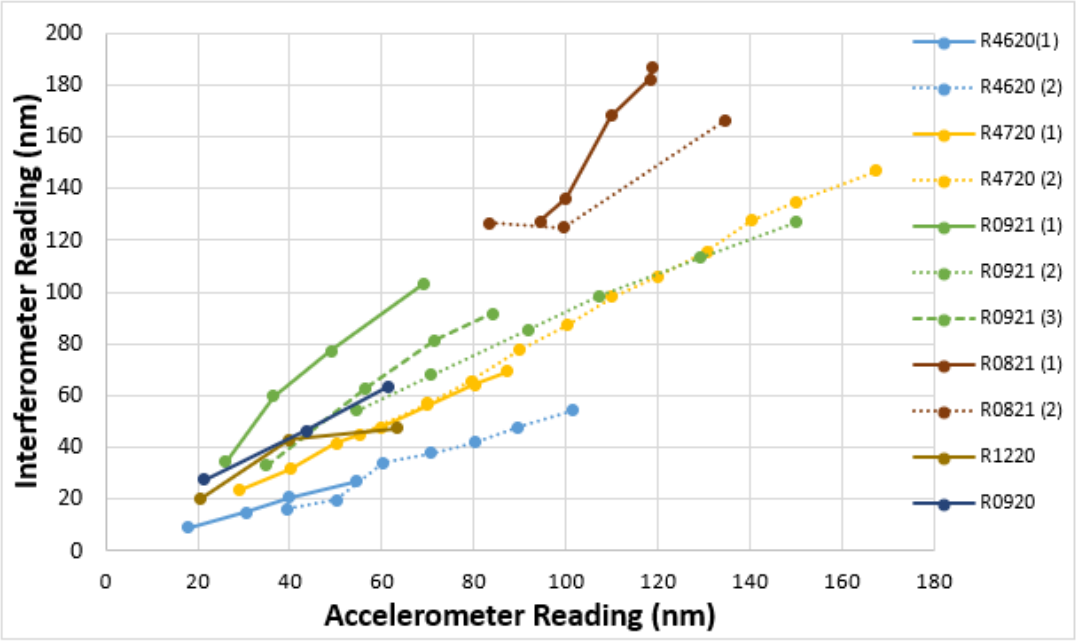

Figure 43: Vibration Amplitude as recorded by laser interferometer over Accelerometer reading for various rats, reproduced with permission from Dr. Jonathan Williams

The above results provide confidence that the vibrating devices were capable of delivering vibration at the intended amplitudes throughout the study for the durations specified, thereby enabling the assessment of the effect of said vibration on bone health.

4.2.3 Bone mineral density results

The aim of the animal trial was to measure any effect on vBMD from applying nanovibration to the rat hindlimb. To achieve this, one hind limb was subject to vibration, the other acted as a control. Trabecular bone volume (BV/TV), trabecular bone thickness (Tb.Th), trabecular spacing (Tb.Sp), connectivity and volumetric bone mineral density (vBMD) are assessed following acquisition of the micro-CT scans as described in 3.9, with vBMD considered as the primary outcome. In addition, wet mass and bone areal fraction over the percentage length of the bone are also shown in this section. The results are shown below.

4.2.3.1 Bone mineral density measurements - vibrated bone vs. control

The mean morphometric outcomes of the animal trial are shown below in Figures 44 and 45, for the 40 nm amplitude and 100 nm amplitude animals respectively (N40 and N100). These are shown against a control (the contralateral limb). The metrics displayed in the below graphs are derived from the micro-CT scans. An example of a typical vibration amplitude measurement over the course of a vibration session is also supplied below.

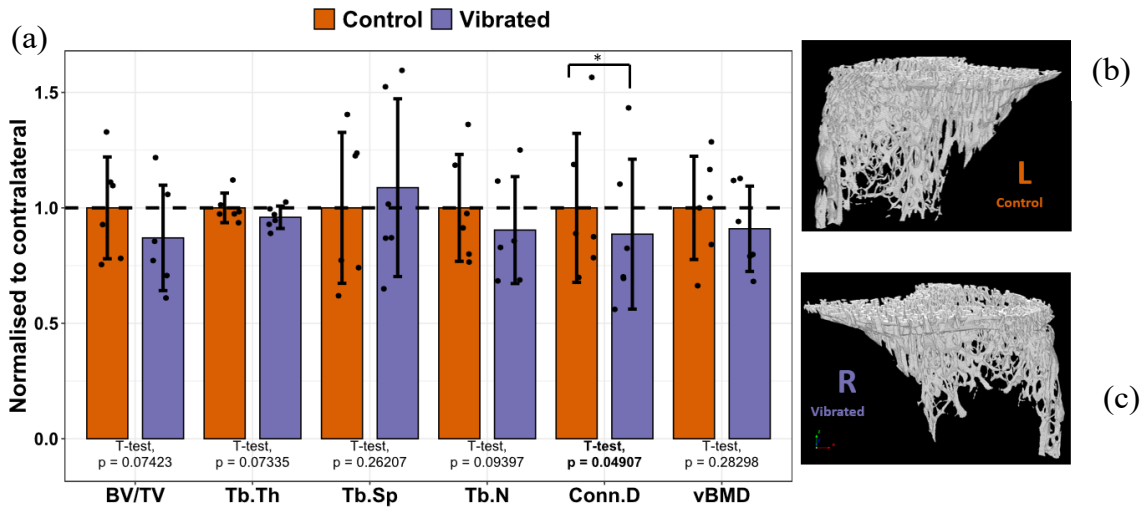

Figure 44: Control vs. vibrated morphometric outcomes for the N40 group of rats; data shown as mean normalised to the control limb values, shown with standard deviation bars (a), a 3D rendered image of generated from the micro-CT scans representing the control leg (b) and the vibrated leg (c)

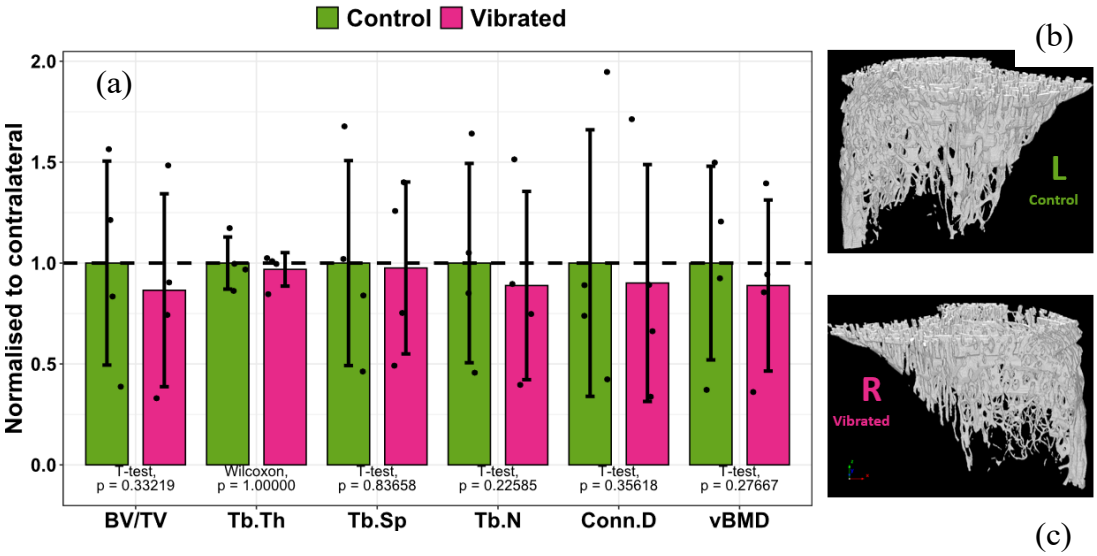

Figure 45: Morphometric outcomes in the N100 group of rats shown as mean normalised against control values, shown with standard deviation (a) and a 3D rendered image of generated from the micro-CT scans representing the control leg (b) and the vibrated leg (c)

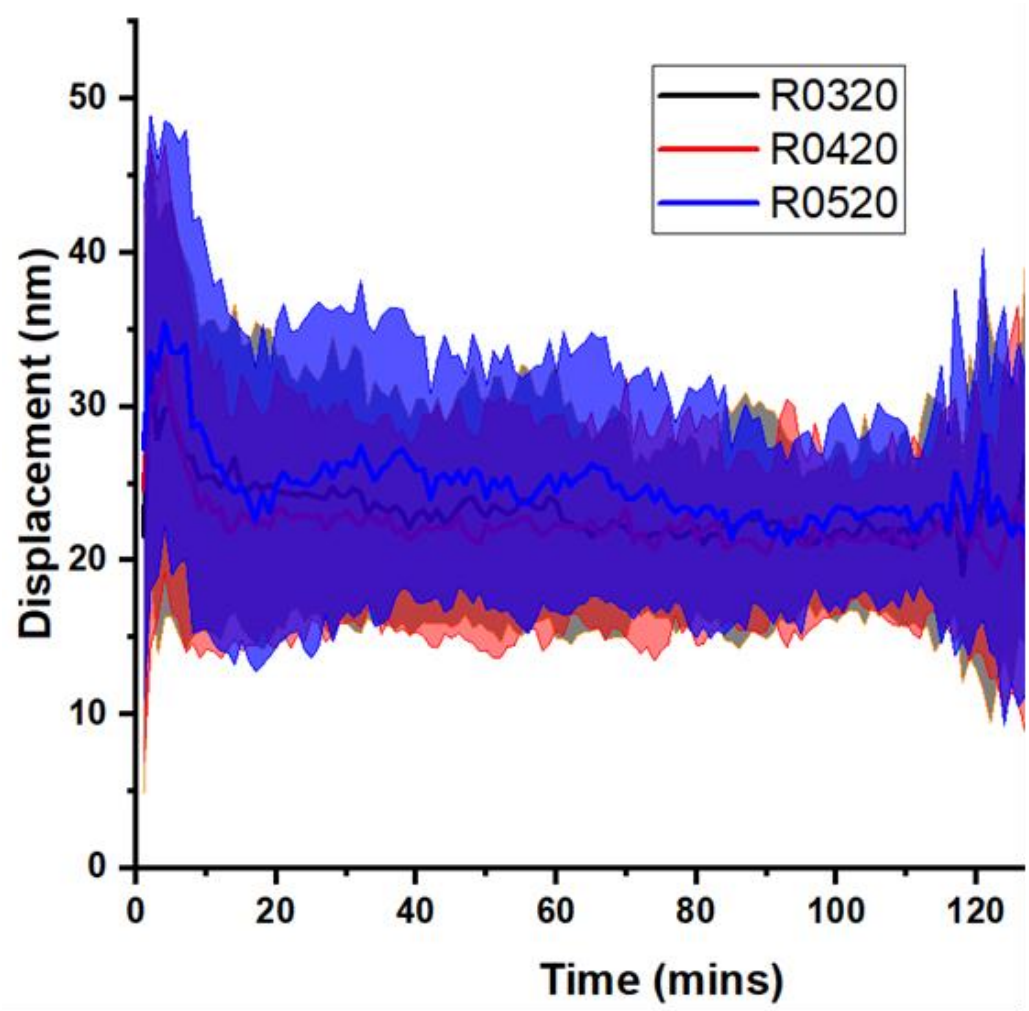

Figure 46: Typical vibration amplitude measurement over the course of a vibration session for 3 animals, superimposed

4.2.3.2 Bone mass measurements vibrated bone vs. control

In the graphs below (Figures 47 and 48), the bone wet mass of the measured hindlimbs is shown, comparing the average vibrated limb bone mass of the tibia and femur against the control limb bones with standard deviation bars to show any observable differences in bone mass per group of rats. These show a decrease of 3% ($p < 0.05$) in bone mass for the N40 group and 4% ($p < 0.01$) in wet bone mass for the N100 group, and no differences were observed in the other groups in terms

of whether the effect of nanovibration intervention reversed the effect of established SCI induced osteoporosis.

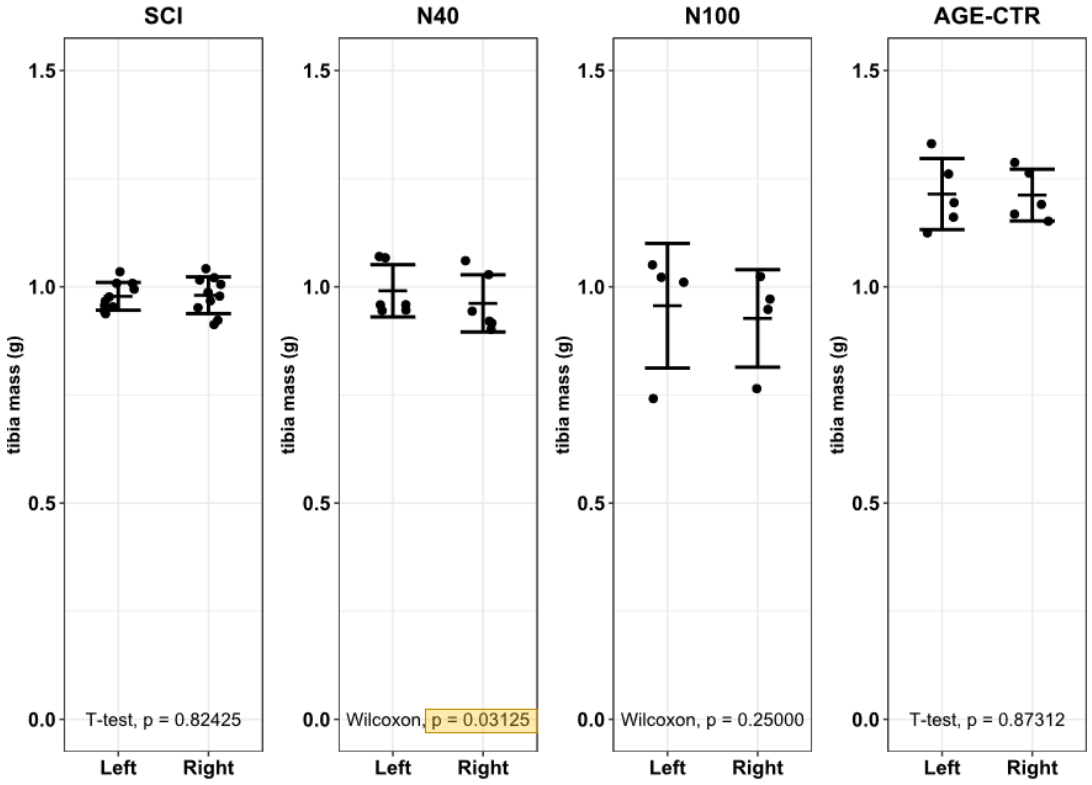

Figure 47: Tibia wet mass for all experimental groups

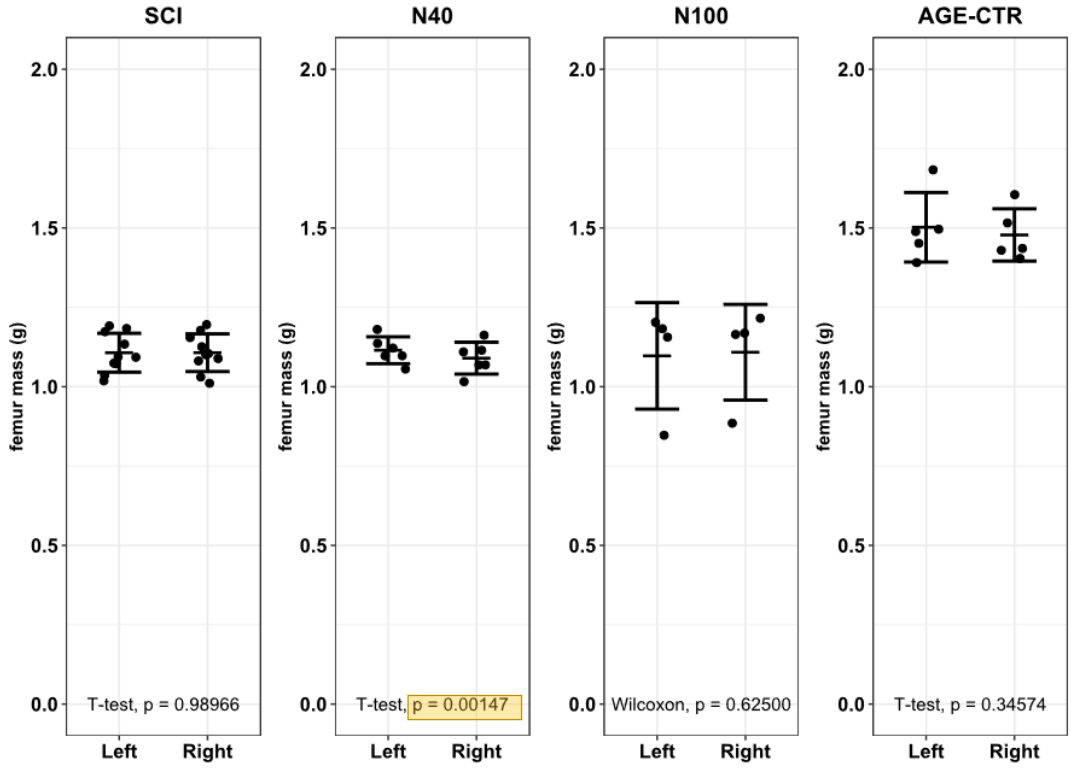

Figure 48: Femur wet mass for all experimental groups

Shown below in Figure 49 is a graph plotting the fraction of trabecular tibia bone area measured via micro-CT scanning from the distal to proximal end of the bone. For comparison, both the vibrated and control legs are shown. This is displayed as a bone area fraction (%), which is given as the proportion of bone present within a cross-sectional 'slice' of the leg, to show the proportion of trabecular bone present at a given area relative to the overall area of the leg.

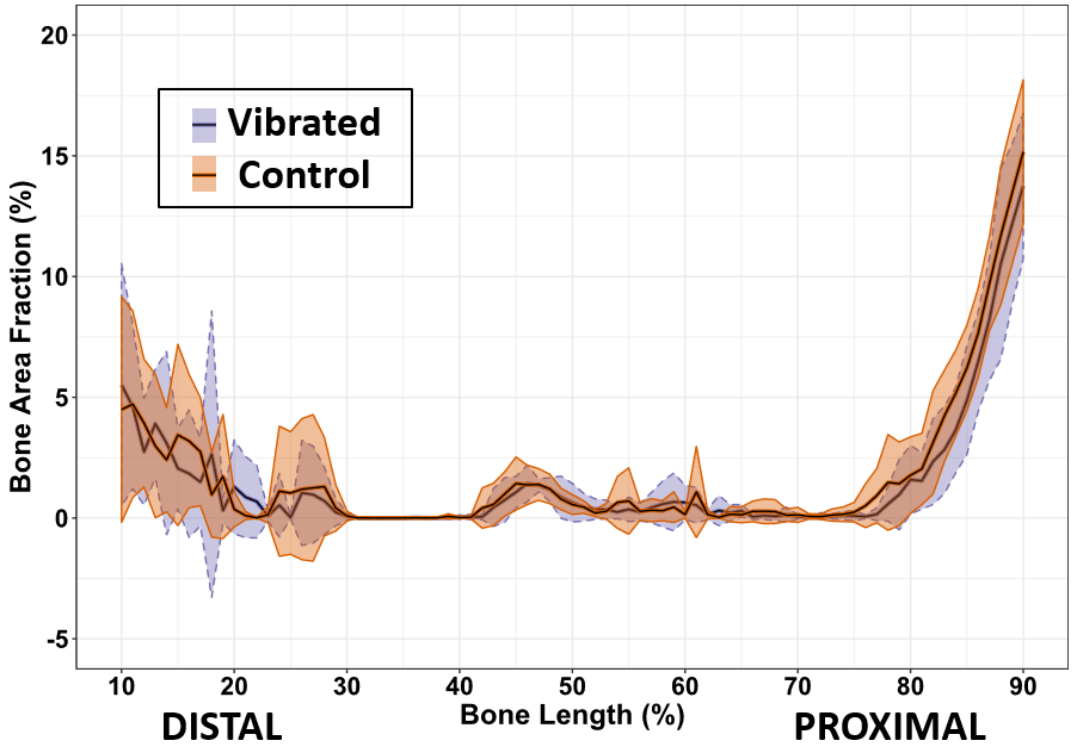

Figure 49: Bone Area Fraction across length of bone in % of bone length of the vibrated and control rats, with standard deviation

The trabecular bone area fraction distribution across the length of the tibia was measured between 10 and 90% of the total bone length as shown. No significant differences were observed between the control and vibrated trabecular bone area fractions. For context, a bone with a higher degree of bone present at each 'slice' taken along the length of the bone would display a higher bone area fraction at that percentage of bone length.

In summary, whilst the device used was capable of delivering vibrations at the expected amplitudes, no measurable effect on bone health was observed from this study. See section 5.2 for further discussion.

4.3 FEA Analysis Results

This section aims to complement the preliminary clinical evaluation and the animal trial experiments to understand how nanovibration is transmitted through bone, soft tissue and via the transducer to introduce vibration to the target area at the magnitudes anticipated in practice and over a frequency range of 500 to 5000 Hz. In addition, the harmonic response of bone was visually represented to show how intensely vibrations are transmitted into and through the bone. Due to the complexity of the bone region and the inability to directly validate the model, the FEA modelling results presented here should be used to gain an understanding of the behaviour of bone in a qualitative sense to inform later results rather than provide quantitative numerical predictions of vibration amplitude change through the bone region.

Results from the FEA harmonic response analyses were taken from the 1-D analysis through the axis of the transducer element model, organised by experiment type as described in the methodology section 4.3.1 and are shown below as resolved by Ansys 17.0.

To enable comparison with results from subsequent bovine distal femur experiments (see section 4.4.2), the frequencies examined were 500 Hz, 1000 Hz, 2000 Hz, 4000 Hz, and 5000 Hz. The variable assessed is directional deformation in the direction of vibration being applied (displayed in metres, as computed by Ansys Workbench). From these analyses, the average vibration amplitude was calculated. The average was then normalised in order to facilitate comparison between results at different amplitudes.

Due to the nature of the simulation, a statistical analysis was not performed on these results, as a simulation is by nature non-statistical.

In order to identify dominant factors that affect the vibration amplitude in the bone, simulations were carried out using three basic shapes for models; a simple block (cube), an armed block and a femur shape, to gain an initial understanding of how transmission is affected by the following progressive changes:

- changing the model shape
- representing variations on internal material properties with a lower-density bone region
- including a disc model of the transducer element
- including a soft tissue proxy between the transducer element and the bone model.

4.3.1 Effect of Model Shape and Composition on Vibration Amplitude

The model shape of the distal femur was made increasingly complex as described in the methods section 3.10.1 in order to model the transmission of nanovibration through the complex structure of bone. Additional modelling features were added to further replicate a realistic simulation, such as a separate model for the transducer and a soft tissue disc added between the transducer model and the bone model. Each combination of features was simulated separately as displayed in the table below in order to identify which features caused the most notable effects on vibration amplitude.

The results for a frequency of 1000 Hz are shown in the table below. A complete list of model types and frequency measured is shown in Appendix 4.

Table 11: Table of Average Amplitudes, Normalised and Absolute, as measured during the FEA simulation at 1000Hz

Simulation Type	Average Amplitude (m)	Normalised Amplitude (against x 1 x 10^{-6})
Block Model, Single Material	**1.01 x 10^{-6}**	*1.012*
Block Model, Composite Material	**1.01 x 10^{-6}**	*1.006*
Block Model, Single Material, Transducer Model Only	**1.02 x 10^{-6}**	*1.021*
Armed Block Model, Single Material, Transducer Model Only	**1.01 x 10^{-6}**	*1.008*
Armed Block Model, Composite Material, Transducer Model Only	**1.01 x 10^{-6}**	*1.006*
Femur Model, Single Material, Transducer Model Only	**1.04 x 10^{-6}**	*1.037*
Femur Model, Composite Material, Transducer Model Only	**1.02 x 10^{-6}**	*1.023*
Block Model, Composite Material, Transducer & Soft Tissue Model	**1.23 x 10^{-8}**	*0.012*
Femur Model, Single Material, Transducer & Soft Tissue Model	**3.01 x 10^{-7}**	*0.301*
Femur Model, Composite Material, Transducer & Soft Tissue Model	**1.63 x 10^{-9}**	*0.002*

To highlight the effect of the model setup on vibration amplitude visually, the following graphs are shown below, displaying both the average amplitude and the normalised amplitude. The most notable element in the results is the effect the soft tissue proxy had in reducing the vibration transmission. This is shown more clearly in the graphs below (Figure 50) as the drop in transmission following the

introduction of soft tissue proxy to the model is clearly evidenced. This has implications for using nanovibration to affect target areas of bone which are covered in soft tissue.

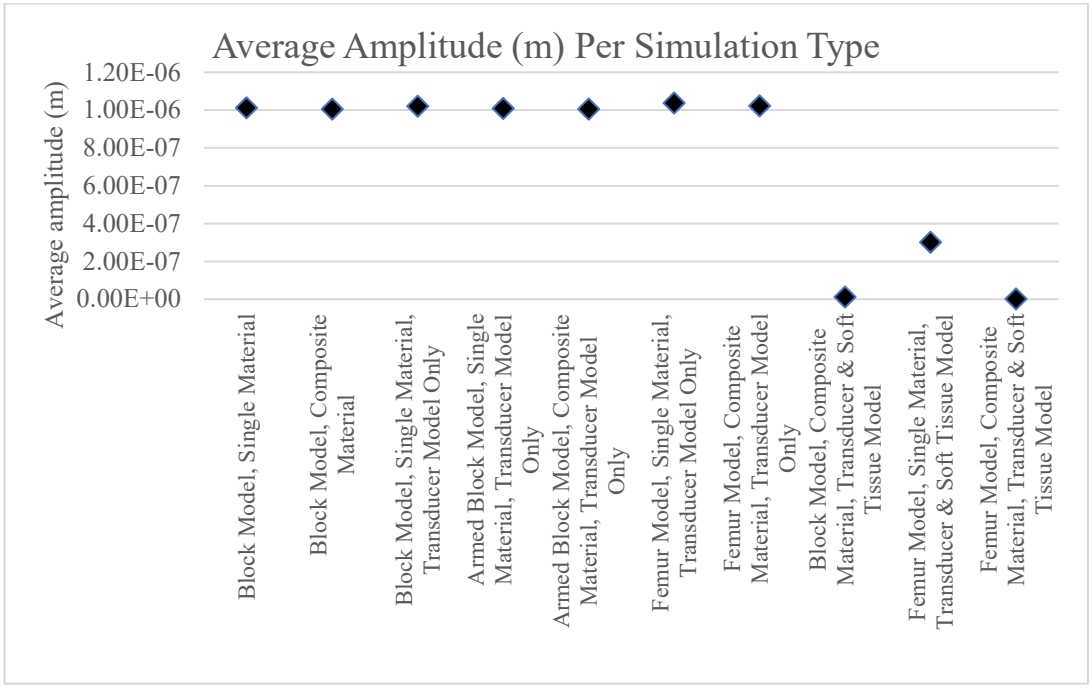

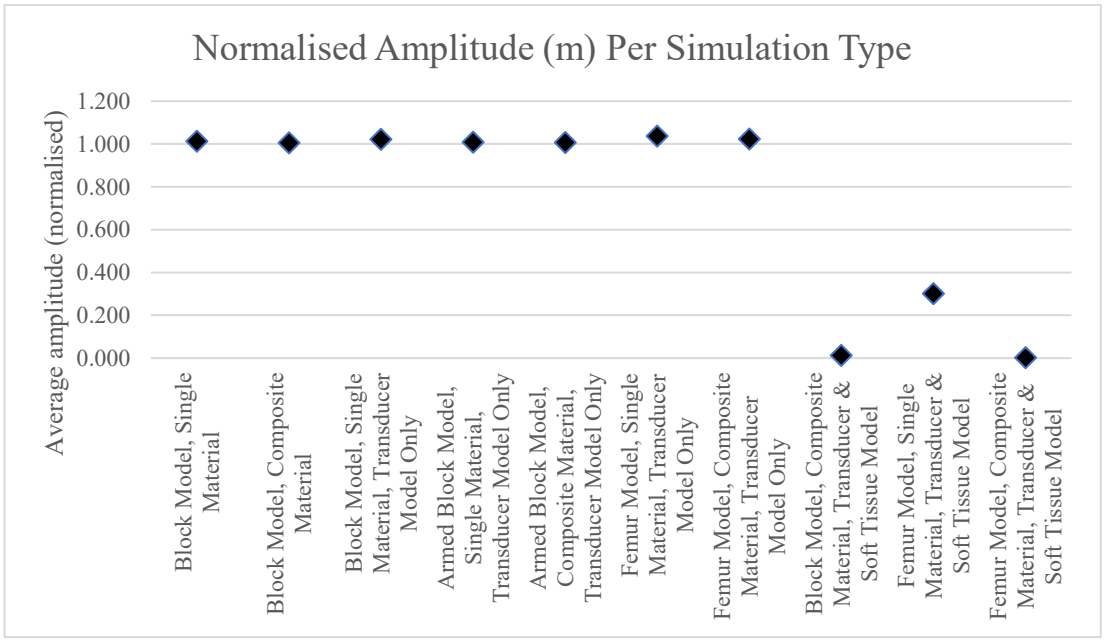

Figure 50: Average and normalised average amplitudes per simulation type showing change in simulation result with added complexity elements

In addition to observing the effect of varying model setups on vibration amplitude, the effect of frequency is also summarised in the following table 10. The results for the composite femur model with transducer disc and soft tissue layer are shown to investigate how vibration amplitude is affected over the range of frequencies applied.

Table 12: Table of Simulated Amplitude and Normalised Amplitude per frequency for the Femur Model, Composite Material, Transducer and Soft Tissue

Simulation Type	**Frequency**	**Average Amplitude (m)**	**Normalised Amplitude (against x 1 x 10^{-6})**
Femur Model, Composite Material, Transducer & Soft Tissue Model	500	**1.01 x 10^{-8}**	0.010
	1000	**1.63 x 10^{-9}**	0.002
	2000	**1.01 x 10^{-8}**	0.010
	4000	**1.62 x 10^{-8}**	0.016
	5000	**1.75 x 10^{-9}**	0.002

Based on the results, which line up in an approximate manner to results observed in section 4.4, some conclusions can be drawn:

- The primary source of vibration amplitude reduction is expected to be transmission between hard and soft media.
- Only minor changes in overall amplitude were observed by changing the geometry, although the distribution of vibration amplitude is altered visibly by differing geometries.

- No resonant effects were observed within the vibrations examined in this study.

Whilst direct numerical comparisons should be treated with caution, the results would indicate a decrease in vibration amplitude from the transducer to the target region of bone of a factor of approximately 500 and 1000; this means that for every μm of vibration at the transducer, approximately 1 - 2 nm is expected to be observed within the bone region for bones of comparable size as those included in this FEA study.

Of relevance to the animal study is the observation that vibration amplitude is not lost in a significant manner within the bone region itself, indicating that a vibration amplitude measured on the bone surface will correspond approximately to the vibration amplitude within the bone, even within the trabecular region; this supports the animal studies performed by indicating that the vibration delivered and observed on the bone surface (see figure 43) was delivered to the bone interior regions as intended.

4.3.2 Visualisation of Vibration Transmission using FEA Heat Map

The mathematical FEA modelling indicated an inconsistent transmission of vibration through the CAD models created. In order to visualise how this would typically appear during the simulations, a heat map was created to allow the simulated wave transmission to be observed.

The following illustration (Figure 51) is of the vibration model on the composite armed block model with transducer element assuming a ‘fixed’ constraint on the base of the arm to represent the bone being held in place at the cortical shaft. This

shape gives the clearest visual representation of the vibration transmission in the model.

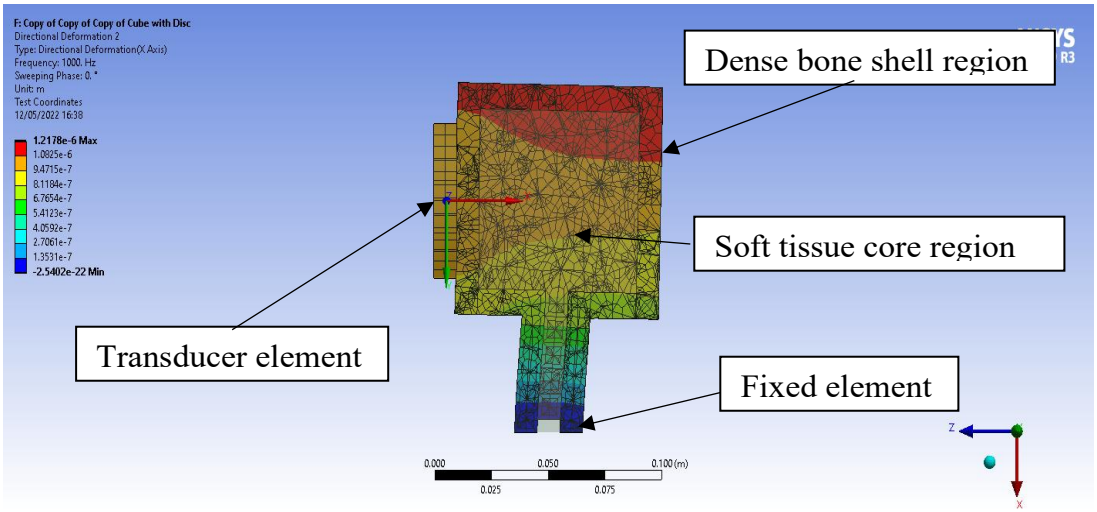

Figure 51: Cross-sectional view of Ansys frequency response of a simplified bone model with a composite structure of trabecular and cortical material regions, transducer element, and femoral shaft at 1000 Hz

The heat map provides a visual representation of the variety of transmission amplitudes experienced within the shape. The fixed element of the model experiences the lowest transmission of vibration amplitude as shown in the image above, and the area which experiences the highest vibration amplitude is shown by the red area at the top of the shape, unattached, above the level of the transducer and with a higher level of transmission amplitude than the area directly adjacent to the vibration source.

These results highlight the variations in measurements between vibration frequencies and geometrical complexities. It can be seen from the summary table that shapes with added geometrical features, such as differences in material properties between regions (for example the two regions in a composite block model, or the soft tissue and transducer element regions) had the effect of reducing

the vibration amplitude returned by the simulations; this indicates, in accordance with our understanding of vibration transmission, that boundaries between low-density and high-density regions will reduce vibration amplitude, which would constitute a challenge for ensuring that the desired vibration amplitude is present at the target region. As frequency increases it was also shown to alter the vibration amplitude measured, albeit in an inconsistent manner; it is therefore expected that frequency will affect the output vibration, however expectations of exact vibration amplitude measured is reserved until later experiments on realistic material substitutes in section 4.4.2.

Due to difficulties in validating these FEA simulations, these results were used only to inform how the vibration amplitude could be qualitatively altered by changes in geometry, material property and frequency. In subsequent experiments on physical models, the quantitative changes in vibration within the bone region was measured to complement the FEA simulation results (see results section 4.4.2).

4.3.3 FEA on 19 mm Synthetic Gel Disc

The FEA analysis on a 19 mm thick synthetic gel disc aimed at simulating soft tissue via a proxy synthetic gel disc is shown below (Figure 52 and 53) in order to visualise and anticipate the behaviour of vibration transmitting through a similarly dimensioned region of soft tissue, which was used in later experiments on bovine samples (section 4.4.1, 4.4.2). A diagram of the FEA set-up displaying regions and vibration direction, as well as a FEA render of the experiment is shown below. All boundary conditions were set to sliding to represent there being no bonded boundary between the soft tissue and the transducer plate.

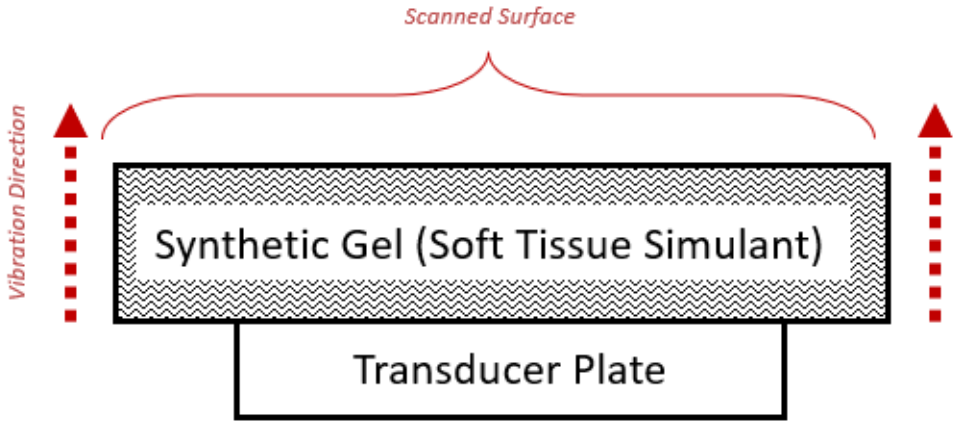

Figure 52: Diagram of the FEA synthetic gel set-up

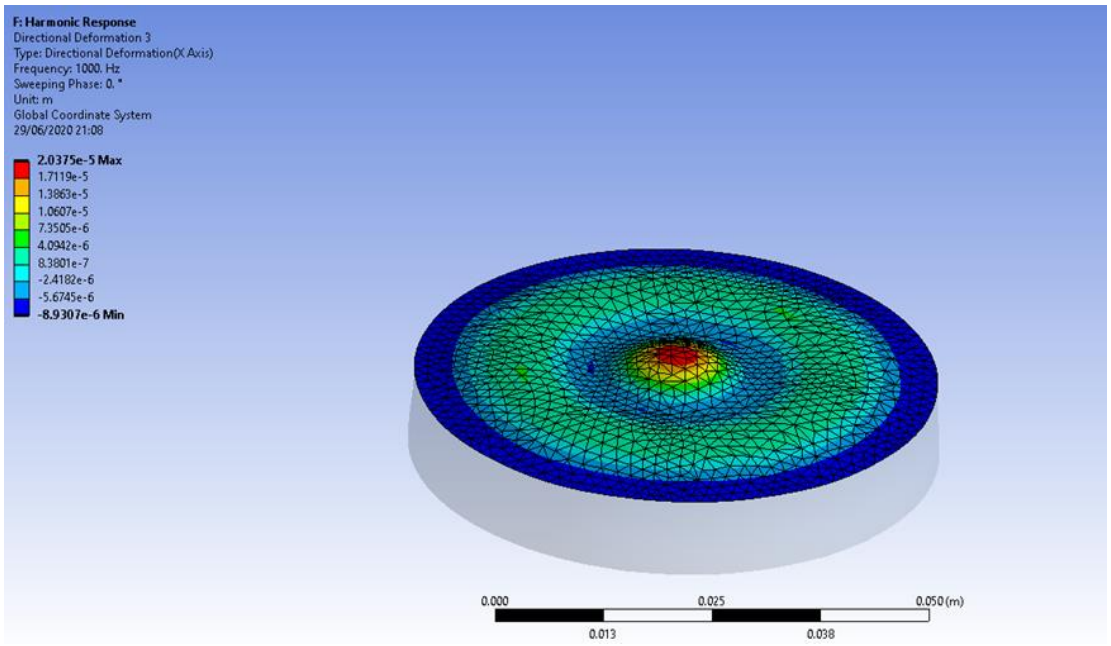

Figure 53: FEA directional displacement analysis of 19mm thick soft tissue disc showing vibration amplitude distribution across disc surface

The results from this simulation show that the highest vibration amplitude was at the centre of the disc (red) and vibration is progressively less until the vibration is lost at the edge of the disc shown in blue. Notably there are concentric rings of vibration around the centre. This indicates the potential for standing waves where no or reduced vibration is experienced as the transmission is cancelled out by

vibration bouncing back towards the transmission source. In this simulation, the peak amplitude experienced was 20,300 μm with the vibration amplitude decreasing from the centre to 4,090 μm on the nearest concentric ring. Similarly for the above FEA simulations on simplified femur models, the FEA results here are interpreted qualitatively and not quantitatively, and further direct measurements using SLI were performed on samples of the same size and dimensions in future experiments on bovine bone. By viewing both FEA tests in tandem, an expectation of vibration amplitude in soft tissues in isolation and when assembled in a simplified bone femoral model can be gained.

4.4 Bovine Femur Vibration Results

This section details the results pertaining to tests performed on bovine distal femur samples. These include:

- Vibration amplitude heat maps from SLI scans to show vibration spread over the surface of the bone and peak surface amplitude, complemented by vibration amplitude measured inside the bovine femur trabecular region by the accelerometer to compare vibration on both the surface and inside of the bone.
- Subsequent, in-depth studies on vibration amplitude at varying points inside the trabecular region of the bone, measured by single-point interferometer, to further characterise with greater resolution the vibration behaviour as delivered by the wearable nanovibration device.
- Additional studies on specific aspects of the device design are also covered in this section to guide potential recommendations for future designs.

The results provide information for subsequent discussion and recommendations regarding the design of the wearable vibration device, the effectiveness of the device to provide vibration to the target area, and the effectiveness of the application of nanovibration to increasing the BMD at the target area of bone.

Whilst limitations to this study can be expected due to differences in mass affecting the performance of the transducer, and the differences in size potentially affecting the quantification of vibration reduction due to the presence of possible attenuation through the bone, the study is expected to capture the complexity between regions of bone and the overall approximate geometry of human bone. Gels are used for accessibility and ease of use and are given exaggerated proportions to observe the effects of transmission as part of the experiment and may behave in an idealised manner compared to organic tissues. Therefore, numerical quantities are not expected to replicate those that would exist in a human femur but should inform how vibrations at the stated frequencies behaves in realistic bone media and to estimate the order of magnitudes by which vibration amplitude may be reduced in practice.

4.4.1 Initial Bovine Femur Experiments

4.4.1.1 SLI Vibration Scan on Bovine Femur Condyle Surface

The set of experiments detailed in section 3.11.2 provided SLI vibration scan data to create a visual representation of the spread of vibration over the surface of the bovine bone sample. The measurement methods used during this experiment were SLI measurements taken on the bone surface.

The visual representation makes it easier to see:

- Where the most intense vibration is experienced in relation to the transducer on the opposing bone surface.
- How quickly the intensity of the vibration is lost as it travels over the bone surface.

This provides an insight into where the vibration is delivered effectively and the physical range within which the wearable device can be anticipated to function. This in turn informed the design of the wearable device by providing information regarding the importance of position for the transducer to maximise vibration to the target area and indicates the effectiveness of the vibration experienced by the wearer.

The vibrating device applied to the condyle of the bovine femur sample generated a displacement on the opposite side of the femur. Using the SLI, it was possible to measure the vibration amplitude across the opposite surface. The SLI returned a series of vibration amplitudes that corresponded to a specific point on the measured surface of the bone.

In order to view these vibration scans as heat maps, the SLI scans were imported into Matlab and arranged showing vibration amplitude in nm over the position in 2 dimensions of the bone surface.

The peak vibration amplitude, averaged between the two scans performed, is given as 1.5 nm (standard deviation = 0.3 nm), and the scans show a drop-off from the peak vibration amplitude region, which halves in amplitude at approximately 4 cm from peak. This shows the drop-off in amplitude from the beam centre. The heat-map shown in figure 45 below was recorded on the bone surface of a bovine

sample with 1 layer of 19 mm thick humimic.com #0 gel to simulate a layer of soft tissue.

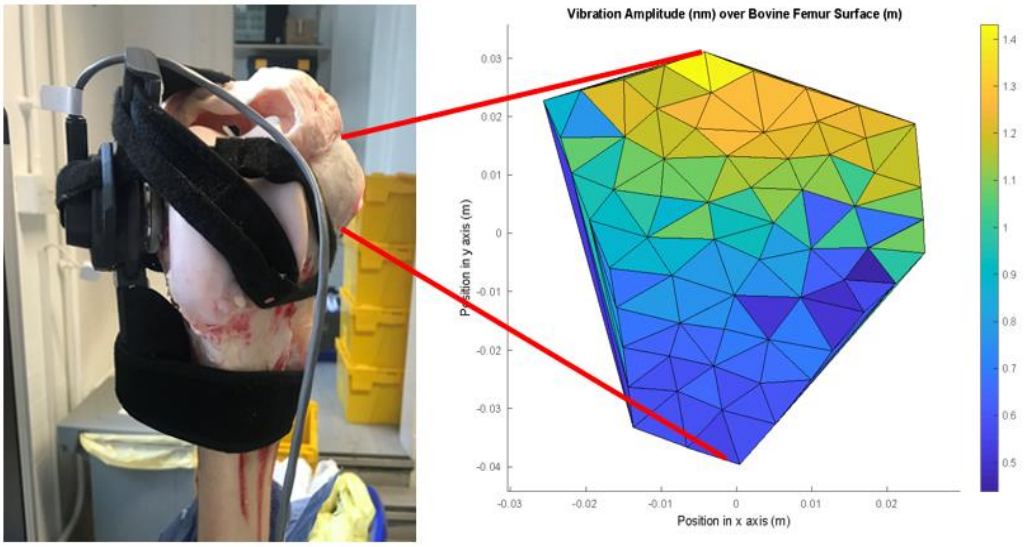

Figure 54: SLI vibration amplitude scan at 1000 Hz over target region of bovine bone (nm) showing vibration amplitude distribution and target region assessed

In the above figure, the heat map is representative of the vibration amplitude on the bone surface opposite the transducer. The bone surface represented on the heat map is identified by the red lines.

Features to note from the heat map are that the most intense vibration is experienced in the area immediately opposite the transducer on the opposite side of the bone. This is illustrated by the yellow colour on the map.

4.4.1.2 Accelerometery Measurement inside Trabecular Bone Region

During the SLI investigations described above, readings were taken by an ACH-01 accelerometer inserted at the midway point in the trabecular bone region of the bovine femur. To measure vibration transmission through soft tissue, a layer of soft synthetic humimic.com gel soft tissue proxy of increasing thickness (6 mm to

19 mm) was inserted between the transducer surface and the bone surface and the vibration amplitude at the accelerometer recorded again.

The summary of the accelerometer readings for each thickness of soft gel is shown in the table 11 below.

Table 13: Vibration amplitude at accelerometer (inside bone, trabecular region) for varying thicknesses of soft gel used as padding.

Thickness of Gel (mm)	**Vibration Amplitude at Accelerometer (nm)**
No gel	8.65
6	3.01
11	2.95
15	1.52
19	1.89

These values are consistent with the peak vibration amplitude measured at the surface of the bone, as compared with the SLI measurement readings described in the prior section and provide confidence that, as anticipated from the FEA models described earlier, the vibration is travelling from the transducer to the opposite side of the bone and vibrating the trabecular bone region.

Thickness of gel is measured prior to assembly in the model and applied until good surface contact (no gaps) are achieved. Excessive force was avoided where possible. Due to variations in bone surface geometry, the results shown here are expected to demonstrate some variability; however this is viewed as indicative of real-life application.

Overall it can be seen that the absence or reduction of synthetic gel leads to an increase in measured vibration, however due to the low sample size of bovine femurs at this stage of experimentation, only non-statistical observations were made at this stage to inform later experimentation. The data is presented below in graphical form, overall showing a reduction in vibration amplitude as gel thickness increases.

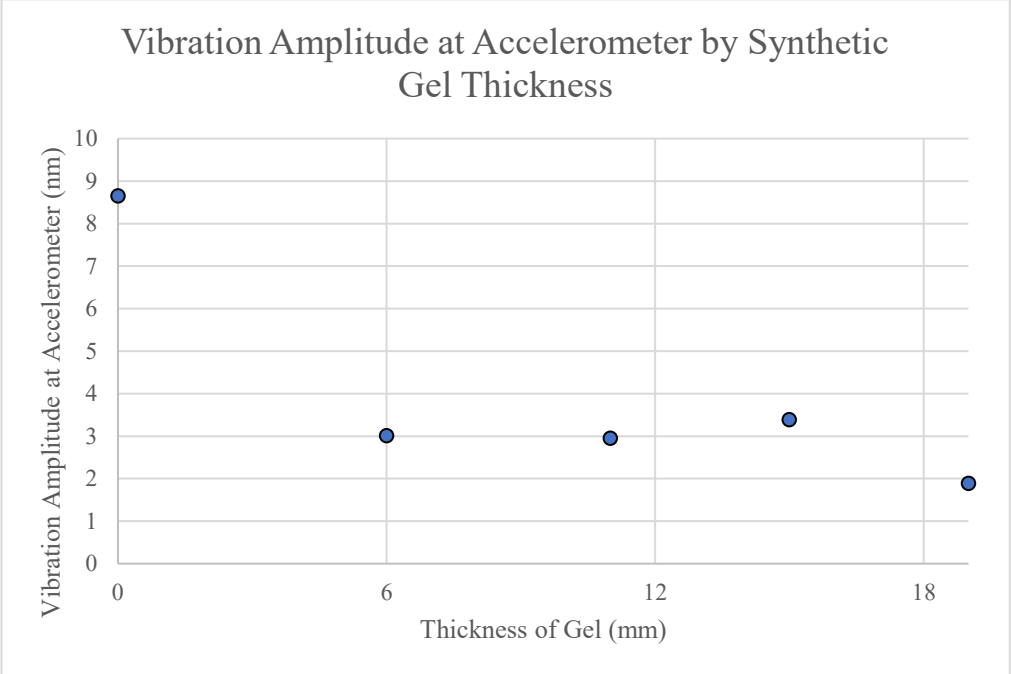

Figure 55: Vibration Amplitude at Accelerometer by Synthetic Gel Thickness

4.4.1.3 SLI Scan on Humimic Soft Tissue Proxy

To complement the measurements made using accelerometer and bone surface measurements, an SLI scan on a layer of #3 Humimic synthetic polymer gel soft tissue proxy was carried out. The SLI scan was imported into Matlab and displayed as a heat map using the same technique as for the SLI measurement on the bone condyle surface in order to visualise the vibration amplitude through a layer of flesh prior to reaching the bone.

The vibrating transducer had a diameter of 4.4 cm, the diameter of the gel was 5 cm. The measurements were taken with a view to clarifying:

- the extent to which vibration amplitude was lost laterally through the gel,
- the extent to which vibration amplitude was reduced through varying thickness of gel.

The measurements are shown visually via the summary table 12 below as well as 3 heat maps showing vibration at the transducer without the gel soft tissue proxy, and vibration frequency through 19 mm and 38 mm gel soft tissue proxies respectively. The transmission amplitude was found by taking an average of the highest 25 points.

Table 14: Summary of vibration amplitude as measured during the SLI studies

	Transducer & 9 mm Technogel Layer	**19 mm gel**	**38 mm gel**
Average Peak Transmission Amplitude	747 nm	62.5 nm	17.9 nm

For comparison the SLI scan on the transducer layer (transducer & Technogel layer) is shown in Figure 56 below, featuring a section of static table for comparison, which demonstrates a high vibration amplitude nearly an order of magnitude higher. Here the vibration amplitude halves at roughly 0.2 cm from peak (near-centre).

As for the SLI scan above, the average amplitude at the centre is found by taking the average of the highest 25 points, resulting in an average vibration amplitude of 747 nm.

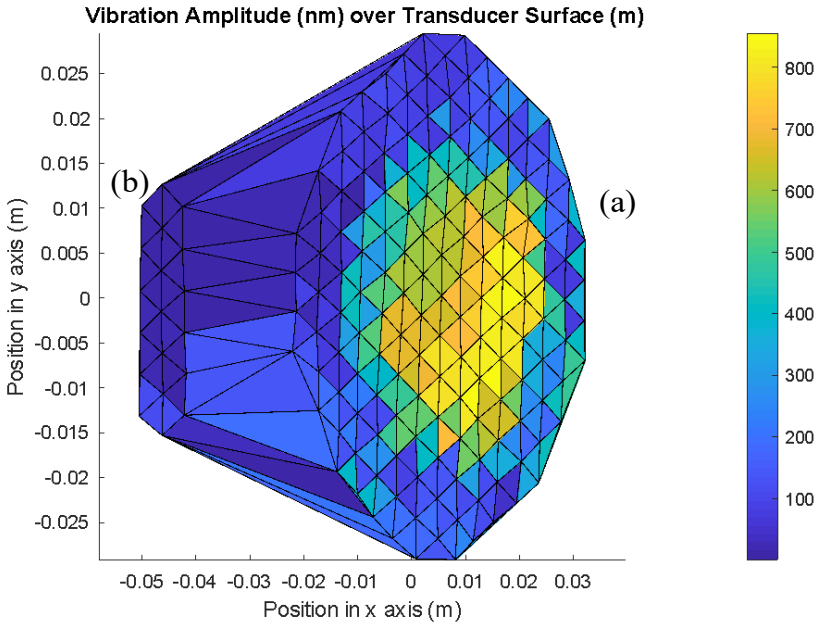

Figure 56: SLI Scan of transducer with technogel padding layer (9mm thick) (b) in nm with reference scan of bench (b), showing peak vibration amplitude and its radial decay

Figure 57 below shows a heat-map of the SLI as performed on the transducer & Technogel padding layer with 19 mm of soft tissue proxy layered on top. Whilst a drop-off in vibration amplitude is expected, it is noted that vibration at the edges of the gel display a vibration amplitude of 10 nm, indicating that vibration is transmitted through the gel outwards as well as directly in the axis of vibration transmission.

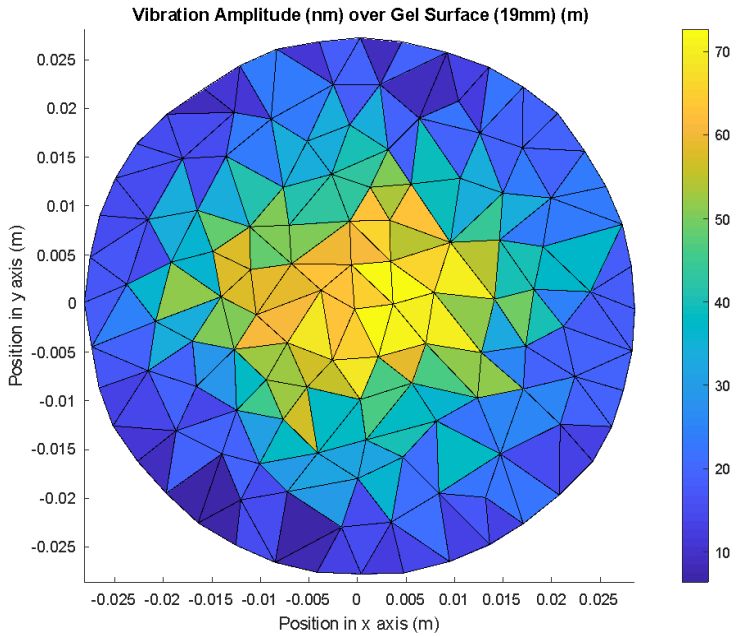

Figure 57: SLI Vibration Amplitude Scan over surface of 19mm thick soft tissue disc (nm) as measured by scanning laser interferometry, drawn in Matlab

The vibration amplitude is highest in the centre of the gel disc, directly above the transducer disc and behaves in a manner consistent with the previously described FEA analysis of a disc of same dimensions and given material properties. The vibration amplitude in the centre of the disc (as shown in the yellow region in Figure 57) was identified as being 62.45 nm, determined by averaging the top highest 25 points in the scan.

When comparing the vibration on the gel surface against the vibrations measured inside the trabecular bone region and on the surface of the bovine femurs, the vibration amplitude at the top of the gel is higher. This indicates the loss of vibration amplitude at the transmission boundary between the two materials. Some loss was anticipated from transmission between the boundaries of the media.

In order to compare the vibration scan shown above against the same vibration through a layer of gel twice as thick, below is shown the vibration amplitude map of the two layers of 19 mm thick gel stacked on one another. This formed a layer of soft gel 38 mm thick; enabling to view the effect of a doubling of thickness of synthetic gel. The transducer positioning and output was consistent with the single gel layer, and the resulting heat map of the vibration amplitude over the surface is shown in Figure 58 below.

The average vibration amplitude at the centre was taken by averaging the highest 25 points, returning a vibration amplitude of 17.9 nm across both scans taken, showing a notable decrease in vibration amplitude measured.

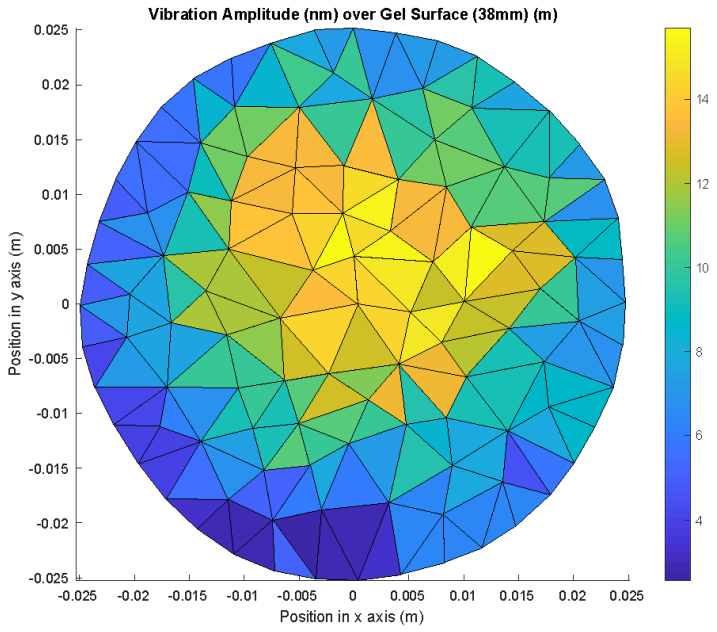

Figure 58: Vibration amplitude (nm) map of SLI Scan (nm) of 38 mm thick gel layer as measured by scanning laser interferometry, drawn in Matlab

4.4.1.4 Summary of Bovine Femur SLI Test

As the purpose of the measurements performed in sections 4.3 and 4.4 are to gain a picture of how the vibration amplitude changes between different regions of the target area (transducer surface, soft tissue, trabecular region of bone, bone surface), the above measurements can be summarised in table 15 below.

Table 15: Summary of vibration amplitude as recorded during Bovine femur SLI test and complimentary scans on transducer and soft gel layer

Location	At the Transducer	Through 19 mm Layer of Muscle Gel	At the Central Interior of Bone (Accelerometer), with 19 mm Layer of Muscle Gel	At the Opposite Bone Surface, with 19 mm Layer of Muscle Gel
Vibration Amplitude (nm)	747.0	62.5	1.9	1.5

From this the vibration can be shown to reduce by a factor of approximately 12 from the transducer to the surface of the gel before transmitting into the bone proper, and then a further factor of 33 between the layer of gel and the bone. The vibration amplitude then does not reduce much between the centre of the bone and the opposing surface, as suggested by the FEA results. Due to the experiment only featuring one accelerometer within the bone at the midpoint, it is difficult to quantify the degree of vibration that is lost within the bone trabecular region, however it is of note that the vibration amplitude is similar to the vibration amplitude at the opposing bone surface (1.9 to 1.5 nm), possibly indicating that attenuation is not a major factor in vibration reduction.

This gives an indication of how the vibration amplitude decreases significantly with each added increase of thickness and/or material. The experiment in the next

section aims to examine the vibration transmission through the internal changes within the bovine bone.

4.4.2 Follow-up Bovine Femur Experiments

4.4.2.1 Single Point Interferometry at 1cm increments through Drilled Bovine Femur

This section shows results from the set of experiments on drilled bovine femurs as described in section 3.11.3. Based on the FEA modelling, the working assumptions were that:

- Vibration at the transducer provides the maximum level of vibration.
- Vibration is likely to reduce as it passes through the different layers of bone, soft tissue and Technogel padding due to vibration amplitudes lost as a result of transmission between media regions.

The aim of this set of experiments was to measure the transmission of vibration through different media using the vibration device. The measurements taken are described below.

The amplitudes delivered at a range of frequencies (500, 1000, 2000, 4000 and 5000 Hz) were measured at successive 1 cm intervals through the bovine femur bone sample. The range of frequencies in addition to the target rate of 1000 Hz was examined to gain any potential indication of waveform effects and to observe possible vibration behaviour other than pistoning. The measurements were taken at 1 cm intervals through the bone to provide information on vibration transmission through different bone composition, primarily in the trabecular region.

A full table in Appendix 6 shows the average recorded amplitude in nanometres for each frequency measured at each depth. Also displayed is the number of different samples considered for each depth; as different bones had differing dimensions, not all bones could support depths above a certain amount. Due to measurement difficulties, measurements at some depths were also infeasible.

Across the range of 500 – 5000 Hz, the vibration amplitudes measured remained of the order of a few to tens of nm (approx. 1 – 53 nm). No resonant effects or substantial attenuation across the bone depth was observed.

Relative to the driving surface, the frequencies at 500, 1000, and 2000 Hz were comparable whereas the vibrations measured at 4000 Hz and 5000 Hz were higher; however due to the low vibration amplitudes measured in nm the higher amplitudes are believed to be partly due to a noise floor elevating the measurements.

These are presented below as graphs of vibration amplitude over drill depth at each 1 cm interval from the bone surface (= 0cm). The vibration amplitudes are achieved by averaging vibration amplitudes recorded at each drill depth from each bone sample shown in figure 59. As shown in Appendix 6, different depths had different repeat numbers due to the dimensional limits of the bone (that is to say, a bone that was only 8 cm thick could not accommodate 9 measurement points with 1 cm intervals). A total of 6 samples were measured across all tests.

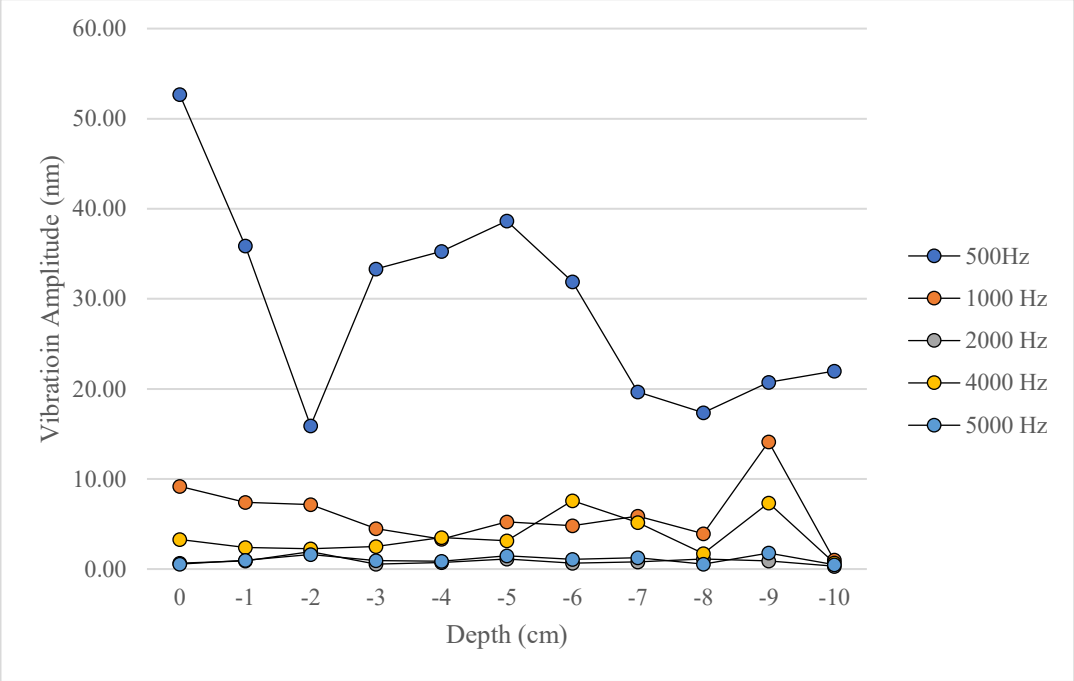

Figure 59: Graph of vibration amplitude as measured in the drilled bovine femur (nm) at 500 Hz, 1000 Hz, 2000 Hz, 4000 Hz, and 5000 Hz over drill depth in 1 cm increments.

From the above information, there was no clear evidence of standing waves at any frequency or anything other than pistoning outside of some unusual variation at 500 Hz, as exhibited by the consistent vibration amplitude across the depth of the bone samples for each frequency other than 500 Hz.

At 500 Hz it is interesting to note a consistent hump at -3 to -6 cm depth, however it is unclear what this is attributable to. This may be the result of a resonant effect at that region at 500 Hz, or the result of experimental error. It is not believed to be the result of a standing wave as the wavelength at 500 Hz would be in excess of the dimensions of the bone.

For very low amplitudes it was noted that some measurements were difficult to separate from a likely noise floor at higher frequencies (particularly 5000 Hz), as amplitudes below 1 nm were difficult to measure using SLI on the bone surface.

As described in the methodology section, once each bone sample was drilled through, a measurement was taken on the vibrating transducer plate, which allowed the vibration amplitudes to be normalised against the vibration on the transducer surface for each frequency. This was done to show the proportion of vibration amplitude transmitted into the bone.The normalised average results are shown in the graph below (figure 60) for a visual representation.

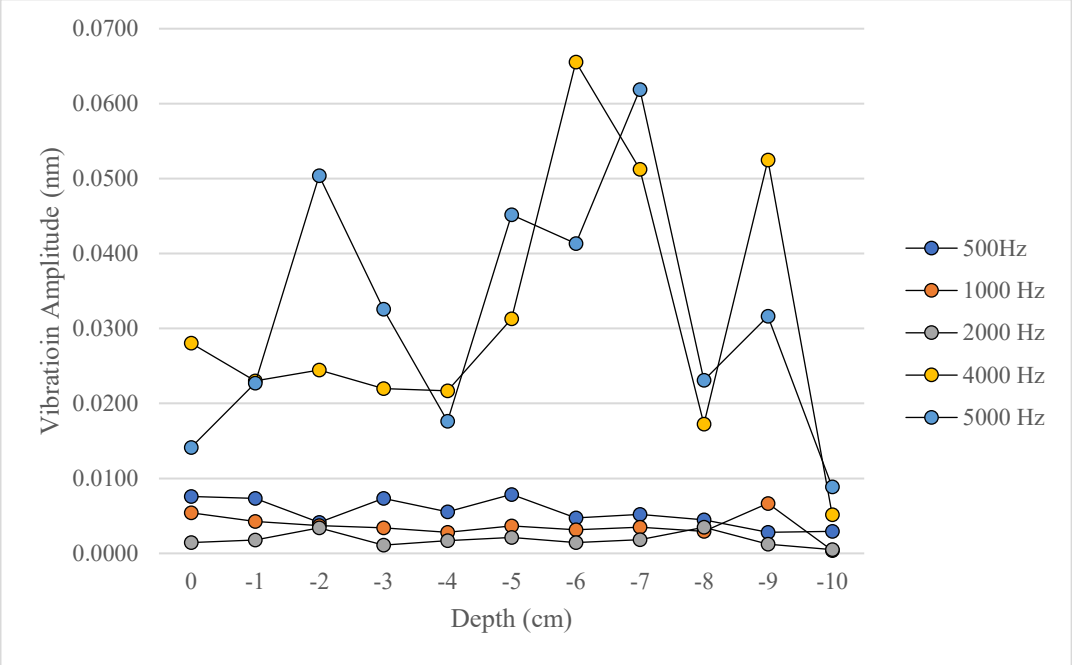

Figure 60: Normalised vibration amplitude in drilled bovine femur samples (normalised to transducer vibration amplitude whilst active on bone) over drill depth in 1 cm increments at 500, 1000, 2000, 4000, and 5000 Hz.

Due to the vibration amplitude of the transducer being much higher than the vibration inside the bone due to transmission losses, the proportion of vibration amplitude transmitted into the bone is evidently small. This is comparable with the FEA modelling which suggested a loss in amplitude by a factor of 0.002 (Femur Model, Composite Material, Transducer & Soft Tissue Model).

An Anova single factor test reveals that the frequency has a significant impact on vibration amplitude ($p < 0.05$). Due to concerns regarding the possibility of a noise floor affecting the frequencies with lower absolute amplitudes (4000 Hz and 5000 Hz) a single factor Anova test was also performed for frequencies 500 through 2000 Hz, which also revealed that the means significantly differed ($p < 0.05$).

4.4.2.2 Bone Femur Vibration Comparison With & Without Technogel Padding

Similarly to the results given above, vibration amplitude over drill depth in 1 cm increments was recorded on bovine samples (n = 5) both with and without the Technogel padding used with the wearable device in order to assess the effect of the soft padding material on vibration amplitude in the bone. The results shown in figure 61 below are for the target frequency of 1000 Hz, graphs for all other frequencies measured are contained in Appendix 5.

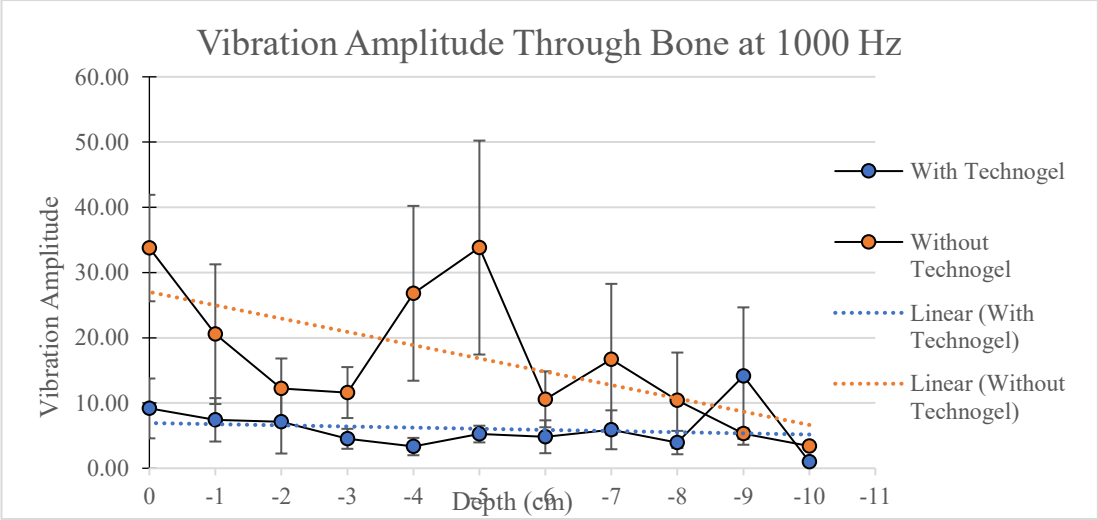

Figure 61: Graph of vibration amplitude over bone with and without technogel (nm), with standard error bars per depth interval and linear trendlines

These graphs show an overall decrease in vibration amplitude measured in the bone due to the Technogel padding, which is consistent with the FEA analysis including a layer of soft material reducing the overall vibration amplitude significantly. It's noted also that the standard error for each measurement point was reduced for the measurements taken featuring the Technogel padding layer.

By averaging the vibration amplitude through the bone, it can be seen that the transducer with a layer of technogel padding generated an average of 6.0 nm in the bone whereas the transducer without padding generated 16.8 nm. A two-sample t-test assuming unequal variances was performed on the datasets and a significant difference was identified between the two means ($p = 0.003 < 0.05$). It can therefore be concluded that technogel is a significant factor

For comparison, a graph showing the same amplitude normalised against the vibration amplitude measured at the transducer surface is shown in figure 62 below to highlight any differences in the proportion of vibration amplitude transmitted between the transducer and the bone region measured as affected by the Technogel padding.

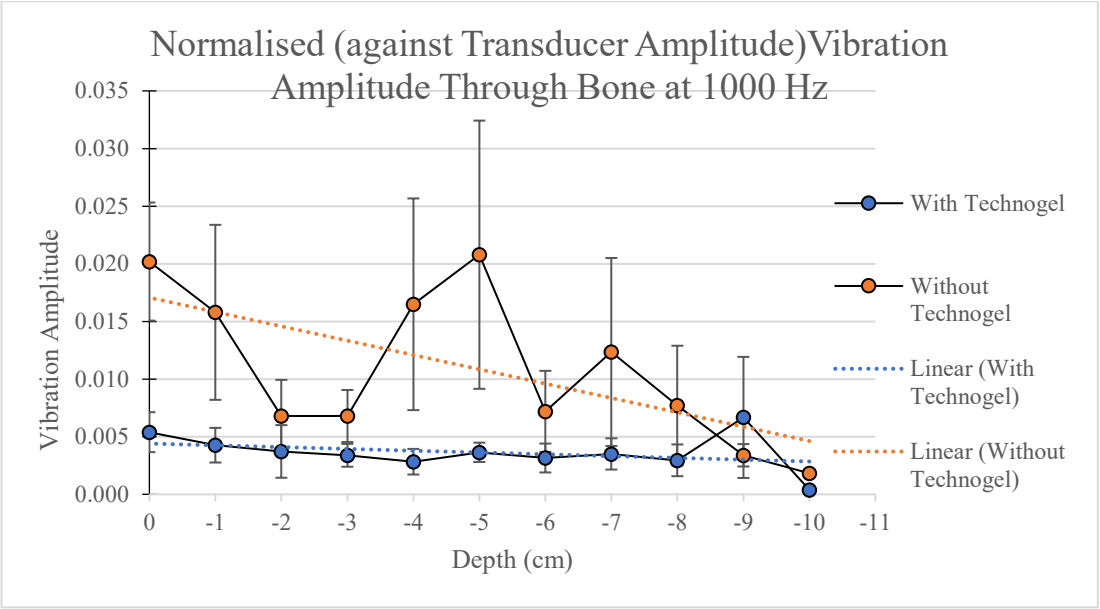

Figure 62: Graph of normalised vibration amplitude over bone with and without technogel (nm), with standard error bars per depth interval and linear trendlines

4.4.2.3 Comparison of Transducer Type Vibration Measurements on Single Bone Femur

In the following graph (figure 63) a comparison of vibration amplitude delivered using a voice-coil transducer and delivered by a piezo-block transducer is shown. The amplitude averages were taken by averaging out vibration amplitudes as measured on the same bovine femur repeated multiple times (n = 6) normalised against the vibration amplitude on the transducer surface. Standard error bars are included, calculated by taking the standard deviation and dividing by the square root of the count for each frequency. The normalised vibration amplitude for 5000 Hz is not included as the vibration amplitude provided by the piezoblock was not sufficient to pass the noise floor of the single-point interferometer, resulting in an inability to measure at that frequency

At 1000 Hz a two-sample t-test assuming unequal variances was performed on the datasets belonging to the piezo-block vibration amplitude and the voice-coil transducer vibration amplitude, revealing a significant difference between the two ($p = 0.02 < 0.05$).

The non-normalised graph showing the vibration amplitudes is shown in figure 64 below, also with standard error bars.

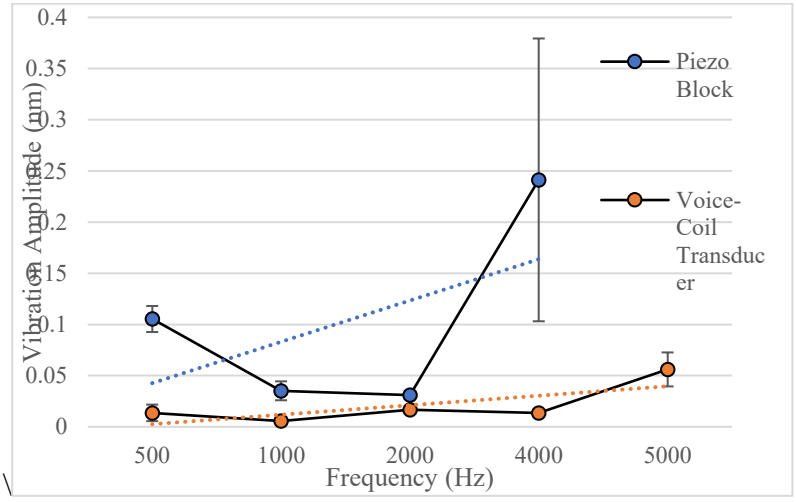

Figure 63: Comparison between vibration on bovine bone surface as delivered by a piezoblock transducer and the standard voice-coil transducer used in the device prototype (normalised to transducer surface vibration) (n=6) displaying standard deviation and linear

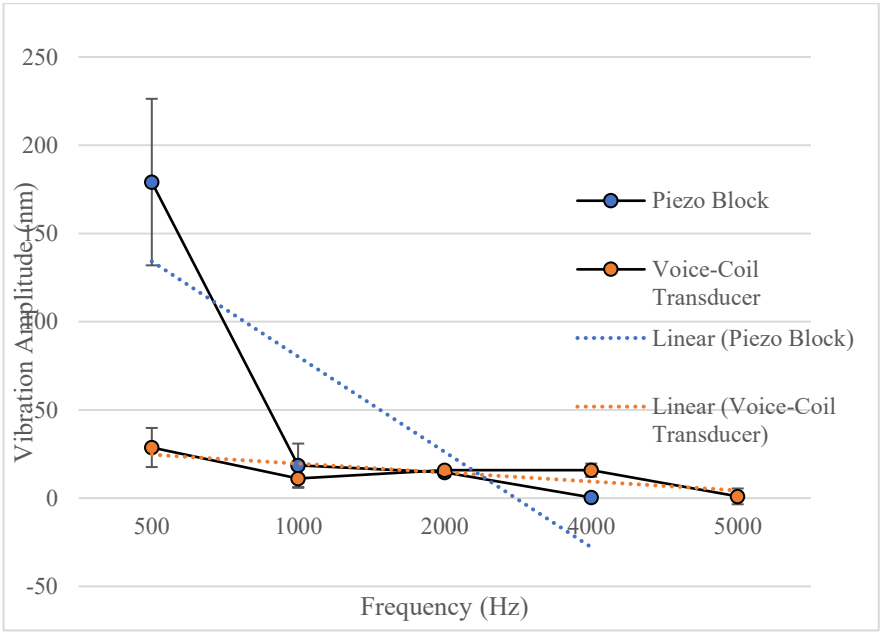

Figure 64: Comparison between vibration on bovine bone surface as delivered by a piezoblock transducer and the standard voice-coil transducer used in the device prototype (nm) (n = 6) displaying standard deviation and linear trendlines

These graphs show the differing capacity to deliver nanovibration into the femur for each type of transducer. The different capacities indicate that the target frequency has a bearing on the choice of transducer.

At the selected vibration amplitude of 1000 Hz, the piezo-electric transducer was comparable in output to the voice-coil transducer; however for lower frequency vibration the piezoblock transducer was far more effective at delivering large amplitudes of vibration. Should alternative vibration frequencies be explored as part of further work, the capacity of the selected transducer to deliver vibration amplitude to the target area should be selected based on frequency dependant metrics; potentially favouring voice-coil transducers for larger ranges of vibration (as the voice-coil transducer demonstrated a relatively flat response across all

selected vibration amplitudes) whereas piezo-electric transducers may be more effective at certain frequencies.

4.4.2.4 Repeat Application Measurements on Bone Femur

The following graph (figure 65) shows the results from the vibrating device being applied on the same bone sample repeatedly (n = 6) with and without Technogel in order to observe any significant operator based effects from multiple applications. As for the results above, this was done both with and without the Technogel padding for each frequency and with standard error bars.

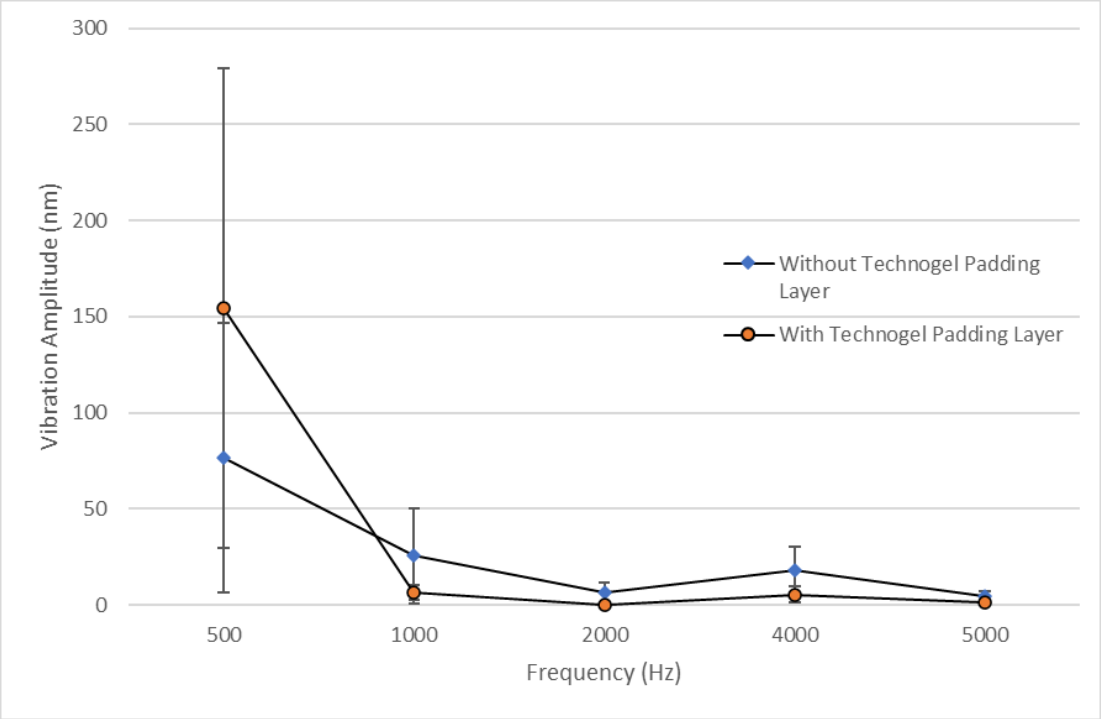

Figure 65: Average vibration Amplitude with repeat Application of vibrating device (n=6) with standard deviation bars.

Using two-sample t-tests assuming unequal variances, no significant difference was found between the two datasets at 500 Hz ($p = 0.21 > 0.05$) or 1000 Hz ($p = 0.06 > 0.05$). A significant difference was confirmed for 2000 Hz ($p = 0.03 < 0.05$), 4000 Hz ($p = 0.04 < 0.05$) and 5000 Hz ($p = 0.02 < 0.05$).

For further discussion on the significance of the vibration transmission experiments and the FEA analysis results, see section 5.3.

4.5 Summary of Key Findings

Across all experiments done as part of this project, the key findings relevant to discussion can be summarised by the following points:

- Out of 3 target regions assessed (ankle/distal femur, proximal tibia, distal femur), the distal femur was selected as the target region for further study in this project due to reliable readings and measurable vibration amplitude (2.4 nm for the Follow Up Investigation at the University of Strathclyde).
- Wearable device could be reliably worn up to 2 hours during the Preliminary Clinical Evaluation, with maximum use time over the 60 sessions approximatively 3 hours. Vibration amplitude measured during sessions was overall stable and consistent, demonstrating a feasible device concept with maximum duration limitations.
- Animal trials showed null results for effect of nanovibration at the dose delivered. No issues in vibration transmission were observed based on tests comparing vibration on animal bone surface to vibration amplitudes detected by the accelerometers.
- FEA testing suggests primary factor for vibration loss at target frequencies are transmission/reflection at boundaries of soft/hard materials. Distance from centre of vibration transducer axis shown to be a factor affecting vibration amplitude.
- Bovine sample transmission studies confirmed vibration presence inside trabecular bone region. Vibration amplitudes are described based on depth

within the bone region from the opposing surface, allowing for comparison between vibration amplitude detected by accelerometer or interferometer and bone surface and vibration within bone.

- Additional vibration transmissions quantifying vibration lost from use of additional padding layers and alternative transducer types were explored, demonstrating significant vibration amplitude decrease due to technogel padding under the conditions observed.

5. Discussion

In order to investigate the feasibility for using nanovibration delivery devices as a possible avenue for osteoporosis treatment, the original work in this thesis was to design and build bespoke wearable devices to apply consistent, controlled and measurable nanovibration to a target area of bone.

From the results, the key findings of this work are the following:

- The device was designed and capable of delivering measurable, repeatable and consistent nanovibration to the target area and was usable by participants with SCI injuries; limitations on duration of use and areas for improvement were identified as part of the Preliminary Clinical Evaluation.
- Vibration transmission at the specified frequencies was possible and measurable through the bone at the target regions. Transitions between soft and hard biological media are shown to cause very large reductions in amplitude.

- No therapeutic benefit was detected during the animal trial and the application of nanovibration did not have a positive effect on BMD at the doses investigated.

This section aims to discuss the outcomes, constraints and implications for future development under three main areas for discussion:

- Commentary on the design of the bespoke vibration devices and factors relating to their validation as a concept. The first objective of this project is to determine the viability of using vibration delivery devices as a usable therapeutic tool in practice; that is to say, can it be worn by the target group, and what improvements need to be made to facilitate its use?
- The effectiveness of applying nanovibration to increase BMD as a therapy as investigated via animal trials. Whilst the study of nanovibration as a mechanism to stimulate osteoblastogenesis and promote bone health is ongoing, based on the existing literature, can this method be considered viable for use in in-vivo applications?
- The effectiveness of the device to transmit vibration to and through bone at the target frequencies. Can confidence be gained that the vibration delivery is reaching the target site and can the vibration transmission be characterised in terms useful to future work?

5.1 Wearable Device Design Discussion

The clinical wearable prototype and the animal trial prototype were designed, developed and used in investigations to transmit controlled and measured nanovibration to the target area of bone as described in sections 3.5, 3.6 and 3.7,

and as shown by the results of 4.1 it was demonstrated that overall as a proof-of-concept, a wearable therapy device is feasible. Specific areas in which the prototype was successful as well as areas for improvement are detailed below.

In order to produce the devices on time and to budget, decisions were made based on a number of criteria which both influenced the outcome of the design and provided input for any future investigation. Firstly, the target group of participants who had suffered an SCI resulted in a very small pool of candidates as described in section 3.7. Due to the very small number of participants in the preliminary clinical evaluation, there are limits to the conclusions that can be drawn from the study, and a broader group of osteoporosis patients with less acute issues would allow a wider sample of participants able to apply any vibration device for longer periods of time. A higher volume of results would have the benefit of improving the statistical validity of results as well as potentially highlighting ergonomic and functional issues requiring design refinement.

However, it is noted that the participant who engaged in the study was capable of successfully wearing the device for extended periods of time, allowing for the collection of performance data necessary for the evaluation of the device's use. This by itself indicates that as a proof-of-concept the device design has promise, as the intended user group presents significant challenges to simply completing a study. The results as shown in section 4.1.4.1 indicate that the participant was overall able to use the device continuously for between 2 and 4 hours. After a number of sessions, the participant chose to limit the use of the device to 2 hours, which is represented in Figure 37. This indicates that over extended application durations the device proved cumbersome to wear, which is thought to be due to a

variety of factors including the bulk of the device and a reported negative effect the device had on the participant's mobility.

Due to the limited pool of participants for the preliminary clinical evaluation, commentary on the efficacy of the design is supplemented with the data from the initial and follow-up investigations at the University of Strathclyde, as detailed in results sections 4.1.1 and 4.1.2.

5.1.1. Wearable Device Overview

The clinical wearable device and the device used in the animal trials were made using Creo and 3D printing as described in section 3.3 and 3.4. However, using 3D printing resulted in a more bulky and heavy design than would be achieved using, for example, injection moulding; this is due to the relative fragility of the layers of polymer material used in 3D printing that are unable to withstand forces that are not aligned with the direction of the print or the direction of the filament (110). As the consequences of the device snapping and presenting a sharp edge were considered to be catastrophic, the parts were over-designed to withstand the forces the straps would apply to the arms which added strength but also bulk to the device. As bulk was cited by the participant as a factor limiting the device's use, this is an element that should be scrutinised carefully for any future designs.

3D printing had the advantage, however, of retaining the possibility for rapidly designed custom components designed to suit particularly challenging geometries or participant preferences without the need to adjust complicated and expensive mould tools. Whilst this aspect of 3D printing was not ultimately used during the study, this is a cost effective and time responsive production method which can be

used advantageously if combined with surface scans of a participant to engineer highly tailored components.

The size and bulk of the 3D printed components was made more portable by its capacity to remove the modular arms, allowing it to take up less space in a transport bag. Due to the size of bought-in components in the electronics box, however, it was not possible to reduce the size of the box containing the battery, the circuitry, and the data-card. This meant that transporting the electronics box was always burdensome for both the participant and the investigators. Similarly, the bought-in components such as the transducer imposed a minimum size requirement on the wearable device, as the transducer used was by necessity its tallest component.

The bulky nature of the build had implications for the portability of the device and the amount of time it was comfortable to wear. During the trials, consideration was given to integrating the design of the device with pre-existing equipment, for example placing the electronics box within a bag on the rear or beneath wheelchairs, however these concepts were not implemented during the investigation. They may, however, exist as avenues for future design iterations for similar devices.

5.1.2 Nanovibration Transducer & Accelerometer

The transducer selected was successful in delivering vibration of the desired frequency to the target region as measured by the ACH-01 accelerometer during use, however it required a considerable degree of vibration at the transducer surface to transmit the vibration in measurable quantities. This is thought to be due

to the mass of the target area combined with losses in vibration amplitude primarily due to transmission/reflection which is increased by the presence of soft tissue layers or intermediary padding, as suggested by measurements described in section 4.4 and supported by understanding of acoustic media (67; 68; 69).

Those same losses due to transmission/reflection also posed a difficulty when measuring the vibration on the far side of the target region, in most cases the medial side of the knee joint (or ankle, in the case of the investigations at the University of Strathclyde). However, the ACH-01 accelerometer proved functional as a means of detecting vibration at 1000 Hz consistently and without noise at the vibration amplitudes investigated.

Both the transducer and accelerometer surface required a wide, flat surface on which to rest in order to transmit a consistent amount of vibration to and from the target region. For the transducer, a larger surface was beneficial to ensure a wider area would receive the nanovibration, requiring both appropriate positioning and a means of conforming to the geometry of the target surface. For this prototype device, the Technogel padding layer fulfilled this function, and it is noted that in section 4.4.2.2 the technogel layer resulted in a lower standard deviation when normalised against the transducer amplitude. This supports the use of a padding layer as a means of assisting in the conformance of the transducer surface against the target region, and it can be assumed that this would be beneficial in a similar sense for the accelerometer. However, the use of soft intermediary materials inevitably has a negative effect on vibration amplitude transmitted due to losses from transmission/reflection.

It is suggested that an array of smaller transducers would allow greater flexibility of design and make it easier for multiple smaller transducers to have more than one point of contact across the target region. It is theorised that this would result in a larger area would be reached by the 1000 Hz vibration and also help reduce the overall height of the transducer side of the device, which would help address the issue of bulk. For the purposes of this study, however, multiple transducers introduced the possibility of interference between the vibration waves which would compromise the transmission measurement and recording and hinder the usefulness of this study; for this initial prototype, it was preferred to use a single vibration source to simplify the overall vibration delivery system and make a straightforward measurement at the accelerometer. For future devices, for which the presence of vibration in the target region was better validated, an array of smaller transducers would be of particular interest to explore.

The most effective transducer for the vibration frequency and amplitude is also a subject for further discussion. The in-vitro research used piezo transducers due to their ability to deliver very precise frequencies in bioreactors. The use of piezo and voice-coil transducers was compared in the bovine bone experiments in section 4.4.2.3.

What can be seen from Figure 64 and Figure 65 is that the piezoelectric transducer used was more successful at delivering a higher proportion of vibration relative to the vibration of the transducer element compared to the voice-coil transducer it was noted that the amplitude the piezo-transducer was capable of emitting was very low and either likely heavily affected by the noise floor (4000 Hz) or unable to be measurable at all (5000 Hz). This was due to the voltage the piezo-transducer

required to drive at higher frequencies. This indicates that whilst the piezo-transducer was not suitable for prototyping at this stage, it may present a viable alternative for future designs should the transducer become capable of delivering higher vibration amplitudes.

As the performance of the transducer type depends on the amplitude/frequency applied, the selection of which transducer to use depends on the requirements of the bone vibration project and could be regarded as an independent subject to be resolved.

5.1.3 Electronics - Clinical Wearable Device

As a means of controlling and monitoring the output of the wearable device during use, the electronic equipment described in section 3.2 was effective; using the electronics box, it was possible for a user to modify the vibration output to the required levels in response to visual feedback from the red and green lights on the front of the box. The data-collection method of storing the data to the SD card was also effective and allowed the investigators to retrieve the necessary data at regular intervals.

Due to the constraints on the project, however, many of the components and circuitry were by necessity large, in particular the need for a battery that could power the device for the required amount of time (up to four hours). This resulted in a bulky electronics box as described in above sections. However, the bulky format and the static nature of the set-up had the effect of shortening the amount of time that vibration was applied via the device, in turn reducing the potential impact of the device to address BMD.

During the clinical trials the wires connecting the wearable device to the electronics to the box rendered the device difficult to move during use without pulling on the wearable device. This would mean the participant was most comfortable when stationary during the application of the device.

In terms of the functions that the electronics components needed to fulfil, this aspect of the device design is considered successful; it is only due to its size that it was rendered uncomfortable to use. If this form of design is further explored, miniaturising the circuitry via circuit printing, as well as removing the need to have data-collection functionality reducing further the need for additional circuitry may prove to be valuable approaches for making what is a successful proof-of-concept more viable for long-term use.

5.1.4 Future Work & Design Suggestions

Following from the above commentary on the device and its ability to deliver vibration to the target region, there are several suggestions for improvements to the design. These are, improvements to the manufacturing and component design, improvements to the electronics implementation, and the nanovibration delivery and monitoring.

The device would likely be rendered less bulky and more flexible if alternative means of manufacturing the components were used; as the device manufacturing was limited to 3D printing for convenience and cost, this was not able to be fully explored during the project beyond speculation.

Injection moulding or forming would allow for alternative materials to be used that are more flexible whilst still being tough enough to support the stresses the

device was subject to, such as High-Density Polyethylene (HDPE) (111). In particular, the modular arms would conform to the shape of the leg limbs better if manufactured from a thinner and more flexible material, which would assist in reducing the overall device profile; this was unachievable with the 3D printed PLA filament available for this prototype.

3D printing may, however, prove valuable in the application of the device to alternative target regions such as the ankle. In combination with scanning technology, it is possible that 3D printing might allow a manufacturer to customise the shape of the arms to the geometry of the specific user. In the initial and follow-up investigations, the primary challenge when applying vibration to the ankle was the variations in geometry between participants and the prominence of the malleolus that rendered it challenging to design a one-size-fits-all component. A resin-based 3D printing technology able to design more flexible components whilst retaining the flexibility and customizability of 3D printing might present a more optimal scenario (112).

As discussed in 5.1.3, it would be worthwhile to print the circuits used in the electronics box and to reduce the size of the batteries used. This would only become cost-effective when producing higher volumes of components, but would help in reducing the overall bulk of the device when combined with the electronics box.

Reducing the overall bulk and reducing the profile may contribute to making the device more accessible for longer durations of use. In particular, if it is able to be

made with a low enough profile to be worn under trousers, this would allow it to be worn more comfortably and in more social settings.

The reduction of the device profile depends on changing the transducer type to a slimmer variety, or alternatively by designing an array of smaller transducers that could wrap around the target region. At the time of completing the preliminary clinical evaluation, an ‘array sock’ was beginning to be developed, but was cut short due to the occurrence of COVID-19.

Finally, it is suggested that similar technologies be applied to existing equipment, such as wheelchairs or hospital beds. By designing the equipment directly into equipment already in use, the possibility for saving on space may allow the device to be used in conditions and settings that are unavailable if it needs to be applied separately.

During the clinical and animal trials it became clear that the device would benefit from being unobtrusive and easy to move with, indicating a need to miniaturise the device further as well as making it independent of connecting power leads and data recording mechanisms.

5.2 Animal Trial Discussion - Using nanovibration to affect BMD

The animal trial provided the opportunity to assess the capacity for nanovibration, delivered at 1000 Hz, to treat or assist in reversing osteoporosis following SCI, and thereby fulfil the clinical need to develop methods of treating osteoporosis that do not require the direct loading of bones or strenuous exercise.

This section discusses the results gathered as part of the animal trials as well as comments on the capacity of the miniaturised device to deliver the nanovibration.

5.2.1 Effect of the Nanovibration Therapy

In-vitro nanovibration results on cells showed initial promise that the nanovibration technology may provide therapeutic benefit, however the results described in section 4.2 indicate that no significant or observable vBMD change in vivo occurred following delivery of the degree of vibration therapy applied. This can be seen in section 4.2.3.1, with no significant effect on bone mineral density observed in the stimulated limb compared to the control limb. The only parameter measured that showed a significant difference was in connectivity density, indicating a significant ($p < 0.05$) decrease in the vibrated limb compared to the control.

This is an overall null result that may be due to one or more factors; the nanovibration delivered to the region may have no biological effect or may not have a biological effect at the doses delivered, the cells used in-vitro and those found in-vivo may exhibit a fundamental difference in function, there may be an effect but it was too minor to detect using the sample sizes used in this studied, or that the effect may be present, but is masked by the severity of the SCI-induced bone loss used in this study. Given that in-vitro the vibration has an effect on mesenchymal stem cells as described in literature, it is considered unlikely that no effect would be present, as the cells present in the target region are not fundamentally changed or different; it is considered more probable that the effect in life biological media is however much reduced compared to in-vitro to the point of becoming impractical to observe a positive change.

Whilst no significant improvement in can be observed, it can be noted that the morphological factors and the bone mineral density have lower mean

measurement results for the vibrated limb than for the control. Instead, a significant decrease was observed during the measurement of wet bone mass.

The vibrated limb for the N40 group showed a reduced overall bone mass in the vibrated limb as compared to the control. This could be a result of restraining the limb being vibrated during the vibration session leading to lower mass. The spasticity of the animals may also have resulted in higher bone mass in the control limb due to muscle-bone loading. No other significant differences were observed.

This causes questions to be asked regarding why the vibration therapy, which was shown to be effective in-vitro, was ineffective in-vivo. Several possibilities may be considered.

It was proposed that the bone loss caused in the SCI rats was too rapid and severe a model, and any potential reduction in bone loss due to the therapy would be too difficult to measure compared to the overwhelming reduction in bone loss due to the SCI, which is known to be severe (11, 12). This would mean that in order to overcome the drastic reduction in BMD, a larger dose than is realistically feasible for this prototype would have been required in order to produce an observable effect using a SCI model.

As suggested above, it was also considered that by applying a mass to the vibrated limb and inhibiting the spastic response in that limb, the limb being vibrated was in fact subject to less muscle loading resulting from natural movement. This lack of loading in the vibrated limb may counter any positive effect caused by the vibration itself. Due to the rats' inherent behaviour, restraining the leg under vibration was considered a necessary feature of the study and therefore may

constitute a limitation. As bone health is partially dependant on mechanical loading, by inhibiting natural loading an adverse effect may counter any positive effect delivered by the device.

Either, or both, of the above factors may mean that the dosage of nanovibration delivered would need to be higher to compensate. The dosage itself may also have simply not been sufficient to observe an effect, independently of other factors. In-vitro, mesenchymal stem cells would be stimulated for continuous 24-hour periods (2; 94; 95; 96), whereas the rats were only subject to the therapy for up to 4 hours, with the duration in most cases lower depending on rat tolerance. Whilst it is not practicable to increase the duration of vibration during sessions due to the tolerance of the rats in the current form of this study, it is considered that the session duration and quantity of vibration delivered to the rats during these sessions may have been a major factor in understanding why nanovibration displays positive results in-vitro, but not as a result of this in-vivo investigation.

It should be noted that in similar experiments featuring vibration delivery to rats, positive effects were observed; Shuxin Sun et. al. (77) were able to observe a partial reduction in bone loss during a study on rats using LIPUS techniques for session durations as low as 20 minutes, and others have been shown to deliver positive results in other contexts. Whilst there are methodological differences between these studies and the work presented here, it is believed that BMD can be positively affected by therapeutic vibration, but either the type of vibration applied (lower frequency over longer durations) or an experimental limitation may be a possible cause of the differences in results.

The capacity of the device to deliver vibration throughout a therapy session, which may also have an effect on the efficacy of the trial is discussed in the following section.

5.2.2 Efficacy of Vibration Delivery during the Animal Trial

It can be seen from the graph showing time spent by the rat in the pouch (section 4.2.2.1 figure 42) that different rats had varying levels of tolerance for the treatment, resulting in a variety of overall dose levels of nanovibration delivered. Over the experiment duration of 38 days, the amount of hours spent in the pouch and subject to the nanovibration therapy ranged between 30 and 110 hours. The capacity of the rat to support the treatment may have presented a major limiting factor in the device's ability to deliver a level of vibration that would have a therapeutic effect.

The original concept that the animals would be free-moving had to be changed as the electronic leads providing power and allowing measurement were not compatible with free moving animals and the rats would make every effort to get free from the constraint. Restraining the rats to allow vibration to be applied and measured had a number of effects; it limited the time the rats could be subjected to vibration so limiting the potential benefit and it reduced the rats' natural movement, which is known to help maintain BMD via muscle loading. In addition, the vibrated leg was fixed whilst being vibrated in contrast to the control leg which reduced the natural movement still further and may have resulted in outweighing any potential benefit from the applied vibration.

Regarding the device's ability to deliver the necessary degree of vibration amplitude to the bone, however, it can be seen from the graph relating vibration measured on the surface of the animal skin to the vibration amplitude on the bone in figure 43, section 4.2.2.2 that the device was able to deliver the required vibration onto the surface of the bone, and that when using the accelerometer to measure the vibration on the surface of the skin, that this reading would be representative of the vibration amplitude delivered. This is based on the assumption that the vibration amplitude measured on the surface of the bone by laser interferometry would be consistent with the vibration through the thickness of the target area of the bone, an assumption that is explored in more detail in section 5.3 as vibration characterisation in the bone is discussed there.

The degree of vibration amplitude is consistent with vibration amplitude levels reported in literature of the order of 40 nm and above, delivered continuously to cells over 24 hours (compared to 2 – 4 hours for the animals in the trial). Measurements taken on the bone surface of test animals in section 4.2.2.2 indicate that the vibration amplitude is comparable to those delivered in-vitro and from FEA and transmission studies on bone it is believed that surface-level vibration measurements would be comparable with vibration amplitudes inside the bone. It would therefore be reasonable to conclude that the vibration amplitude by itself ought to be sufficient to match the in-vitro levels. This leaves the session duration as a possible cause of such a stark difference between in-vitro and in-vivo results in this set of experiments and an area of attention when looking at potential future work.

5.2.3 Future Studies & Work

From the results discussed in the above section, it is clear that the effect of nanovibration as a therapy did not have the desired positive effect on BMD. As speculated, this may be due to experimental limitations, such as the length of a nanovibration session. Whilst this could be lengthened in a later study in order to increase the dosage of nanovibration delivered to the limb, some practical challenges would first need to be addressed.

Most importantly, it would be required for the rat to undergo the treatment for a longer, uninterrupted duration. As it is understandably not possible to coerce the rat into behaving differently to its nature, as it will naturally try to get rid of any encumbrance, this leaves a few options available for future studies of this kind. Redesigning the harness to be wearable by a rat able to roam freely in a cage might present a first option; this would however necessitate a significant redesign and likely further miniaturisation of the device.

It could also be possible to directly vibrate the rat cage. This would present questions regarding the degree of vibration amplitude transmitted to the rat via the cage floor, however, and this uncertainty would need to be answered in order to gain confidence that the nanovibration is being transmitted into the target area.

Alternatively, a less severe means of causing an osteoporotic response (in this case, via a spinal transection operation) may allow for any possible positive therapeutic response to be measurable.

5.3 Vibration Characterisation in Bone

As observed in the initial and follow-up investigations at the University of Strathclyde in section 4.1.1 and 4.1.2, it was feasible from even early prototypes of the device to measure vibration transmitted from the transducer element of the prototype device through the bone to the accelerometer on the opposite side.

Whilst this provided confidence that nanovibration at 1000 Hz was being transmitted through the target area, as there was no other logical path for the vibration to take before reaching the accelerometer, the question of how much vibration amplitude relative to the accelerometer or transducer was present in the bone, and in what region, was left unquantified at this point in the project.

The two primary methods used to predict the behaviour of the vibration inside the bone, particularly in the trabecular region which was the target of this vibration therapy, was to construct a simplified model using FEA to outline the factors contributing to vibration transmission, and then to directly measure the vibration inside bovine bone samples as a proxy for human bone via laser interferometry. The outcomes of both methods are discussed in the following sections.

All results are made on the assumption that the bone regions behave as a bulk media; in reality, the bone environment is highly anisotropic and has a complex geometry. Fluid behaviour within the bone region (such as marrow or adipose tissue) are also not represented. Whilst the effect of such small geometrical features and changes in material property were not expected to have a significant effect on the vibration of bone at 1000 Hz, as the wavelength of 1000 Hz in bone is many orders of magnitude larger than the dimension of an individual trabeculae,

bone pore, or other geometrical feature, it remains a limitation that micro-scale vibration distributions are not considered as part of the following results which may affect the experience of individual marrow stem cells targeted by the nanovibration.

5.3.1 FEA Analysis Discussion

There were two objectives that the FEA analysis of the simplified models aimed to achieve: support the measurements observed via accelerometery and interferometry by predicting vibration amplitude inside the bone and on its surface at a comparable level, and to provide a representative behaviour model of how the vibration affects the directional displacement of the bone to assist in visualising the vibration transmission in-vivo.

As shown in section 4.3.1, the complexity of the model was increased iteratively in order to identify the largest contributors to changes in vibration amplitude. It was anticipated prior to commencing that creating more than one bulk media region, thereby introducing a change in media would result in reflection/transmission, however this was only observed to a significant degree in the model types that introduced, specifically, a soft tissue layer between the transducer model and the bone model, as shown in Figure 50.

The existence of two separate media in the bone itself (to represent the trabecular bone in the core of the bone model and the cortical bone region serving as its ‘shell’) did not make a large difference to the vibration amplitude results displayed by Ansys.

It is reasonable to anticipate from the FEA modelling that the most complex model in terms of shapes and components, and also the one that should represent most faithfully the transitions in region (Femur Model, Composite Material, Transducer & Soft Tissue Model), should be the most accurate in terms of the predicted vibration amplitude it provides.

This is supported by the vibration amplitude it suggests (0.002 of the transducer amplitude at 1000 Hz). These values are of similar orders of magnitude to those observed and measured inside the bone as seen in the follow up bovine experiments in section 4.4.2 (0.36% of the transducer amplitude on average at 1000 Hz).

This indicates, as an example, that for every micrometre of vibration amplitude at the surface of the transducer, an estimated 2 nm would be detectable inside the bone according to the FEA simulations, or 3.6 nm according to the vibrations measured inside the bovine femur. Whilst these are likely underestimations due to the differences in mass between a bovine and human femur, it highlights the degree of vibration required at the transducer in order to deliver even nanovibration at the target region. In order to replicate vibration levels seen in-vitro, 15 μm of vibration would be required.

This allows the conclusion to be drawn that the primary drivers of vibration amplitude reduction would be a combination of the soft tissue material between the transducer and the bone (this would, in a practical context, be any padding material combined with any soft flesh, muscle, skin, or adipose at that region) and the shape of the bone. As seen in the other models, where these factors are not

present, there is no decrease in vibration amplitude of the magnitude anticipated from real-life measured results. Notably, the presence of soft tissue seems especially important as its presence in other model types also caused a large dip in amplitude, particularly when combined with a more realistic bone geometry.

As shown from the heat maps generated in section 4.3.2, there is no obvious wave effect or evidence of compression/rarefaction within the bone region. Instead, the bone pistons back and forth in the direction of vibration, with the exception of the 'arm' representing the cortical shaft, which is stationary due to the 'fixed' constraint used. This provides confidence that the entirety of the bone is subject to an applied vibration, and that there are no node points where no vibration occurs. This is substantiated in section 4.4.1 and 4.4.2 using bovine bone samples.

It should be noted that the FEA modelling provided does not include attenuative effects, and these may contribute to the differences observed in real-life models. However, given the degree of accuracy displayed by these models, it is anticipated that attenuation has a lesser effect overall compared to reflection/transmission on the wave amplitude through the bone.

5.3.2 Vibration Characterisation in Bovine Bone

From the results shown in section 4.4.1 and 4.4.2, it is immediately clear that vibration was, as predicted by the FEA in earlier sections, present in the bone. During the initial bovine experiment results in 4.4.1, it was observed that the vibration in the approximate centre of the trabecular region (where the accelerometer was placed) ranged from 1.52 nm to 8.65 nm depending on the degree of soft material between the transducer element and the bone.

Compared to the FEA, there were differences in vibration application that are believed to have an effect on the vibration delivery; namely, due to the irregular geometry of the bone condyle upon which the transducer element was applied, it was difficult to gain a significant surface area to apply the transducer element to.

The SLI measurements on the surface displayed that the vibration amplitude was highest at a given point on the bone surface approximately in line with the transducer location, and then decayed across the surface. This effect is assumed to also be present within the trabecular region of bone.

The results from section 4.4.2 allow for commentary on the behaviour of vibration within the trabecular region to a greater degree. Whilst it was not anticipated from the FEA that wave effects or significant attenuation effects would occur (which would manifest as peaks and troughs in the measurements, or a gradual decline in amplitude from the transducer), it is valuable to confirm this using the vibration measurements seen in section 4.4.2.1.

Variation in vibration amplitude through the bone can be seen, however, which might highlight either a high degree of experimental variation or complexities in internal bone geometry that manifest as different vibration amplitudes (for example, on the edge of a given trabecula as opposed to a region of marrow/adipose tissue). Whilst care was taken to apply the transducer device as consistently as possible, it can be seen from the repeat application measurements on a single bone in 4.4.2.4 that there was considerable variation between measurements.

This is thought to be due to minute differences in transducer positioning, orientation, and contact with the bone that was difficult to control during the experiment due to the bone condyle geometry, the hardness and slipperiness of the bone surface, and reflective tape adhesion (particularly within the bone itself). Whilst this might serve to conceal any notable vibration effects that manifest as amplitude changes whose amplitude is less than the standard deviation of the repeat application experiment, it is not believed to be sufficient to discount the presence of vibration of at 1000 Hz on average 6.05 nm (0 - 12.98 nm CI = 95%; values lower than 0 discounted).

It can be seen from the normalised results that only a small fraction of vibration amplitude is successfully transmitted into the bone. The proportion of vibration amplitude in the bone compared to the vibration amplitude as measured on the transducer surface ranges between 0.0018 nm and 0.031 nm depending on frequency (0.0036 nm at 1000 Hz). It can be seen in Figure 60 that higher frequency vibration appears to be more successful at transmitting amplitude through the bone relative to the vibration at the transducer by a large factor (approximately 10). However there is also considerably more relative variation across the depth of the bone at high frequencies; this is possibly due to the lower absolute amplitude leading to a greater impact from the noise floor and small vibrations in the room and during the measurements.

It is worth comparing the efficacy of the piezo-block transducer compared to the voice-coil transducer in terms of the frequency at which they drive the vibration; at lower frequencies, the piezo-block appears to have greater success at delivering a larger proportion of vibration amplitude into the bone region compared to the

voice-coil transducer, however was unable to deliver detectable vibration amplitude at all at 5000 Hz, and it is believed that noise floor may be contributing to the results seen at 4000 Hz in Figure 63.

This indicates that depending on target frequency, for future prototypes that potentially use different frequencies for different applications, selecting the appropriate style of transducer will be an important design consideration. Overall the voice-coil transducer appears more reliable across low and mid-range frequencies, however the piezo-block may be more appropriate for very low-frequency applications. The selection of transducer type may be a valid subject for future work in this area due to the design considerations.

Whilst the results outlined in sections 4.4.1 and 4.4.2 go a long way towards granting confidence that vibration is transmitted successfully in an observable fashion within bone, and also relates the vibration amplitude at the bone surface and transducer surface with vibration within the bone, there are areas in which these studies could be improved upon. These experiments treat the trabecular region as an overall homogeneous media, which in reality is not the case; individual trabeculae and viscous bone-marrow have different vibration behaviours that the resolution of this experiment was not able to capture. Additionally, for very high frequencies, noise-floor interference became an obstacle to gaining accurate measurements.

It should be considered for future study, should this avenue be considered valuable, to investigate the vibration amplitude on an even smaller resolution (possibly by isolating trabeculae) and performing more exhaustive tests on bone

marrow regions. An improvement to experimental design may also allow for a lowering of the noise floor and, therefore, a more representative measurement at high frequencies. Lastly, it is obvious that there are geometrical and mass differences between a human femur and a bovine femur; due to the differences in mass and scale, it may have been more difficult for the voice-coil transducer especially to drive the bovine femoral head. Whilst a smaller size femur would be more challenging to measure in some regards, and availability of human femurs is limited, a more accurate-to-life sample would be undeniably more representative.

5.4 Summary of Future Work

From the results and discussion in this section, several avenues for future work are suggested due to either limitations of the study and discoveries made as a result of the work done.

Engineering improvements can be made to the device design based on observations made from the preliminary clinical evaluation and vibration characterisation. These can be viewed as independent from the biological outcomes observed in the animal trial, and can be applied to different methods of delivering a vibrational mechanical stimulation to a target region.

- Miniaturisation of the design should be a priority for any future device in order to improve the accessibility of the wearable device for any patient group. Whilst the wearability of the device was demonstrated successfully, the duration of use was limited by the bulk of the design. These may be achieved in part by making compact design choices as well as by dropping the need to perform vibration measurements during the study.

- Vibrational measurements during the wearing of the device may be forgone on the condition that sufficient confidence can be gained that vibration continues to be delivered constantly over the duration of vibration. This may be achievable by use of vibration transmission studies on representative biological samples or sufficiently adequate alternatives in order to provide confidence of vibration transmission without directly measuring vibration output during use and thereby remove the need for measurement components and systems added to the wearable device.
- The use of wearable devices may be adaptable to methods other than nanovibration delivery such as LIPUS therapy.

Additional work to explore the effects of vibration on BMD in-vivo is clearly required.

- Whilst there are practical limitations to extending the dose, given the difference in observed effects between the animal trials and in-vivo trials, it is worth considering designing a trial that enables continuous delivery of nanovibration over comparable durations to the in-vitro studies done.
- Allowing animals that partake in an animal trial to use their full range of motion may remove a bone-growth inhibiting factor.
- Investigating a less severe bone loss model may enable the observation of effects on BMD otherwise concealed by the dramatic bone loss caused by SCI.

Overall, the project has investigated the practical limits of delivering therapeutic vibration to participants suffering from SCI; it has been demonstrated that it can

be done with ergonomic limitations and monitor the vibration levels during use. The ergonomic limitations can be at least partially addressed through adjustments to design and engineering, which are worth considering irrespective of type of vibration intended to be delivered.

Additionally, steps towards quantifying the degree by which vibration amplitude is reduced through the bone region have been made, which are expected to be of assistance to any future project using lower-frequency vibration through bone. It is shown that there are serious challenges to delivering meaningful vibration amplitudes to the bone region, but that it can be possible to estimate at least in approximate terms the vibration amplitude at the target area.

6. Conclusion

At the completion of this project, the goal of designing and implementing a prototype wearable vibration device as well as investigating the viability of low-amplitude, low-frequency vibration as a potential therapy was achieved and implemented.

It remains important to pursue alternative therapies that have the potential to be used to improve outcomes for osteoporosis in order to reduce the costs inherent in an ageing population and importantly to increase the benefit of a greater quality of life and provide insight into their realistic implementation for future research.

Whilst many of the practical engineering challenges associated with a wearable device capable of being used by a patient suffering an SCI were addressed at least in part, it is clear from the work done on animals that the vibration amplitude and frequency using the device designed resulted in a null outcome. Whilst this in itself

informs research being performed on cells in-vitro, it is noteworthy to address the areas in which the design was successful. It was able to be worn for extended durations without a break and was capable of delivering measurable vibration amplitudes at the nanoscale, as confirmed by benchtop measurements carried out on bovine samples. Characterisation of the vibration inside the bone was also performed to form a basis for future work, as this frequency range remains little-explored compared to ultrasound mechanics or static mechanics. Greater understanding of the practical limitations of a wearable device was also achieved and can be used as feedback for future devices, whether these are used to deliver low-frequency vibration, a different form of vibration such as low-intensity pulsed ultrasound, or a different targeted therapy system.

As a prototype, it is believed to be worthwhile to view this body of work as a foundation for future devices in this category. Alterations to design may be considered using smaller components capable of forming a reduced profile; with a robust confidence level in the presence of vibration in the bone achieved, the need to constantly measure the vibration on the far side of the target region may also be measured with less sensitive apparatus or foregone entirely, further reducing the components and complexity of the device. As more information on using vibration as a therapy becomes accessible, the frequencies and vibration amplitudes, or variations in patterns, may also be explored. Lastly, it is worth performing more robust measurements within the bone, as the bone in all areas is a complex environment that simulations struggle to capture. Behaviour of vibration on the trabeculae and in the marrow may be different than for the bulk

region. This would necessitate more precise measurement tools and methodologies than was practical here.

Overall, this project demonstrated some success at advancing knowledge with regards to wearable devices, their application to SCI injuries and viability, and how the vibration is delivered and transmitted through the bone.

References

[1], Peter G Childs, Christina A Boyle, Gabriel D Pemberton, Habib Nikukar, Adam S G Curtis, Fiona L Henriquez, Matthew J Dalby, Stuart Reid, 2016, Use of nanoscale mechanical stimulation for control and manipulation of cell behaviour, Acta Biomaterialia, 34, 159-168, 10.1016/j.actbio.2015.11.045

[2], Habib Nikukar, 2013, Nanomechanotransduction of human mesenchymal stem cells an application of medical nanobiotechnology, PhD Thesis, University of Glasgow

[3], Gabriel D Pemberton, Peter Childs, Stuart Reid, Habib Nikukar, P Monica Tsimbouri, Nikolaj Gagegaard, Adam S G Curtis, Matthew J Dalby, 2015, Nanoscale Stimulation of Osteoblastogenesis from Mesenchymal Stel Cells: Nanotopography and Nanokikcing, Nanomedicine, 547-560, 10.2217/nnm.14.134

[4], Gabriel D Pemberton, Peter Childs, Stuart Reid, Nikolaj Gadegaard, Richard Burchmore, Adam S G Curtis, Matthew J Dalby, 2014, Nano-kicking stem cells into making bone, European Cells and Materials, Vol.28, Suppl. 4, 13

[5], NICE, 2017, Osteoporosis: assessing the risk of fragility fracture, National Institute for Health and Care Excellence

[6], National Institute for Health and Care Excellence, 2018, NICE impact falls and fragility fractures

[7], Royal Osteoporosis Society, 2022, ICS0035 Written evidence submitted by the Royal Osteoporosis Society, Royal Osteoporosis Society

[8], Tumay Sozen, Lale Ozisik, Nursel Calik Basaran, 2017, An overview and management of osteoporosis, European Journal of Rheumatology, 4(1), 46-56, 10.5152/eurjrheum.2016.048

[9], NIH Consensus Development Panel on Osteoporosis Prevention Diagnosis and Therapy, 2001, Osteoporosis Prevention, Diagnosis, and Therpy, JAMA: The Journal of the American Medical Association

[10], WHO Scientific Group on the Prevention and Management of Osteoporosis, 2003, Prevention and management of osteoporosis: Repowr of a WHO scientific group, https://iris.who.int/handle/10665/42841

[11], D E Garland, C A Steward, R H Adkins, S S Hu, C Rosen, F J Liotta, D A Weinstein, 1992, Osteoporosis After Spinal Cord Injury, Journal of Orthopaedic Research, 10, 371-378, 10.1002/jor.1100100309

[12], Sheng-Dan, Jiang Li-Yang, Dai Lei-Sheng Jiang, 2006, Osteoporosis After Spinal Cord Injury, Osteoporosis International, 17, 180-192, 10.1007/s00198-005-2028-8

[13], Shaun N Robertson, Paul Campsie, Peter G Childs, Fiona Madsen, Hannah Donnely, Fiona L Henriquez, William G Machay, Manuel Salmeron-Sanchez, Monica P Tsimbouri, Craig Williams, Matthew J Dalby, Stuart Reid, 2018, Control of cell behaviours through

nanovibrational stimulation: nanokicking, Philosophical Transactions, 10.1098/rsta.2017.0290

[14], L M Giangregorio, A Papaioannou, N J MacIntyre, M C Ashe, A Heinonen, K Shipp, J Wark, S McGill, H Keller, R Jain, J Laprade, A M Cheung, 2014, Too Fit To Fracture: exercise recommendations for individuals with osteoporosis or osteoporotic vertebral fracture, Osteoporosis International, 25, 3, 821-835, 10.1007/s00198-013-2523-2

[15], Julia O Totosy sde Zepetnek, Lora M Giangregorio, B Catharine Craven, 2009, Whole-body vibration as potential intervention for people with low bone mineral density and osteoporosis: a review, Journal of Rehabilitation Research and Development, 46, 4, 529-542, 10.1682/jrrd.2008.09.0136

[16], S M Szollar, E M Martin, D J Sartoris, J G Parthemore, L J Deftos, 1998, Bone mineral density and indexes of bone metabolism in spinal cord injury, American Journal of Physical Medicine and Rehabilitation, 77, 1, 28-35, 10.1097/00002060-199801000-00005

[17], Jonathan A. Williams, Paul Campsie, Richard Gibson, Olivia Johnson-Love, Anna Werner, Mark Sprott, Ryan Meechan, Carmen Huesa, James F. C. Windmill, Mariel Purcell, Sylvie Coupaud, Matthew J Dalby, Peter Childs, John S Riddel, Stuart Reid, 2024, Developing and Investigating a Nanovibration Intervention for the Prevention/Reversal of Bone Loss Following Spinal Cord Injury, ACS Nano, 18, 17630-17641

[18], Patricia A Downey, Michael I Siegel, 2006, Bone biology and the clinical implications for osteoporosis, Physical Therapy, 86, 1, 77-91, 10.1093/ptj/86.1.77

[19], J A Buckwalter, M J Glimcher, R R Cooper, R Recker, 1995, Bone biology and the clinical implications for osteoporosis, The Jurnal of Bone and Joint Surgery, 77, 8, 1276-1289

[20], Joana Caetano-Lopes, Helena Canhao, Joao Eurico Fonesca, 2007, Osteoblasts and bone formation, Sociedade Portuguesa de Rheumatologia, 32, 2, 103-110

[21], Jenneke Klein-Nulend, Peter J Nijweide, Elisabeth H Burger, 2003, Osteocyte and Bone Structure, Bone Biology and Structure, 1, 5-10

[22], Arkady Rutkovskiy, Kare-Olav Stenslokken, Ingvar Jarle Vaage, 2016, Osteoblast Differentiation at a Glance, Medical Science Monitor Basic Research, 22, 95-106, 10.12659/MSMBR.901142

[23], Shinjiro Takata, Natsuo Yasui, 2001, Disuse Osteoporosis, The Journal of Medical Investigation, 17, 180-192, 10.1007/s00198-005-2028-8

[24], S B Arnaud, D J Sherrard, N Maloney, R T Maloney, R T Whalen, P Fung, 1992, Effects of 1-week head-down tilt bed rest on bone formation and the calcium endocrine system, Aviation, 63, 1, 14-20

[25], Pekka Kannus, Markku Jarvinen, Harri Sievanen, Pekka Oja, Ilkka Vuori, 1994, Osteoporosis in men with a history of tibial fracture, Journal of Bone and Mineral Research, 9, 3, 423-429, 10.1002/jbmr.5650090319

[26], U.S. Department of Health and Human Services, 2004, Bone Health and Osteoporosis: A Report of the Surgeon General, U.S. Department of Health and Human Services, Office of the Surgeon General

[27], B Lawrence Riggs, Sundeep Khosla, L Joseph Melton, 2002, Sex Stereoids and the construction and cosnervation of the adult skeleton, Endocrine Reviews, 279-302, 10.1210/edrv.23.3.0465

[28], Peter Pietschmann, Martina Rauner, Wolfgang Sipos, Katharina Kershan-Shindl, 2008, OsteoporosisL An Age-Related and Gender-Specific Disease - A Mini-Review, Gerontology, 55, 10.1159%2F000166209

[29], Ricardo A Battaglino, Antonio A Lazzari, Eric Garshick, Lestlie R Morse, 2012, Spinal cord injury-induced osteoporosis: pathogenesis and emerging therapies, Current Osteoporosis Research, 10, 4, 278-285, 10.1007/s11914-012-0117-0

[30], National Institute fof Neurological Disorders and Stroke, 2025, Last accessed Jan. 2025, available from: https://www.ninds.nih.gov/health-information/disorders/spinal-cord-injury

[31], M Dauty, B Perrouin Verbe, Y Maugars, C Dubois, J F Mathe, 2000, Supralesional and sublesional bone mineral density in spinal cord-injured patients, Bone, 27, 2, 305-309, 10.1016/S8756-3282(00)00326-4

[32], A El Maghraoui, C Roux, 2008, DXA scanning in clinical practice, QJM, 101, 8, 6055-617, 10.1093/qjmed/hcn022

[33], Paul E Konahan, Bruce H Hasegawa, Thomas Beyer, 2003, X-Ray-Based Attenuation Correction for Positron Emission Tomography/Computed Tomography Scanners, Seminars in Nuclear Medicine, XXXIII, 3, 166-179, 10.1053/snuc.2003.127307

[34], Jack Wang, John C Thornton, Mary Horlick, Carmelo Formica, Wei Wang, Maike Rahn, Richard N Pierson Jr., 1999, Dual-X-Ray Absorptiometry in Pediatric Studies:

Changing Scan Modes Alters Bone and Body Composition Measurements, Journal of Clinical Densitometry, 2, 135-141, 10.1385/JCD:2:2:135

[35], J P van den Bergh, P Szulc, A M Cheung, M Bouxsein, K Engelke, R Chapurlat, 2020, The clinical application of high-resolution peripheral computed tomography (HR-pQCT) in adults: state of the art and future directions, Osteoporosis International, 32, 1465-1485, 10.1007/s00198-021-05999-z

[36], Yebin Jiang, Jenny Zhao, Er-Yuan Liao, Ru-Chan Dai, Xian-Ping Wu, Harry K Genant, 2005, Application of micro-CT assessment of 3-D bone microstructure in preclinical and clinical studies, Journal of Bone and Mineral Research, 27, 122-131

[37], Riana Lo Bu, Rose Fluss, Yashraj Srivastava, Rafael De la Garza Ramos, Saikiran G Murthy, Reza Yassari, Yaroslav Gelfand, 2025, Hounsfield Unit Utilization in Cervical Spine for Bone Quality Assessment: A scoping Review, Journal of Clinical Medicine, 14, 442, 10.3390/jcm14020442

[38], Murray J Favus, 2010, Bisphosphonates for Osteoporosis, Clinical Therapeutics, 363, 2027-2035, 10.1056/NEJMct1004903

[39], Nelson B Watts, Dima L Diab, 2010, Long-Term Use of Bisphosphonates in Osteoporosis, The Journal of clinical endocrinology and metabolism, 95, 4, 1555-1565, 10.1210/jc.2009-1947

[40], R G G Russel, N B Watts, F H Ebetino, M J Rogers, 2008, Mechanisms of action of bisphosphonates: similarities and differences and their potential influence on clinical efficacy, Osteoporosis International, 19, 733-759, 10.1007/s00198-007-0540-8

[41], Sarah Zaheer, Meryl LeBoff, E Michael Lewiecki, 2015, Denosumab for the Treatment of Osteoporosis, Expert Opinion on Drug Metabolism and Toxicology, 11, 3, 461-470, 10.1517/17425255.2015.1000860

[42], Michael R McClung, 2017, Sclerostin antibodies in osteoporosis: latest evidence and therapeutic potential, Therapeutic Advances in Musculoskeletal Disease, 9, 10, 263-270, 10.1177/1759720X17726744

[43], Stephanie Fabre, Thomas Funck-Brentano, Martine Cohen-Solal, 2020, Anti-Sclerostin Antibodies in Osteoporosis and Other Bone Diseases, Journal of Clinical Medicine, 9, 11, 3439, 10.3390/jcm9113439

[44], Ean G Phillips, Luck A Beggs, Fan Ye, Christine F Conover, Darren T Beck, Dana M Otzel, Payal Ghosh, Anna C F Bassit, Stephen E Borst, Joshua F Yarrow, 2018, Effects of pharmacologic sclerostin inhibition or testosterone administration on soleus muscle atrophy in rodents after spinal cord injury, PLOS ONE, 13, 3, 1-18, 10.1371/journal.pone.0194440

[45], Julius Wolff, 1870, Ueber de innere Architectur der Knocken und ihre Bedeutung fur die Frage vom Knockenwacschsthum, Archiv fur pathologische Anatomie Virchovs Archiv, 5, 389-453

[46], Daniela Grimm, Jirka Grosse, Markus Wehland, Vivek Mann, Janne Elin Reseland, Alamelu Sundaresan, Thomas Juhl Corydon, 2016, The impact of microgravity on bone in humans, Bone, 87, 44-56, 10.1016/j.bone.2015.12.057

[47], Guideo Schroder, Andreas Knauerhase, Guenther Kundt, Hans-Christof Schober, 2012, Effects of physical therapy on quality of life in osteoporosis patients - a randomized clinical trial, Health and Quality of Life Outcomes, 10, 101, 10.1186/1477-7525-10-101

[48], Charles F Kunkel, A M Erika Scremin, Brian Eisenberg, Jose F Garcia, Susan Roberts, Sylvia Martinez, 1993, Effect of "standing" on spasticity, contracture and osteoporosis in maralyzed males, Archives of Physical Medicine and Rehabilitation, 74, 1, 73-78

[49], Anne L Friedlander, Harry K Genant, Steven Sadowsky, Nancy N Byl, Claus C Gluer, 1995, A two-year program of aerobics and weight-training enhances bone mineral density of young women, Journal of Bone and Mineral Research, 10, 4, 574-585, 10.1002/jbmr.5650100410

[50], Christine Snow-Harter, Mary L Bouxsine, Barbara T Lewis, Dennis R Carter, Robert Marcus, 1992, Effects of resistance and endurance exercise intervention trial, Journal of Bone and Mineral Research, 7, 7, 761-769, 10.1002/jbmr.5650070706

[51], D S Ditor, A E Latimer, K A Martin Ginis, K P Arbour, N McCarteney, A L Hicks, 2003, Maintenance of exercise participation in individuals with spinal cord injury: effects on quality of life, stress and pain, Spinal Cord, 41, 446-450

[52], Martin Ginis, Kathleen A, A L Hicks, Audrey L, 2005, Exercise Research Issues in the Spinal Cord Injured Population, Exercise and Sport Sciences Reviews, 33, 1, 49-53

[53], Debra Bemben, Christina Stark, Redha Taiar, Mario Bernardo-Filho, 2018, Relevance of Whole-Body Vibration Exercises on Muscle Strength/Power and Bone of Elderly Individuals, Dose Response: An International Journal, 10.1177/1559325818813066

[54], H M Frost, 1996, Perspectives: a proposed general model of the "mechanostat" (suggestions from a new skeletal-biologic paradigm), Anatomica Record, 244, 2, 1339-1347, 10.1002/(sici)1097-0185(199602)244:2%3C139::aid-ar1%3E3.0.co;2-x

[55], S Stewart, A Darwood, S Masouros, C Higgins, A Ramasamy, 2020, Mechanotransduction in osteogenesis, Bone Joint Research, 9, 1, 1-14, 10.1302/2046-3758.91.bjr-2019-0043.r2

[56], Ruan Xiang-yan , Jin Feng-yu, Peng Shou-li, Sun Yun-Gao, 2008, Effects of vibration therapy on bone mineral density in postmenopausal women with osteoporosis, Chinese Medical Journal, 121, 13, 1155-1158

[57], Cosimo Roberto Russo, Fulvio Lauretani, Stefania Bandinelli, Benedetta Bartali, Chara Cavazzini, Jack M Guralnik, Luigi Ferrucci, 2003, High-Frequency Vibration Training Increases Muscle Power in Postmenopausal Women, Archives of Physical Medicine and Rehabilitation, 84, 12, 1854-1857, 10.1016/s0003-9993(03)00357-5

[58], S Dudley-Javoroski, M A Petrie, C L McHenry, R E Amelon, P K Saha, R K Shields, 2015, Bone architecture adaptations after spinal cord injury: impact of long-term vibration of a constrained lower limb, Osteoporosis International, 27, 3, 1149-1160, 10.1007/s00198-015-3326-4

[59], Ronald Davis, Charlotte Sanborn, David Nichols, David M Bazett-Jones, Eric Dugan, 2010, The Effects of Whle Body Vibration on Bone Mineral Density for a Person with a Spinal Cord Injury: A Case Study, Adapted Physical Activity Quarterly, 27, 60-72

[60], Lisa-Ann Wuermser, Lisa A Beck, Jeffry L Lamb, Elizabeth J Atkinson, Shreyasee Amin, 2014, The effect of low-magnitude whole body vibration on bone density and microstructure in men and women with chronic motor complete paraplegia, Journal of Spinal Cord Medicine, 38, 2, 178-186, 10.1179/2045772313Y.0000000191

[61], Clinton Rubin, A Simon Turner, Steven Bain, Craig Mallinckrodt, Kenneth McLeod, 2001, Low mechanical signals strengthen long bones, Nature, 412, 603-604, 10.1038/35088122

[62], Juha Kiiski, Ari Heinonen, Tepo I Jarvinen, Pekka Kannus, Harri Sievanen, 2008, Transmission of Vertical Whole Body Vibration to the Human Body, Journal of Bone and Mineral Research, 28, 8, 1318-1325, 0.1359/JBMR.080315

[63], Ditte Beck Jepsen, Katja Thomsen, Stinus Hansen, Niklas Rye Jorgensen, Tahir Masud, Jesper Ryg, 2017, Effect of whole-body vibration exercise in preventing falls and fractures: a systematic review and meta-analysis, BMJ Open, 7, 1-14, 10.1136/bmjopen-2017-018342

[64], L C Oliveira, R G Oliveira, D A A Pires-Oliveira, 2016, Effects of whole body vibration on bone mineral density in postmenopausal women: a systemic review and meta-analysis, Osteoporosis International, 27, 2913-2933, 10.1007/s00198-016-3618-3

[65], Lubomira Slatkovska, Shabbir M H Alibhai, Joseph Beyene, Hanxian Hu, Alice Demaras, Angela M Cheung, 2011, Effects of 12 months of whole-body vibration therapy on bone density and structure in postmenopausal women: a randomized trial, Annals of internal medicine, 155, 10, 668-679, 10.7326/0003-4819-155-10-201111150-00005

[66], S J Warden, K L Bennel, B Matthews, D J Brown, J M McMeeken, J D Wark, 2001, Efficacy of Low-intensity Pulsed Ultrasound in the Prevention of Osteoporosis Folowing Spinal Cord Injury, Bone, 29, 5, 431-436, 10.1016/S8756-3282(01)00599-3

[67], Brian F G Katz, 2000, Method to resolve microphone and sample location errors in the two-microphone duct measurement method, Journal of the Acoustics Society of America, 108, 2231-2237, 10.1121/1.1314318

[68], Kenneth J W Taylor, P N T Wells, 1989, Tissue characterisation, Ultrasound in Medicine & Biology, 15, 5, 421-428

[69], A F Seybert, D F Ross, 1976, Experimental determination of acoustic properties using a two-microphone random-excitation technique, Journal of the Acoustical Society of America, 61, 5, 1362-1370

[70], C M Langton, C F Njeh, 2008, The measurement of broadband ultrasonic attenuation in cancellous bone - a review of the science and technology, IEEE Transactions on NanoBioscience, 55, 7, 1546-1554, 10.1109/tuffc.2008.831

[71], M Choffie, 1994, Low-intensity pulsed ultrasound and effects on ununited fractures, Orthopaedic Health Conference, Sao Paolo

[72], T K Kristiansen, J P Ryaby, J McCabe, J J Frey, L R Roe, 1997, Accelerated Healing of Distal Radial Fractures with the Use of Specific, Low-Intensity Ultrasound. A Multicenter, Prospective, Randomized, Double-Blind, Placebo-Controlled Study, The Journal of Bone & Joint Surgery, 79, 7, 961-973

[73], Sjoerd Rutten, Peter A Nolte, Clara M Korstjens, Marion A Van Duin, Jenneke Klein-Nulend, 2008, Low-intensity pulsed ultrasound increased bone volume, osteoid thickness and mineral apposition rate in the area of fracture healing in patients with a delayed union of the osteomized fibula, Bone, 43, 438-354, 10.1016/j.bone.2008.04.010

[74], P A Nolte, A ven der Krans, P Patka, I M Janssenm J P Ryaby, G H Albers, 2001, Low-Intensity Pulsed Ultrasound in the Treatment of Nonunions, The Journal of Trauma: Injury, Infection, and Critical Care, 51, 4, 693-703

[75], C M Korstjens, R H H van der Rijt, G H R Albers, C M Semeins, J Klein-Nulend, 2008, Low-intensity pulsed ultrasound affects human articular chondrocytes in vitro, Medical & Biological Engineering & Computing, 46, 1263-1270, 10.1007/s11517-008-0409-9

[76], Yan Tan, Yang Guo, Amanda B Reed-Maldonaldo, Zheng Li, Guitling Lin, Shu-Jie Xia, Tom F Lue, 2021, Low-intensity pulsed ultrasound stimulates proliferation of stem/progenitor cells: what we need to know to translate basic science research into clinical applications, Asian Journal of Andrology, 23, 602-610, 10.4103/aja.aja_25_21

[77], Shuxin Sun, Lijun Sun, Yiying Kang, Liang Tang, Yi-Xian Qin, Dean Ta, 2020, Therapeutic effects of low-intensity pulsed ultrasound on osteoporosis in ovariectomized rats: intensity-dependant study, Ultrasound in Medicine & Biology, 46, 1, 108-121

[78], Daniela C I Carvalho, Alberto Cliquet, 2004, The Action of Low-Intensity Pulsed Ultrasound in Bones of Osteopenic Rats, Artificial Organs, 28, 1

[79], Dieter Gebauer, Edgar Mayr, Ernst Orthner, John P Ryaby, 2005, Low-intensity pulsed ultrasound: effects on nonunions, Ultrasound in Medicine & Biology, 31, 10, 1391-1402, 10.1016/j.ultrasmedbio.2005.06.002

[80], Jonathan H Lee, Kenneth J McLeod, 2000, Morphologic Responses of Osteoblast-like Cells in Monolayer Culture to ELF Electromagnetic Fields, Bioelectromagnetics, 21, 129-136

[81], C H Lohmann, Z Schwartz, Y Liu, H Guerkov, D D Dean, B Simon, B D Boyan, 2000, Pulsed Electromagnetic Field Stimulation of MG63 Osteoblast-like Cells Affects Differentiation and Local Factor Production, Journal of Orthopaedic Research, 18, 637-647, 10.1002/jor.1100180417

[82], J R Mauney, S Sjostorm, J Blumberg, R Horan, J P O'Leary, G Vunjak-Novakovic, V Volloch, D L Kaplan, 2004, Mechanical stimulation promotes osteogenic differentiation of human bone marrow stromal cells on 3-D partially demineralized bone scaffolds in vitro, Calcified Tissue International, 74, 5, 458-468, 10.1007/s00223-003-0104-7

[83], Boon Chin Heng, Tong Cao, Lawrence Walter Stanton, Paul robson, Bjorn Olsen, 2004, Strategies for Directing the Differentiation of Stem Cells Into the Osteogenic Lineage In Vitro, Journal of Bone and Mineral Research, 19, 9, 1379-1394, 10.1359/JBMR.040714

[84], D W Murray, N Rushton, 1990, The Effect of Strain on Bone Cell Prostaglandin 32 Release: A New Experimental Method, Calcified Tissue International, 47, 35-39

[85], Cornelia Neidlinger-Wilke, Hans-Joachim Wilke, Lutz Claes, 1994, Cyclic Stretching of Human Osteoblasts Affects Proliferation and Metabolism: A New Experimental Method and its Application, Journal of Orthopaedic Research, 12, 70-78, 10.1002/jor.1100120109

[86], C T Brighton, B Strafford, S B Gross, D F Leatherwood, J L Williams, S R Pollack, 1991, The proliferative and synthetic response of isolated calvarial bone cells of rats to cyclic biaxial mechanical strain, The Journal of Bone & Joint Surgery, 73, 320-331

[87], Daijang Du, Katsuko S Furukawa, Takashi Ushida, 2008, 3D Culture of Osteoblast-Like Cells by Unidirectional or Oscillatory Flow for Bone Tissue Engineering, Biotechnology and Bioengineering, 102, 6, 1670-1678, 10.1002/bit.22214

[88], E H Burger, J Klein-Nulend, J P Veldhuijzen, 1992, Mechanical stress and osteogenesis in vitro, Journal of Bone and Mineral Research, 2, 397-401, 10.1002/jbmr.5650071406

[89], Robin M Delaine-Smith, Gwendolen C Reilly, 2012, Mesenchymal stem cell responses to mechanical stimuli, Muscles, Ligaments and Tendons Journal, 16, 3, 169-180

[90], C E Sarraf, W R Otto, M Eastwood, 2011, In vitro mesenchymal stem cell differentiation after mechanical stimulation, Cell Proliferation, 44, 99-108, 10.1111/j.1365-2184.2010.00740.x

[91], Craig A Simmons, Sean Matlis, Amanda J Thornton, Shaoqiong Chen, Cun-Yu Wang, David J Mooney, 2003, Cyclic strain enhances matrix mineralization by adult human mesenchymal stem cells via the extracellular signal-regulated kinase (ERK1/2) signalling pathway, Journal of Biomechanics, 44, 1087-1096, 10.1016/S0021-9290(03)00110-6

[92], Yang-Kao Wang, Christopher S Chen, 2013, Cell adhesion and mechanical stimulation in the regulation of mesenchymal stem cell differentiation, Journal of Cellular & Molecular Medicine, 17, 7, 823-832, 10.1111/jcmm.12061

[93], Guenaelle Bouet, Magali Cruel, Coralie Laurent, Laurence Vico, Luc Malaval, David Marchat, 2016, Validation of an in vitro 3D bone culture model with perfused and mechanically stressed ceramic scaffold, eCells and Materials Journal, 29, 250-267, ffhal-01272415

[94], Adam Curtis, Chris Wilkinson, 1997, Topological control of cells, Biomaterials, 18, 1573-1583, 10.1016/S0142-9612(97)00144-0

[95], Ramanathan Vaidyanathan, Adam Curtis, Margaret Mullin, 2011, Entry of large nanoparticles into cells aided by nanoscale mechanical stimulation, Journal of Nanoparticle Research, 13, 5301-5309, 10.1007/s11051-011-0516-7

[96], Adam S G Curtis, Stuart Reid, Iain Martin, Ramanathan Vaidyanathan, Carol-Anne Smith, Habib Nikukar, Matthew J Dalby, 2013, Cell Interactions at the Nanoscale: Piezoelectric Stimulation, IEEE Transactions on NanoBioscience, 12, 3, 247-254

[97], Rong Peng, Xiang Yao, Bin Cao, Jian Tang, Jiandong Ding, 2012, The effect of culture conditions on the adipogenic and osteogenic inductions of mesenchymal stem cells on micropatterned surfaces, Biomaterials, 33, 6008-6019, 10.1016/j.biomaterials.2012.05.010

[98], Jennifer S Park, Julia S Chu, Anch D Tsou, Rokhaya Dlop, Zenyu Tang, Aijun Wang, Song Li, 2011, The Effect of Matrix Stiffness on the Differentiation of Mesenchymal Stem Cells in Response to TGF-β, Biomaterials, 32, 16, 3921-3930, 10.1016/j.biomaterials.2011.02.019

[99], M J P Biggs, R G Richards, S McFarlane, C D W Wilkinson, R O C Oreffo, M J Dalby, 2008, Adhesion formation of primary human osteoblasts and the functional response of mesenchymal stem cells to 330 nm deep microgrooves, Journal of the Royal Society Interface, 5, 1231-1242, 10.1098/rsif.2008.0035

[100], Matthew J Dalby, Mathis O Riehle, Duncan S Sutherland, Hossein Agheli, Adam S G Curtis, 2004, Use of nanotopography to study mechanotransduction in fibroblasts - methods and perspectives, European Journal of Cell Biology, 83, 159-169, 10.1078/0171-9335-00369

[101], Dan Wu, Andrea Smanou, Anna Diez-Escudero, Cecilia Persson, 2020, 3D -printed PLA/HA composite structures as synthetic trabecular bone: A feasibility study using fused deposition modelling, Journal of the Mechanical Behaviour of Biomedical Materials, 103, 10.1016/j.jmbbm.2019.103608

[102], Ana Grzeszczak, Susanne Lewin, Olle Eriksson, Johan Kreuger, Cecilia Persson, 2021, The Potential of Stereolithography for 3D Printing of Synthetic Trabecular Bone Structures, Materials, 13, 14, 10.3390/ma14133712

[103], Bryan Kaye, Connor Randall, Daniel Walsh, Paul Hansma, 2012, The Effects of Freezing on the Mechanical Properties of Bone, The Open Bone Journal, 4, 14-19, 10.2174/1876525401204010014

[104], H J Jung, Gautum Vangipuram, Matthew B Fisher, Guoguang Yang, Shanling Hsu, John Bianchi, Chad Ronholdt, Savio L Y Woo, 2011, The Effects of Multiple Freeze-Thaw Cycles on the Biomechanical Properties of the Human Bone-Patellar Tendon-one Allograft, Journal of Orthopaedic Research, 1193-1198, 10.1002/jor.21373

[105], Y N Feng, Y P Li, C L Liu, Z J Zhang, 2018, Assessing the elastic properties of skeletal muscle and tendon using shearwave ultrasound elastology and MyotonPRO, Scientific Reports, 8:17064, 10.1038/s41598-018-34719-7

[106], Gregor Pirnat, Matevz Marincic, Miha Ravnik, Matjaz Humar, 2024, Quantifying local stiffness and forces in soft biological tissues using droplet optical microcavities, Applied Physical Sciences, 121, 4, 1-9

[107], V K Strivastava, 2017, A Review on Advances in Rapid Prototype 3D Printing of Multi-Functional Applications, Science and Technology, 7, 1, 4-24, 10.5923/j.scit.20170701.02

[108], Bradford Cannon, James J O'Leary, Joseph W O'Neil, Robert Steinsieck, 1950, An Approach to the Treatment of Pressure Sores, Annals of Surgery, 132, 4, 760-777, 10.1097/00000658-195010000-00013

[109], John E McDermott, Pierce E Scranton, James V Rogers, 2004, Variations in Fibular Position, Talar Length and Anterior Talofibular Ligament Length, American Orthopaedic Foot & Ankle Society, 25, 9, 625-629, 10.1177/107110070402500905

[110], Rui Zou, Yang Xia, Shiyi Liu, Ping Hu, Wenbin Hou, Qingyuan Hu, Chunlai Shan, 2016, Isotropic and anisotropic elasticity and yielding of 3D printed material, Composites Part B: Engineering, 99, 506-513, 10.1016/j.compositesb.2016.06.009

[111], H J Kwon, P Y B Jar, 2007, Toughness of high-density polyethylene in shear fracture, International Journal of Fracture, 145, 123-133, 10.1007/s10704-007-9110-5

[112], Bolzica Bojovic, Zorana Golubovic, Ljubisa Petrov, Aleksa Milovanovic, Aleksandar Sedmak, Zarko Miskovic, Milos Milosevic, 2023, Comparative Mechanical Analysis of PLA and ABS Materials in Filament and Resin Form, New Trends in Engineering Research, 114-131

Appendix

Appendix 1: ACH-01 Datasheet

dimensions

ACCELEROMETER ACH-01

SPECIFICATIONS

- Piezoelectric Accelerometer
- Wide Bandwidth; AC Coupled
- Ultra Low Power
- High G Ranges

The ACH-01 is an inexpensive, general purpose accelerometer with outstanding performance characteristics. The use of piezoelectric polymer film in the ACH-01 provides many cost/performance advantages that allow it to be used in a wide range of applications where the use of traditional accelerometer technology is impractical. It is specifically designed for high volume applications which require the permanent installation of an accelerometer.

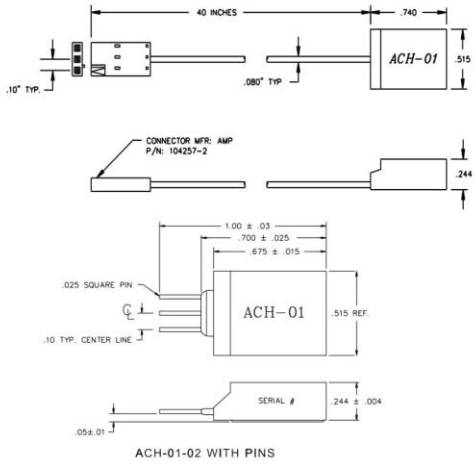

ACH-01-02 WITH PINS

FEATURES

- Wide Frequency Response
- Excellent Phase Response
- Small Temperature Dependence
- Wide Supply Voltage Range
- Excellent Linearity
- Very High Resonant Frequency
- Wide Dynamic Range
- Low Transverse Sensitivity
- Wide Temperature Range
- Low Impedance Output
- Ultra Low Power

APPLICATIONS

- Machine Health Monitoring
- Model Analysis
- Automotive Sensors
- Appliances
- Feedback Control Systems

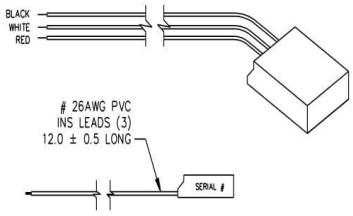

ACH-01-04 WITH WIRES

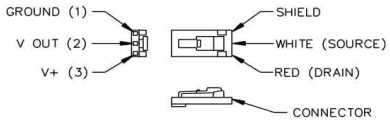

CONNECTOR DETAIL

PERFORMANCE SPECIFICATIONS

PERFORMANCE (T=25°C)	Symbol	Min	Typ	Max	Units
Sensitivity	M_o	7	9	11	mV/g
Lower Frequency Limit (1)	f_l	--	2	5	Hz
Upper Frequency Limit(1)	f_u	10	20	--	kHz
Equivalent Noise Floor 10Hz 100Hz 1kHz		 -- -- --	 130 20 6	 -- -- --	$\mu g/\sqrt{Hz}$
Dynamic Range	--	≤150	--	--	g
Linearity	--	--	0.1	1.0	%
Transverse Sensitivity	M_t	--	2.0	5	%
Resonant Frequency	f_o	--	35	--	kHz
Phase Deviation (≤5° Limit)(6)	θ	10	--	10	kHz
Drain Voltage (6)	V+	3	--	40	Volts
Supply Current (6)	I_{dss}	30	--	90	µA
Output Impedance (6)	--	--	20	--	kΩ
ENVIRONMENTAL CHARACTERISTICS					
Operating Temperature (2)	T_o	-40	--	85	°C
Storage Temperature	T_s	-40	--	85	°C
Maximum Shock Level	A_m	1000	--	--	g
Base Strain Sensitivity (3)	--	--	0.3	--	g/µε
Transient Temp Sensitivity (4)	--	--	0.35	--	g/°C
PHYSICAL CHARACTERISTICS					
Weight (5) Cable	W	--	8	--	grams

(1) ≤3 dB limit
(2) ≤2 dB from nominal M_o at 1kHz
(3) @ 250µε in base plane
(4) @ 3Hz LLF
(5) Includes 40" cable and connector
(6) Typical Value

Mounting methods play a critical role in determining the overall performance of any accelerometer. The ACH-01 is no exception. An improperly mounted accelerometer can give erroneous results. We recommend using an Adhesive Mounting Method.

The surface should be flat. The area where the ACH-01 is to be mounted should be thoroughly cleaned to remove any dirt or oil present on the surface. Use a quick setting, viscous methyl cyanoacrylate adhesive such as Loctite's Black Max or any epoxy such as Devcon's 5-Minute epoxy. Apply the adhesive sparingly to one surface following the manufacturer's directions. Apply pressure and allow the adhesive to set. Soft adhesives, such as double-sided tape or pressure sensitive adhesives, should not be used since they can adversely affect the ACH-01's performance. Cable should be adhered to the surface.

There is an interface amplifier available to simplify connection to the ACH-01, the IB-ACH-01. Please see the appropiate data sheet.

In an effort to keep the product cost low, the ACH-01 uses a ceramic substrate as the mounting base. Because of this, the ACH-01 is susceptible to base strain and temperature transient effects. A mechanically rigid and thermally non-conductive mounting surface is highly recommended to limit these effects. MEAS application engineers are available to recommend various mounting arrangements for your specific application.

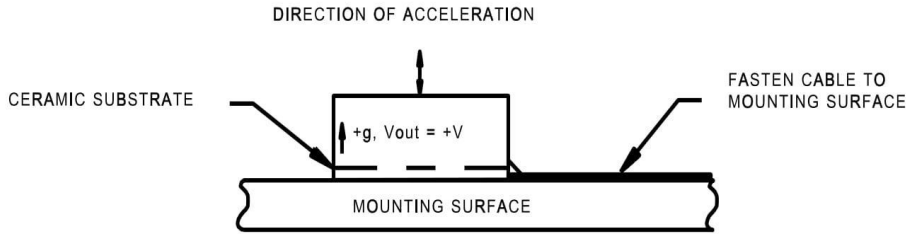

ELECTRICAL INTERFACE CIRCUITS

The accelerometer ACH-01 accommodates various electrical interface circuits. A typical example is provided in the following figure. The ACH-01 equivalent electrical schematic is also shown.

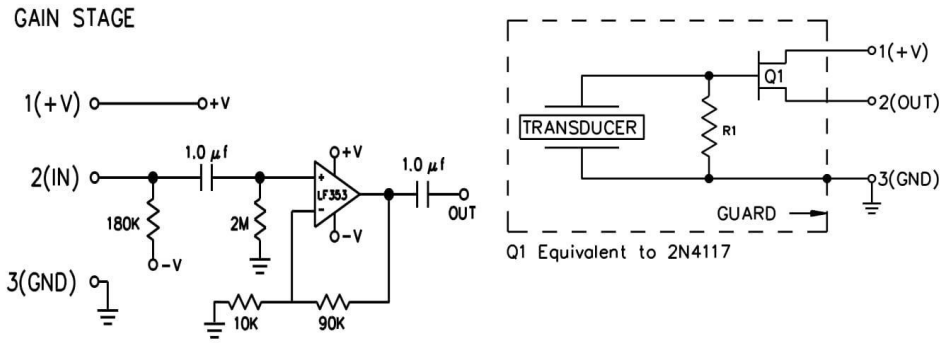

ORDERING INFORMATION

Description	Interface	Model No.	Part No.
Accelerometer	Pins	ACH-01-02	0-1000985-0
	Shielded Cable	ACH-01-03	1-1001220-0
	Discrete Wires	ACH-01-04	1-1001497-0
Amplifier	Amplifier Box	IB-ACH-01	1003058

NORTH AMERICA
Measurement Specialties, Inc.,
a TE Connectivity Company
Tel: +1-800-522-6752
Email: customercare.dtmd@te.com

EUROPE
MEAS Deutschland GmbH
a TE Connectivity Company
Tel: +49-800-440-5100
Email: customercare.dtmd@te.com

ASIA
Measurement Specialties (China), Ltd.,
a TE Connectivity Company
Tel: +86 0400-820-6015
Email: customercare.chdu@te.com

TE.com/sensorsolutions

Appendix 2: Electronics Design Components

Electronics Components:

- AD9833 low power programmable waveform generator (Analog Devices, Massachusetts, United States of America)
- ATMega328 microcontroller (Atmel, California, United States of America)
- OPA37 ultra-low noise operational amplifier (Texas Instruments, Texas, United States of America)
- 10 kΩ rotary potentiometer
- MAX98306 3.7 W power amplifier (SparkFun Electronics, Colorado, United States of America)
- ACH-01 accelerometer (TE Connectivity, Shaffhausen, Switzerland)
- Power amplification circuit (Adafruit Industries, New York, United States of America)
- Arduino Nano microcontroller (Arduino, Massachusetts, United States of America)
- AD736JNZ

Wave Generator Circuit:

The Wave Generator Circuit comprises the following components:

- Seventh order LC elliptical reconstruction filter
- Microcontroller (ATMega328)
- Waveform Generator (AD9833)
- Reconstruction Filter
- Voltage Amplifier (OPA37)
- Power Amplifier (MAX98306)

The seventh order LC elliptical reconstruction filter was used to reduce higher frequency components above 1000 Hz; the signal was then amplified using a non-inverting amplifier circuit featuring an OPA37 OP-AMP, and then featured a user-adjustable amplification stage using a 10 kΩ rotary potentiometer.

The gain of the amplification stage in the wave generator circuit is given by the following formula:

$$GAIN = 1 + \frac{R_{POT}}{R_2},$$

where Rpot is the resistance of the potentiometer.

Vibration Signal Amplifier (Accelerometer):

The vibration signal amplifier comprises the following components:

- Non-inverting amplifier (OPA37)
- Standard inverting amplifier (OPA37)
- RMS to DC signal converter (AD736JNZ)

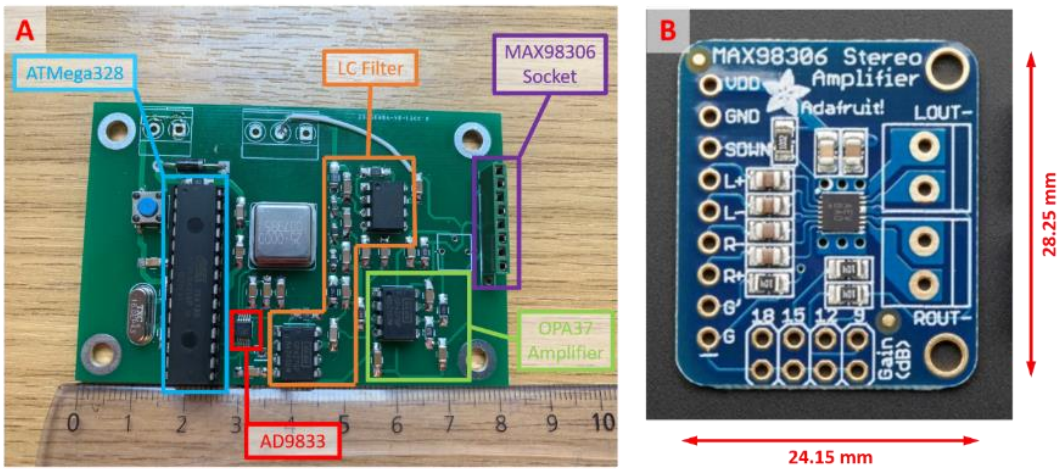

Appendix 3: LB07 Datasheet

样 品 承 认 书

APPROVED SHEER

Customer 客 户:_____

Description 种 类: 共振喇叭LB07 4Ω5W

Customer's P/N 客 户 编 号:_____

Offer Date 提 供 日 期:_____

设 计 DESIGNED	审 核 CHECKED	核 准 APPROVED	客户确认 Approved Signature

承认后请寄回一份
Please return one copy after approved.

深圳市富通盈科技有限公司
深圳市宝安区沙井镇东环路80-4号富威工业园5栋2楼
TEL:0755-27465565

规 格 书

SPEAKER SPECIFICATION

2012 年 11 月 5 日 REV: A0

单 元 型 名Our Model No.		LB07 4Ω5W		适用机种Product Model No:	
客户 Customer				客 户 型 名Customer's Model No :	
规格描述		LB 4Ω5W			
1	适用范围 Applicable Scope				
1.1	类型 Type	永久磁铁动圈式扬声器 permanent-magnet dynamic loudspeaker			
1.2	口径 Dimensions	44 mm			
1.3	功率 Power	额定功率Nominal input 5 W, 最大功率Maximum input 10W			
2	机械特性 mechanical specification				
2.1					
2.2					
3	电气特性: Electrical specification				
3.1	公称阻抗 Nominal Impedance	4Ω ±15% test @200Hz 3 v			
3.2	最低共振周数 Lowest Resonance Frequency	60Hz±20% (@ 3.0 V)			
3.3	出力音压 Output sound Pressure Level	86±3 dB (100、400、800、12000Hz 的平均值@ 500m 3w)			
3.4	实际周波数带域 Effective Frequency Band	F100 ~ 15KHz @ 3.0V 5.0 W			
3.5	失真率 Distortion	5% less @ 5W 800Hz			
3.6	纯音检测Sine Wave Test	正弦波 6.3V 60~2.0K HZ, 串 \ uf 电容时，无异常不良. Must be normal at sine wave			
3.7	极性 Polarity	从SP端子正极输入正电流，另一端输入负电流时，振动板向前推出。 When a positive current is supplied form the speaker the terminal marked (+) and a negative to the other terminal the diaphragm must move toward the front .			
4	信赖性Reliability				
4.1	连 续 负 荷 Load Test	粉红噪音10W连续96小时试验后无异常的不良。 Must be normal after load test :pink noise 5W 96 hours			
4.2	耐 热 性 heat Test	温度70±2℃ 湿度20-25% 16小时试验常温1小时后，无异常不良。 Must be normal after 70±2℃and relative humidity20-25% 16hours and then room temperature 1hour.			
4.3	耐 寒 性 Cold Test	温度-25±3℃ 温度 - % 16小时试验常温1小时后，无异常的不良 Must be normal -25±3℃ and relative humidity - % 16hours and then room temperature 1 hour			
4.4	耐 温 性 Humidity Test	温度40±2℃ 湿度90-95% 48小时试验常温1小时后，无异常的不良。 Must be normal after40±2℃ and relative humidity 90-95% 48 hours and then room temperature 1hour			
批 准 APPRROVED		审 核 CHECKED		制 表 DESINGED	

装 配 工 艺 表

产品编号		产品型号		客 户	

产品形状	安装外径：44mm, 全高：28mm 					
检测	输入电压 V	谐振频率 Hz	有效频宽 Hz	检听频率 Hz	反电动势 V	分频电容 uf
	6.3	50	F100-15K	50-2.0K Hz		
	阻 抗 Ω	直流电阻 Ω	相 位			
	4	3.6	正 向			
包装	外包装	内包装	装入数 pcs	尺寸 cm	体积 M3	毛重 kg
	1		96	29*21*15		20.1

音圈定位	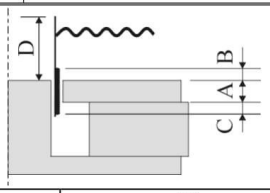				
	A	**B**	**C**	**D1**	**D2**
	3.0	**0.5±0.05**	**0.5±0.05**		

治 具	中心治具型号	音圈治具型号	备 注	充磁电压:>200 V

备注	1	3
	2	4

批　准 APPRROVED		审　核 CHECKED		制　表 DESINGED	

频 响 曲 线

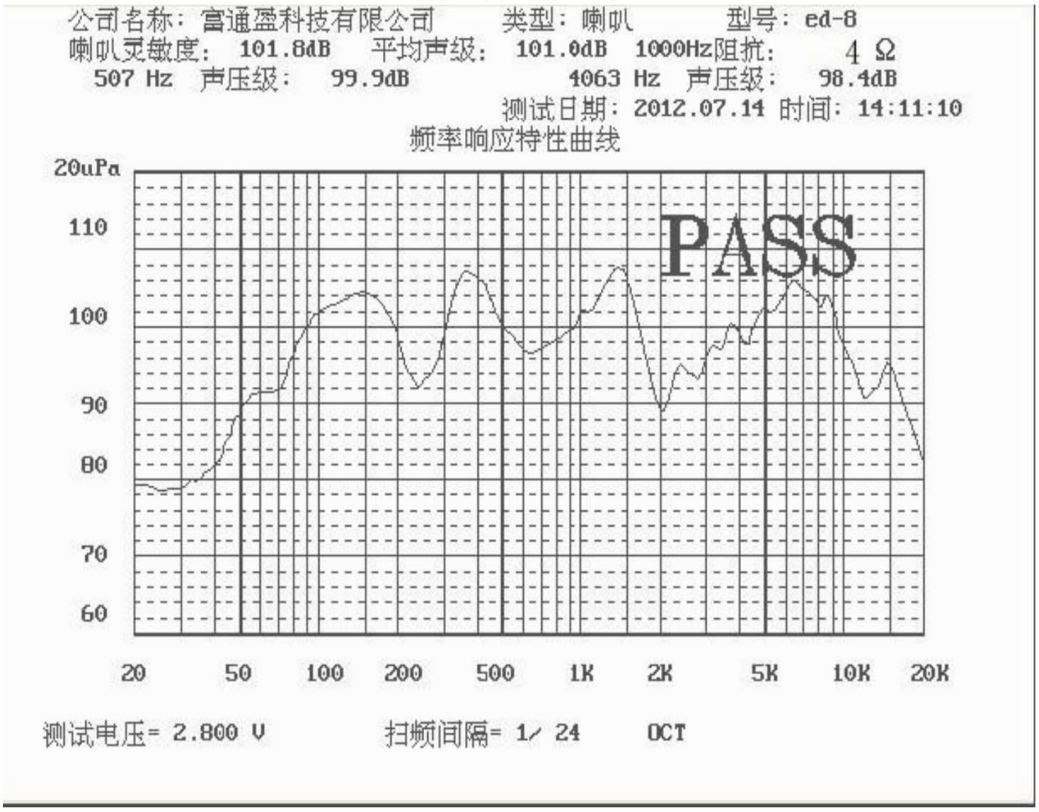
公司名称：富通盈科技有限公司
类型：喇叭
型号：ed-8
喇叭灵敏度： 101.8dB
平均声级： 101.0dB
1000Hz阻抗： 4 Ω
507 Hz 声压级： 99.9dB
4063 Hz 声压级： 98.4dB
测试日期：2012.07.14 时间：14:11:10
频率响应特性曲线
20uPa
110
100
90
80
70
60
PASS
20
50
100
200
500
1K
2K
5K
10K
20K
测试电压= 2.800 V
扫频间隔= 1/ 24
OCT

Appendix 4: User Manual

DEPARTMENT OF BIOMEDICAL ENGINEERING

University of Strathclyde Engineering

Instructions for Knee Nanovibration Device

Contact Information:

Email: **Telephone:**

Note: These instructions are for the right leg

Step 1: Open straps up and lay out as shown.

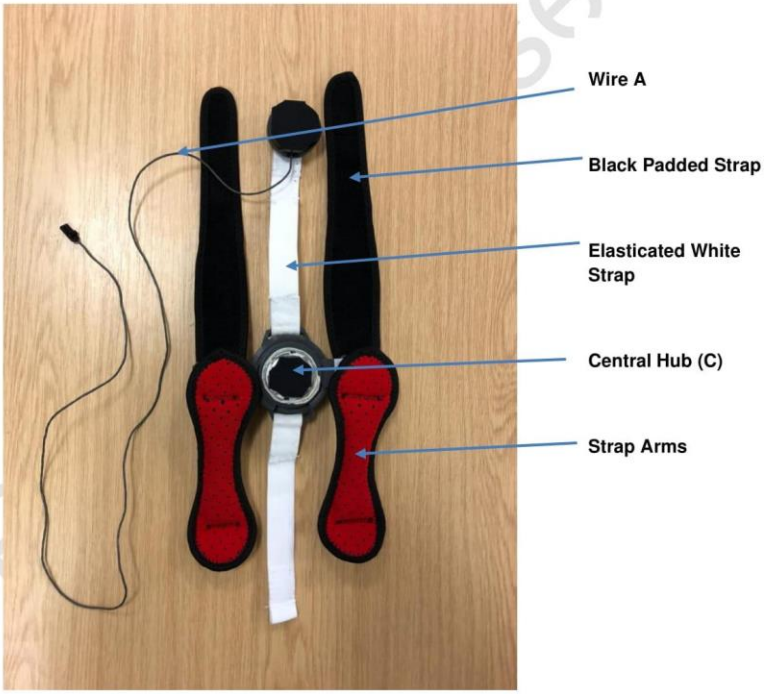

1

Step 2: Adjust device against the outer leg as shown.

Step 3: Position the top strap (labelled T) on the top of the thigh as shown below. The central hub should be positioned against the outer leg and the padded part of the strap should be above the knee. Close the strap at the inside of the leg and tighten it lightly so as to secure the device from falling.

Step 4: Position lower strap (labelled L) on the lower leg below the knee. As with in step 3, close the strap at the inside of the leg and tighten lightly.

Step 5: Rotate central hub so that the white strap passes evenly in-between the two black straps as shown.

Step 6: Shift central hub to be positioned at the end of the lower leg above the knee joint.

Step 7: Position the part A at the end of the white strap against the knee on the opposite side of the central hub. Attach the other end of the white strap on top of the part A to secure in place.

Step 8: Plug in Wire B to Central Hub

Step 9: Connect wires A and B as shown below

Step 10: Turn on the power supply using the ON/OFF button. The red and green lights on the left side of the device will flash for a few seconds to show that the power is on.

> If both red lights continually flash, the unit should be turned off and the issue reported to one of the contacts above.

Step 11: If the green light is on then the setup is good and you can move to step 12.

If the red light on the left is on, then the signal is too high. The signal can be turned down by turning the VOLUME control to the left. If the left red light is still on, loosen straps slightly until green light comes on.

If the red light on the right is on, then the signal is too low. The signal can be increased by turning the VOLUME control to the right. If the red light is still on after turning the volume control all the way to the right, then the device on the leg needs to be readjusted (see step 6)

Step 12: Once the setup is complete, press the DATA button on the left side of the power supply to start recording data.

Step 13: After the time for the therapy is complete press the DATA button to stop recording data.

Step 14: Press the ON/OFF button to power down the device and disconnect the wires A and B.

Step 15: Remove the white strap by detaching part A.

Step 16: Remove the lower black strap.

Step 15: Remove the upper black strap slowly to ensure that the device does not fall, pull device away from leg.

Step 16: Plug in USB cable as shown below and plug to mains. After a 4 hour therapy session, make sure to charge device for at least 4 hours.

Appendix 5: FEA Table of Results

Simulation Type	Frequency	Average Amplitude (m)	Normalised Amplitude (against 1E-6m)
Block Model, Single Material	500	**1.00** x 10^{-6}	1.00 x 10^{0}
	1000	**1.01** x 10^{-6}	1.01 x 10^{0}
	2000	**1.05** x 10^{-6}	1.05 x 10^{0}
	4000	**1.25** x 10^{-6}	1.25 x 10^{0}
	5000	**1.47** x 10^{-6}	1.47 x 10^{0}
Block Model, Composite Material	500	**9.97** x 10^{-7}	9.97 x 10^{-1}
	1000	**1.01** x 10^{-6}	1.01 x 10^{0}
	2000	**1.04** x 10^{-6}	1.04 x 10^{0}
	4000	**1.23** x 10^{-6}	1.23 x 10^{0}
	5000	**1.43** x 10^{-6}	1.43 x 10^{0}
Block Model, Single Material, Transducer Model Only	500	**1.01** x 10^{-6}	1.01 x 10^{0}
	1000	**1.02** x 10^{-6}	1.02 x 10^{0}
	2000	**1.09** x 10^{-6}	1.09 x 10^{0}
	4000	**2.57** x 10^{-6}	2.57 x 10^{0}

Simulation Type	Frequency	Average Amplitude (m)	Normalised Amplitude (against 1E-6m)
	5000	**2.57** x 10^{-6}	2.57 x 10^{0}
Armed Block Model, Single Material, Transducer Model Only	500	**9.93** x 10^{-7}	0.993 x 10^{-1}
	1000	**1.01** x 10^{-6}	1.01 x 10^{0}
	2000	**1.08** x 10^{-6}	1.08 x 10^{0}
	4000	**1.50** x 10^{-6}	1.50 x 10^{0}
	5000	**2.37** x 10^{-6}	2.37 x 10^{0}
Block Model, Composite Material, Transducer & Soft Tissue Model	500	**4.09** x 10^{-8}	4.09 x 10^{-2}
	1000	**1.23** x 10^{-8}	1.23 x 10^{-2}
	2000	**2.86** x 10^{-9}	2.86 x 10^{-3}
	4000	**4.13** x 10^{-9}	4.13 x 10^{-3}
	5000	**1.02** x 10^{-8}	1.02 x 10^{-2}
Armed Block Model, Composite Material, Transducer Model Only	500	**9.89** x 10^{-7}	9.89 x 10^{-1}
	1000	**1.01** x 10^{-6}	1.01E x 10^{0}
	2000	**1.08** x 10^{-6}	1.08 x 10^{0}
	4000	**1.57** x 10^{-6}	1.57 x 10^{0}
	5000	**2.85** x 10^{-6}	2.85 x 10^{0}

Simulation Type	Frequency	Average Amplitude (m)	Normalised Amplitude (against 1E-6m)
Femur Model, Single Material, Transducer Model Only	500	**1.02** x 10^{-6}	1.02 x 10^{0}
	1000	**1.04** x 10^{-6}	1.04 x 10^{0}
	2000	**1.11** x 10^{-6}	1.11 x 10^{0}
	4000	**1.68** x 10^{-6}	1.68 x 10^{0}
	5000	**3.56** x 10^{-6}	3.56 x 10^{0}
Femur Model, Single Material, Transducer & Soft Tissue Model	500	**8.03** x 10^{-9}	8.03 x 10^{-3}
	1000	**3.01** x 10^{-7}	3.01 x 10^{-1}
	2000	**1.30** x 10^{-9}	1.30 x 10^{-3}
	4000	**8.59** x 10^{-10}	8.59 x 10^{-4}
	5000	**7.79** x 10^{-10}	7.79 x 10^{-4}
Femur Model, Composite Material, Transducer Model Only	500	**9.34** x 10^{-7}	9.34 x 10^{-1}
	1000	**1.02** x 10^{-6}	1.02 x 10^{0}
	2000	**4.37** x 10^{-6}	4.37 x 10^{0}
	4000	**6.82** x 10^{-7}	6.82 x 10^{0}
	5000	**8.34** x 10^{-8}	8.34 x 10^{-2}
Femur Model, Composite Material,	500	**1.01** x 10^{-8}	1.01 x 10^{-2}

Simulation Type	Frequency	Average Amplitude (m)	Normalised Amplitude (against 1E-6m)
Transducer & Soft Tissue Model	1000	**1.63** x 10^{-9}	1.63 x 10^{-3}
	2000	**1.01** x 10^{-8}	1.01 x 10^{-2}
	4000	**1.62** x 10^{-8}	1.62 x 10^{-2}
	5000	**1.75** x 10^{-9}	1.75 x 10^{-3}

Appendix 6: Vibration measured from Follow-up Bovine Femur Experiments in nm and normalised against the transducer surface

Vibration Amplitude By Frequency (Hz) and Measurement Depth (cm)						
Depth	**500 Hz**	**1000 Hz**	**2000 Hz**	**4000 Hz**	**5000 Hz**	**Count (n)**
0	52.70	9.17	0.67	3.27	0.54	6
-1	35.87	7.42	0.90	2.40	0.99	5
-2	15.91	7.14	1.93	2.25	1.60	6
-3	33.30	4.51	0.54	2.51	0.93	5
-4	35.27	3.32	0.71	3.50	0.86	5
-5	38.66	5.24	1.12	3.13	1.48	6
-6	31.88	4.82	0.65	7.59	1.09	6
-7	19.67	5.89	0.79	5.16	1.24	4
-8	17.37	3.93	1.11	1.72	0.54	4
-9	20.72	14.13	0.92	7.33	1.77	2
-10	21.98	1.00	0.32	0.69	0.49	1

Normalised Vibration Amplitude By Frequency (Hz) and Measurement Depth (cm)						
Depth	**500 Hz**	**1000 Hz**	**2000 Hz**	**4000 Hz**	**5000 Hz**	**Count (n)**
0	0.0076	0.0054	0.0014	0.0281	0.0141	6
-1	0.0073	0.0043	0.0018	0.0230	0.0227	5
-2	0.0041	0.0037	0.0034	0.0245	0.0504	6
-3	0.0073	0.0034	0.0011	0.0220	0.0326	6
-4	0.0056	0.0028	0.0017	0.0217	0.0176	5
-5	0.0079	0.0036	0.0021	0.0313	0.0452	6
-6	0.0047	0.0032	0.0014	0.0656	0.0413	6
-7	0.0052	0.0035	0.0018	0.0513	0.0619	4
-8	0.0045	0.0030	0.0035	0.0172	0.0231	4
-9	0.0028	0.0067	0.0012	0.0525	0.0317	2
-10	0.0029	0.0004	0.0005	0.0052	0.0089	1

Appendix 7: Vibration amplitude through bovine bone at 500Hz, 1000Hz, 2000Hz, 4000Hz, and 5000Hz in nm and normalised to transducer vibration amplitude